

3
2006

This is to certify that the
dissertation entitled

CRYSTAL GROWTH MECHANISMS IN NATURAL AND
SYNTHETIC DOLOMITE: INSIGHT INTO DOLOMITIZATION
KINETICS

presented by

STEPHEN EMIL KACZMAREK

has been accepted towards fulfillment
of the requirements for the

Ph. D degree in Geological Sciences


Major Professor's Signature

Oct 21, 2005

Date

MSU is an Affirmative Action/Equal Opportunity Institution

LIBRARY
Michigan State
University

PLACE IN RETURN BOX to remove this checkout from your record.
TO AVOID FINES return on or before date due.
MAY BE RECALLED with earlier due date if requested.

DATE DUE	DATE DUE	DATE DUE

**CRYSTAL GROWTH MECHANISMS IN NATURAL AND SYNTHETIC
DOLOMITE: INSIGHT INTO DOLOMITIZATION KINETICS**

By

Stephen Emil Kaczmarek

A Dissertation

**Submitted to
Michigan State University
In partial fulfillment of the requirements
for the degree of**

DOCTOR OF PHILOSOPHY

Department of Geological Sciences

2005

ABSTRACT

CRYSTAL GROWTH MECHANISMS IN NATURAL AND SYNTHETIC DOLOMITE: INSIGHT INTO DOLOMITIZATION KINETICS

By

Stephen Emil Kaczmarek

The lack of dolomite in modern marine setting is a kinetic problem, yet relatively few details about dolomitization are understood. Because the geometries observed on crystal surfaces are dictated by growth and dissolution, and such mechanisms are theoretically related to kinetics, the current study utilizes *ex situ* atomic force microscopy to investigate nanometer-scale features on synthetic and natural dolomites in order to better understand dolomitization.

Following a relatively long induction period, high-temperature synthetic dolomite forms very rapidly. Initial dolomite products are poorly ordered (i.e., nonideal), whereas stoichiometry (61-50 mole% CaCO₃) is dependent on the initial Mg²⁺:Ca²⁺ ratio in solution (R²=0.97). Following initial reactant depletion, dolomite products are stoichiometric and well-ordered (i.e., ideal).

Two distinct nanometer-scale growth features - islands and layers - characterize dolomite growth surfaces. Islands are rounded positive relief features. Layers are broad, flat surfaces with steps. Islands occur on nonideal synthetic dolomite prior to reactant depletion, whereas layers form only after calcite reactant depletion. Counter to theoretical predictions, dolomite nanotopography is independent of the Mg²⁺:Ca²⁺ in solution. Surface nanotopography does respond, however, to changing carbonate flux at the

growth interface following reactant depletion, therefore suggesting that carbonate plays a major role in dolomitization kinetics.

Following chemical etching, ideal synthetic dolomite surfaces exhibit flat layers with deep euhedral pits, whereas nonideal synthetic dolomite surfaces are covered with islands identical to the islands observed on growth surfaces. Chemically etched ideal and nonideal natural dolomites are also characterized by etch pits and islands, respectively. These features are indistinguishable from islands and etch pits observed on synthetic dolomite. Based on models of crystal growth and dissolution, nonideal dolomite surface nanotopography is most consistent with polynuclear growth. Conversely, ideal dolomite is more consistent with spiral growth. These observations indicate that dolomite initially forms by polynuclear growth and is nonideal. Because it is metastable, nonideal dolomite may later be replaced by ideal dolomite.

Due to the similarities between natural and synthetic dolomites, high-temperature experimental findings can serve as a model for interpreting observations from natural low-temperature settings. Therefore, a long induction period followed by rapid growth is the best model to explain the absence of dolomite in modern marine environments.

ACKNOWLEDGEMENTS

Many thanks to my advisor, mentor, and friend Duncan Sibley; it has truly been an honor and a privilege to think about science and life with you over the years. To my committee members Mike Velbel, Lina Patino, and Dave Long for helping to make this project worthy of being proud of. I would like to thank Ewa Danielewicz at the MSU Center for Advanced Microscopy for her help with mastering AFM and SEM techniques. Much appreciation to Loretta Knutson, Jackie “the dude” Bennett, Cathy Caswell, and Marsha Walsh for helping me avoid as many administrative problems as possible. I would also like to recognize family and friends for remaining supportive and interested even when I appeared not to be.

TABLE OF CONTENTS

LIST OF TABLES.....	vii
LIST OF FIGURES.....	viii
1. INTRODUCTION.....	1
1.a. Previous Experimental Work.....	4
1.b. Ca-Enrichment in Natural Dolomite.....	11
1.c. Crystal Growth Mechanisms.....	16
1.d. Chemical Etching.....	24
2. METHODS.....	29
2.a. Dolomite Synthesis.....	29
2.b. X-Ray Diffraction.....	31
2.c. Atomic Force Microscopy.....	35
2.d. Scanning Electron Microscopy.....	38
2.e. Crystal Size Distributions.....	39
3. RESULTS.....	40
3.a. Synthetic Dolomite Reaction.....	40
3.b. Calcite Reactant Experiments.....	44
3.b.1. Reaction Rate.....	44
3.b.2. Dolomite Stoichiometry.....	57
3.b.3. Cation Order.....	65
3.b.4. Solution Chemistry.....	71
3.c. Aragonite Reactant Experiments.....	73
3.c.1. Reaction Rate.....	73
3.c.2. Dolomite Stoichiometry.....	77
3.c.3. Cation Order.....	77
3.d. Synthetic Dolomite Crystal Size Distributions.....	80
3.e. Synthetic Dolomite Surface Nanotopography, AFM.....	80
3.e.1. Calcite Reactant Experiments.....	80
3.e.2. Aragonite Reactant Experiments.....	90
3.f. Synthetic Dolomite Surface Nanotopography, SEM.....	96
3.f.1. Calcite Reactant Experiments.....	96
3.f.2. Aragonite Reactant Experiments.....	105
3.g. Etched Synthetic Dolomite Surface Nanotopography, AFM.....	105
3.h. Natural Dolomite Surface Nanotopography, AFM.....	112
3.i. Natural Dolomite Surface Nanotopography, SEM.....	120

4. DISCUSSION.....	124
4.a. Islands and Layers Are Growth Features.....	124
4.b. Polynuclear Growth.....	127
4.c. Spiral Growth.....	135
4.d. Transition From Polynuclear To Spiral Growth.....	142
4.d.1. Energy.....	143
4.d.2. Carbonate.....	150
4.e. Synthetic Dolomite Stoichiometry.....	159
4.f. Synthetic Dolomite Cation Order.....	161
4.g. Synthetic Dolomite Recrystallization.....	164
4.h. Natural Dolomite Growth Mechanisms.....	167
4.h.1. Nonideal Dolomite And Polynuclear Growth.....	168
4.h.2. Ideal Dolomite And Spiral Growth.....	172
4.i. Surface Nanotopography and Internal Microstructure.....	173
4.j. Similarities Between Synthetic and Natural Dolomites.....	176
4.j.1. Induction Period.....	176
4.j.2. Reaction Rate.....	178
4.j.3. Selective Replacement.....	179
4.j.4. Crystal Size Distributions.....	180
4.j.5. Mimetic Replacement.....	181
4.j.6. Stoichiometry.....	182
4.j.7. Cation Order.....	185
4.k. Implications for Natural Dolomite.....	187
5. CONCLUSIONS.....	207
6. REFERENCES CITED.....	211

LIST OF TABLES

Table 1. Natural dolomite sample list.....	34
Table 2a. Experimental results for high-temperature calcite experiments.....	41
Table 2b. Experimental results for high-temperature aragonite experiments.....	43
Table 3. Induction period times for calcite experiments.....	56
Table 4. Changes in solution $Mg^{2+}:Ca^{2+}$ chemistry at 50% products and 100% products. Column three is the average dolomite stoichiometry observed in the experiments for the initial solution $Mg^{2+}:Ca^{2+}$ in column one.....	72

LIST OF FIGURES

Figure 1. Generalized reaction curve for high-temperature synthetic dolomitization reactions.....	7
Figure 2. Surface expressions of some common crystal growth models.....	17
Figure 3. Diagram showing theoretical growth rates of spiral and polynuclear growth as a function of free energy (after Sunagawa, 1984).....	18
Figure 4. Percent product vs. time for calcite reactant experiment with initial solution $Mg^{2+}:Ca^{2+} = 0.429$	45
Figure 5. Percent product vs. time for calcite reactant experiment with initial solution $Mg^{2+}:Ca^{2+} = 0.50$	46
Figure 6. Percent product vs. time for calcite reactant experiment with initial solution $Mg^{2+}:Ca^{2+} = 0.66$	47
Figure 7. Percent product vs. time for calcite reactant experiment with initial solution $Mg^{2+}:Ca^{2+} = 0.786$	48
Figure 8. Percent product vs. time for calcite reactant experiment with initial solution $Mg^{2+}:Ca^{2+} = 1.0$	49
Figure 9. Percent product vs. time for calcite reactant experiment with initial solution $Mg^{2+}:Ca^{2+} = 1.14$	50
Figure 10. Percent product vs. time for calcite reactant experiment with initial solution $Mg^{2+}:Ca^{2+} = 1.27$	51
Figure 11. Percent product vs. time for calcite reactant experiment with initial solution $Mg^{2+}:Ca^{2+} = 1.5$	52
Figure 12a. Induction period (log-scale) vs. initial solution $Mg^{2+}:Ca^{2+}$ for calcite reactant experiments.....	54
Figure 12b. Induction period (linear-scale) vs. initial solution $Mg^{2+}:Ca^{2+}$ for calcite reactant experiments.....	55
Figure 13. Dolomite stoichiometry vs. initial solution $Mg^{2+}:Ca^{2+}$ for all dolomites formed prior to calcite reactant depletion, calcite reactant experiments, $R^2=0.9688$, $N=69$	58

Figure 14. Dolomite stoichiometry vs. percent product for all dolomites formed prior to calcite reactant depletion, calcite reactant experiments, $R^2=0.023$, $N=69$59

Figure 15. Dolomite stoichiometry vs. percent product for dolomites formed prior to calcite reactant depletion, calcite reactant experiment, initial solution $Mg^{2+}:Ca^{2+} = 0.79$, $R^2=0.0013$60

Figure 16. Dolomite stoichiometry vs. percent product for dolomites formed prior to calcite reactant depletion, calcite reactant experiment, initial solution $Mg^{2+}:Ca^{2+} = 1.27$, $R^2=0.0005$61

Figure 17. Dolomite stoichiometry vs. time for dolomite formed prior to calcite reactant depletion, calcite reactant experiment, initial solution $Mg^{2+}:Ca^{2+} = 0.79$, $R^2=0.0003$63

Figure 18. Dolomite stoichiometry vs. time for dolomites formed prior to calcite reactant depletion, calcite reactant experiment, initial solution $Mg^{2+}:Ca^{2+} = 1.27$, $R^2=0.0097$64

Figure 19. Cation order vs. time for calcite reactant experiment, initial solution $Mg^{2+}:Ca^{2+} = 1.0$. Reactant depletion occurs after ~160 hours.....67

Figure 20. Cation order vs. time for calcite reactant experiment, initial solution $Mg^{2+}:Ca^{2+} = 1.5$. Reactant depletion occurs between 35 and 77 hours.....68

Figure 21. Cation order vs. time for calcite reactant experiment, initial solution $Mg^{2+}:Ca^{2+} = 0.66$. Reactant depletion occurs at ~217 hours.....69

Figure 22. Cation order vs. dolomite stoichiometry for all synthetic dolomites formed prior to calcite reactant depletion. Calcite reactant experiments, $N=69$, $R^2=0.0342$70

Figure 23. Percent product vs. time for aragonite reactant experiment with initial solution $Mg^{2+}:Ca^{2+} = 1.0$74

Figure 24a. SEM photomicrograph showing selective dolomitization of aragonite when both calcite and aragonite are present.....75

Figure 24b. SEM photomicrograph showing randomly oriented dolomite rhombs on an aragonite substrate.....76

Figure 25. Dolomite stoichiometry vs. time for dolomite formed up to 30 hours after the onset of experimental conditions, aragonite reactant experiment, initial solution $Mg^{2+}:Ca^{2+} = 1.0$, $R^2=0.841$78

Figure 26. Cation order vs. time for aragonite reactant experiments, initial solution $Mg^{2+}:Ca^{2+} = 1.0$, $R^2=0.8325$79

Figure 27. Coarse skewed CSD, sample 7-22-02-7. Reactant: 140-160 micron size Iceland spar calcite.....81

Figure 28. Coarse skewed CSD, sample 1-19-87-1. Reactant: reagent grade calcium carbonate.....82

Figure 29. Coarse skewed CSD, sample 1-24-98-1. Reactant: reagent grade calcium carbonate.....83

Figure 30. Coarse skewed CSD, sample 1-17-87-2. Reactant: reagent grade calcium carbonate.....84

Figure 31. Coarse skewed CSD, sample 1-21-87-1. Reactant: reagent grade calcium carbonate.....85

Figure 32. AFM image of a nonideal synthetic dolomite growth surface showing pervasive island nanotopography. Calcite reactant experiment, solution $Mg^{2+}:Ca^{2+} = 1.0$86

Figure 33. AFM image of a nonideal synthetic dolomite showing cross-section of island-covered growth surface. Calcite reactant experiment, solution $Mg^{2+}:Ca^{2+} = 0.66$87

Figure 34. AFM image of a nonideal synthetic dolomite growth surface showing variable nanotopography caused by islands. Calcite reactant experiment, solution $Mg^{2+}:Ca^{2+} = 1.5$89

Figure 35. AFM image of an ideal synthetic dolomite growth surface showing straight-sided steps. Calcite reactant experiment, solution $Mg^{2+}:Ca^{2+} = 1.0$91

Figure 36. AFM image of an ideal synthetic dolomite growth surface showing multiple layers with curved steps. Calcite reactant experiment, solution $Mg^{2+}:Ca^{2+} = 1.5$92

Figure 37a. AFM image and cross-section of an ideal synthetic dolomite growth surface showing an emerging growth layer. Calcite reactant experiment, solution $Mg^{2+}:Ca^{2+} = 0.66$93

Figure 37b. AFM image and cross-section of an ideal synthetic dolomite showing the emerging growth layer disappears into the surface.....94

Figure 38. AFM image of a nonideal synthetic dolomite showing pervasive island nanotopography. Aragonite reactant experiment, solution $Mg^{2+}:Ca^{2+} = 1.0$95

Figure 39. SEM photomicrograph showing crystallographically oriented dolomite rhombs on the edges and corners of the calcite substrate.....	97
Figure 40. SEM photomicrograph showing dolomite growth rhombs on a pitted calcite surface that has been dissolved.....	98
Figure 41. SEM photomicrograph showing a dolomite encrusted calcite grain.....	99
Figure 42. SEM photomicrograph of a small dolomite rhomb on a dolomite surface.	100
Figure 43a. SEM photomicrograph of a nonideal synthetic dolomite surface showing irregular growth nanotopography.....	101
Figure 43b. SEM photomicrograph of the same nonideal synthetic dolomite growth surface at higher magnification showing rounded topographic highs and wavy ledges.....	102
Figure 44a. SEM photomicrograph of an ideal synthetic dolomite showing relatively flat growth surfaces.....	103
Figure 44b. SEM photomicrograph of the same ideal synthetic dolomite at higher magnification showing flat growth surfaces separated by straight-sided steps.....	104
Figure 45. SEM photomicrograph showing gold coating on dolomite grain.....	106
Figure 46. AFM image of an etched synthetic nonideal dolomite showing a pervasive island dissolution surface. Calcite reactant experiment, solution $Mg^{2+}:Ca^{2+} = 0.66$	107
Figure 47. AFM image of an etched ideal synthetic dolomite showing euhedral etch pits. Calcite reactant experiment, solution $Mg^{2+}:Ca^{2+} = 0.66$	109
Figure 48. AFM image of an etched ideal synthetic dolomite showing a high density of euhedral etch pits. Calcite reactant experiment, solution $Mg^{2+}:Ca^{2+} = 1.5$	110
Figure 49. AFM image of an etched ideal synthetic dolomite showing euhedral etch pits and relatively flat inter-pit surfaces. Calcite reactant experiment, solution $Mg^{2+}:Ca^{2+} = 1.27$	111
Figure 50. AFM image of an etched natural nonideal dolomite showing pervasive island-covered surface.....	113

Figure 51. AFM image and cross-section of an etched natural nonideal dolomite showing dissolution island nanotopography..... 114

Figure 52. AFM image of an etched natural nonideal dolomite showing an island-covered surface with voids and depressions.....115

Figure 53. AFM image of an etched natural ideal dolomite showing euhedral etch pits with flat inter-pit layers..... 116

Figure 54. AFM image of an etched natural ideal dolomite showing crystallographically oriented rhombic etch pits..... 117

Figure 55. AFM image of an etched natural ideal dolomite showing euhedral etch pits with rhombic shape.....118

Figure 56. AFM image and cross-section of an etched natural ideal dolomite showing euhedral etch pits with pointed bottoms..... 119

Figure 57. SEM photomicrograph of an unetched natural dolomite surface showing voids (V), steps (S), and debris (D).....121

Figure 58. SEM photomicrograph of an etched natural nonideal dolomite surface. Arrows mark voids (V), steps (S), and debris (D).....122

Figure 59. SEM photomicrograph of a natural ideal dolomite showing a highly irregular and dissolved surface after 10 minutes of etching in dilute acid.....124

Figure 60. AFM image from Heraty (1998) showing amorphous growth islands on a calcite surface in phosphate-doped experiments..... 131

Figure 61. Growth mechanism summary diagram for dolomitization..... 166

Figure 62. 2-theta (i.e. dolomite stoichiometry) vs. percent dolomite for GWP data from Abu Dhabi, $R^2=0.3706$. Note: 2-theta values are proportional to dolomite stoichiometry..... 199

There is a mask of theory over the whole face of nature

- W. Whewell

1. INTRODUCTION

The origin of dolomite, $[\text{CaMg}(\text{CO}_3)_2]$, has been debated extensively for over a decade. Although most geologists now regard dolomite as a sedimentary mineral that forms during the replacement reaction between carbonate sediments and magnesium-rich fluids, no unique geologic environment of dolomitization has been recognized (e.g., Murray and Pray, 1965; Friedman and Sanders, 1967, Folk and Land, 1975; Budd, 1997). Dolomite is found in thick, laterally extensive deposits throughout the rock record, but exists in modern marine environments only in small abundances and few locations. Because dolomite is the thermodynamically stable carbonate phase in seawater, its rare occurrence in modern carbonate-forming marine environments is problematic. Although no universal explanation has emerged, most workers generally agree that the “dolomite problem” is one of kinetics (Land, 1985; Hardie, 1987; Sibley, 1990; Budd, 1997).

Relatively little is known about the reaction details of natural dolomitization aside from the fact that, for most dolomites, no geologic evidence exists of unusual temperature or pressure conditions (Krauskopf and Bird, 1995). However, both the failure to unequivocally synthesize dolomite at temperatures below 100°C (e.g., Usdowski, 1994; Land, 1998) without the aid of bacteria (see Vasconcelos et al., 1995; Warthman et al., 2000) and the lack of a modern analog for massive dolomite deposits have led a number of workers to examine high-temperature synthesis experiments as a means of acquiring information

about dolomite reaction kinetics (Graf and Goldsmith, 1956; Gaines, 1974; Katz and Matthews, 1977; Baker and Kastner, 1981; Sibley et al., 1987; Morrow and Rickets, 1988; Sibley, 1990; Sibley et al., 1994; Kessels et al., 2000). These high-temperature experiments provide insight into the kinetic details of the CaCO_3 to dolomite transformation, yet there exist no theoretical bases for extrapolating kinetic data over the 25-250°C temperature range between sedimentary dolomites and temperatures commonly employed in laboratory experiments. Consequently, applicability of these high-temperature experiments to natural low-temperature systems remains uncertain.

Dolomitization of CaCO_3 requires nucleation and crystal growth, both of which are dictated by thermodynamic, as well as kinetic factors. The details of these processes are in turn reflected in the mineral's texture and microstructure. Knowledge of a crystal's defect microstructure can provide insight to the growth process (e.g., Reeder, 2000). More specifically, different models of crystal growth imply different defect structures. This study will test two hypotheses about the kinetics of dolomitization: 1) high-temperature, synthetic dolomites and low-temperature, natural dolomites have similar growth mechanisms, and 2) the growth mechanisms in dolomite are dictated by $\text{Mg}^{2+}:\text{Ca}^{2+}$ ratios (i.e., the degree of supersaturation) of the dolomitizing solutions. Both hypotheses have a great deal of importance in regard to understanding dolomitization in natural settings. If the first hypothesis is unsubstantiated, the applicability of high-temperature experiments to natural dolomite is tenuous. Support for the second hypothesis

suggests that knowledge of the growth mechanism would allow the possibility of interpreting information about the environment of formation of natural dolomites.

Before proceeding, it is worth noting that both natural and synthetic dolomites are found in a variety of forms that must be distinguished. Dolomite is a complex mineral in which considerable variations occur in the composition and the degree of cation order (Goldsmith and Graf, 1958; Reeder and Wenk, 1979; Reeder, 1992). The term dolomite is used here to describe Ca-Mg carbonates with compositions approximating $m\text{Mg}/m\text{Ca} = 1$ and evidence of cation ordering. For dolomite with non-Mg and non-Ca ions only in trace abundances, stoichiometry is generally expressed in terms of mole percent CaCO_3 . Ideal dolomite, $\text{Ca}_{0.50}\text{Mg}_{0.50}(\text{CO}_3)_2$, refers to dolomites with equal molar quantities of calcium and magnesium that display a relatively high degree of cation order. The structure of ideal dolomite is characterized by alternating A and B cation planes, separated by layers of CO_3 , all of which are stacked along the threefold axis (Reeder, 1981). Both Lippmann (1973) and Reeder (1983) have likened the structure of ideal dolomite to a composite of alternating calcite and magnesite layers. When the criteria of a high degree of cation order and stoichiometric composition are not satisfied, the term nonideal dolomite is appropriate. Nonideal dolomites are most often associated with Ca-enrichment (Reeder, 1983). Although Mg-rich dolomite does occur in nature, its occurrence is relatively rare (Rosen et al., 1989) or poorly documented (Reeder, 2000).

In a number of instances, the term protodolomite (Graf and Goldsmith, 1956) has been used in the literature to describe Ca-Mg carbonates with very

poor or non-existent ordering, the inference being that protodolomite might represent a metastable precursor of well-ordered stoichiometric dolomite for high-temperature experimental dolomites described by Graf and Goldsmith (1956) and natural dolomites as well (Lippmann, 1973; Reeder, 1981). This latter view is consistent with the observation that many recent dolomites are Ca-rich and poorly ordered. Land (1980) has argued against the term protodolomite on the grounds that natural Mg-Ca-carbonate phases often display some degree of cation order and should therefore be considered dolomite. Following this reasoning, the term protodolomite is avoided when describing poorly ordered Ca-Mg-carbonate phases, unless making reference to previously published observations.

1.a. Previous Experimental Work

Several experimental investigations have attempted to identify the thermodynamic and kinetic controls on dolomite formation (Graf and Goldsmith, 1956; Land, 1967; Lippmann, 1973; Gaines, 1974, 1980; Katz and Matthews, 1977; Baker and Kastner, 1981; Sibley and Bartlett, 1987; Sibley et al., 1987a,b; Morrow and Ricketts, 1988; Sibley, 1990; Nordeng and Sibley, 1993; Sibley et al., 1994; Morrow et al., 1994; Kessels et al., 2000). These investigators employed temperatures in excess of 100°C because dolomite has a very low reactivity at lower temperatures (Usdowski, 1994). Moreover, scientists have largely been unsuccessful in synthesizing dolomite inorganically at low temperatures even over very long times (e.g. 30 years, *c.f.* Land, 1998) other than poorly ordered

Ca-rich (nonideal) dolomite (Deer et al., 1992; Deelman, 1981; Busenberg and Plummer, 1989). Katz and Matthews (1977) examined the effects of temperature on the dolomitization rate. They reported that complete dolomitization of calcite took 112 hours at 252°C, 38 hours at 263°C, 14 hours at 274°C, 6 hours at 285°C, and 4 hours at 295°C. From this data, Katz and Matthews (1977) calculated the activation energy for the synthetic dolomite to be 48-50kcal/mol, which they used to invoke the high temperatures needed to synthesize dolomite over reasonable time-scales. Based on experimental data from Gaines (1968), Arvidson and Mackenzie (1997) recalculated the activation energy of ordered (ideal) dolomite to be 42.1kcal/mol. Arvidson and Mackenzie (1999) later calculated the activation energy for poorly ordered calcium-rich dolomite (protodolomite) to be 31.9kcal/mol, approximately 10 kcal/mol less than the value for ideal dolomite. Arvidson and Mackenzie (2000) postulated that the activation energy of dolomite is a function of 1) the energy associated with the dehydration of magnesium ions, and 2) the energy associated with cation ordering. They plotted activation energy (E_a) vs. composition for Ca-Mg carbonates based on a published value for calcite from Kazmierczak et al. (1982) and an extrapolated value for magnesite. Although the experimentally determined activation energy for the nonideal dolomite (protodolomite) used by Arvidson and Mackenzie (1999) was in nearly perfect accord with the value predicted from the extrapolated line between the calcite and magnesite values, the experimentally derived E_a for ideal dolomite was approximately 5.5 kcal/mol greater than the value predicted by the line. Arvidson and Mackenzie (2000)

interpreted the additional energy to represent the effects of cation order in ideal dolomite. The additional energy reported by Arvidson and Mackenzie (2000) for ideal dolomite is in agreement with the E_a of 5.5kcal/mol calculated earlier by Malone et al. (1996) which was determined for the rate of recrystallization of disordered Ca-Mg carbonate phases to ordered dolomite between 149-197°C.

Graf and Goldsmith (1956) formed dolomite by reacting combinations of various Mg-bearing and carbonate-bearing species (calcareous algae, echinoids, Ca-Mg-carbonate gel, aragonite and Mg-carbonate) in hydrothermal bombs at various temperatures. In lower temperature and shorter duration experiments, they observed that initial products (called protodolomite) were compositionally different from the ideal dolomite that was formed in higher temperature and longer duration experiments. Powder X-ray diffraction (XRD) patterns of the initial products (protodolomite) showed expanded unit cell dimensions, which Graf and Goldsmith (1956) interpreted as substitution of larger calcium cations into magnesium sites. The initial products (protodolomite) also exhibited missing superstructure reflections, which they interpreted to indicate an absence of the ideal succession of alternating magnesium and calcium cation planes.

Results of subsequent high-temperature studies demonstrated that the overall reaction curve for the dolomitization reaction is sigmoidal-shaped (Figure 1; Katz and Matthews, 1977; Sibley and Bartlett, 1987; Sibley et al., 1987; Sibley, 1990; Nordeng and Sibley, 1993; Sibley et al., 1994; Kessels et al., 2000), the

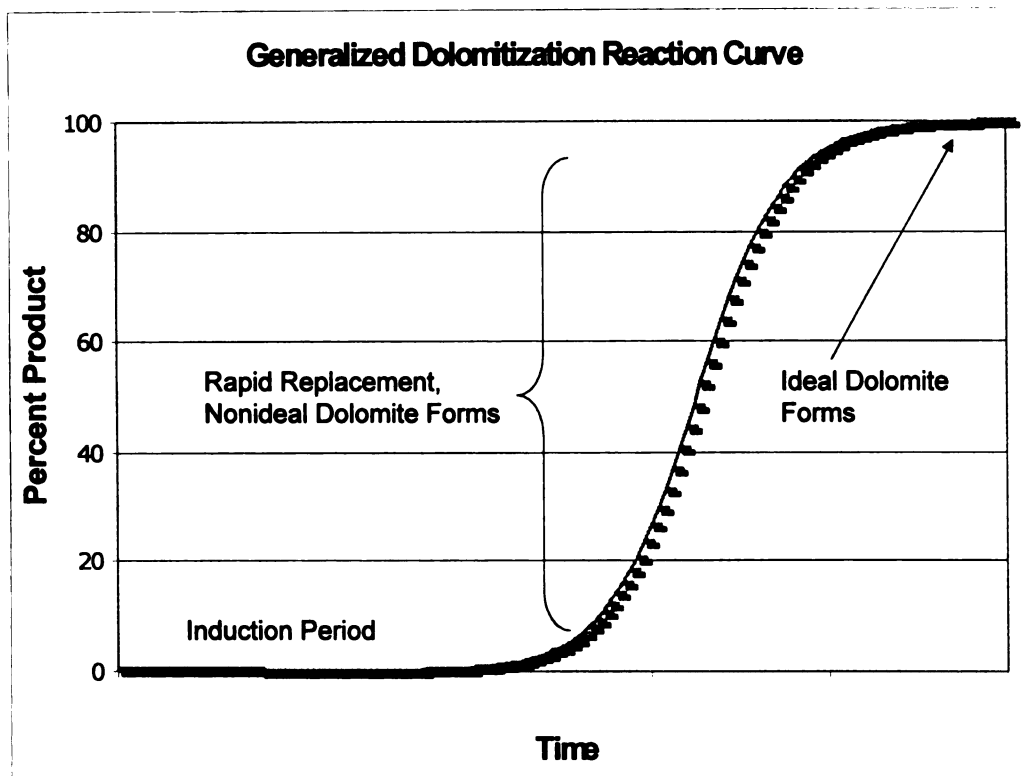


Figure 1. Generalized reaction curve for high-temperature synthetic dolomitization reactions.

slope at any point being a function of growth and nucleation rates (Avrami, 1939). The dolomitization reaction has a relatively long induction period followed by rapid replacement of reactants (Katz and Matthews, 1977; Sibley and Bartlett, 1987; Sibley et al., 1987; Sibley, 1990; Nordeng and Sibley, 1993; Sibley et al., 1994; Kessels et al., 2000). The induction period is the time after the onset of experimental conditions when no dolomite products are detected (Walton, 1969). Sibley et al. (1987) showed that the induction period, as determined by XRD, could be 20% to >80% of the total duration of the reaction. Nordeng and Sibley (1993) conducted thermal cycling experiments to show that nucleation occurs relatively early in the induction period. The length of the induction period is therefore dependent, in part, on the ability to detect small percentages of product. Kessels et al. (2000) showed that the length of the induction period was lowered, but not eliminated when atomic force microscopy was used to detect the presence of reaction products.

The induction period is followed by a rapid replacement stage where calcite dissolves and metastable, nonideal dolomite products form (refer to Figure 1). Following the rapid replacement stage, when all reactants have been consumed, ordered, stoichiometric dolomite forms (Gaines, 1974, 1980; Katz and Matthews, 1977; Baker and Kastner, 1981; Sibley and Bartlett, 1987; Sibley et al., 1987; Morrow and Ricketts, 1988; Sibley, 1990; Nordeng and Sibley, 1993; Sibley et al., 1994; Kessels et al., 2000).

A number of factors have been shown to affect the overall rate at which dolomitization of a carbonate precursor takes place in high-temperature

experiments. These include: $Mg^{2+}:Ca^{2+}$ ratio of the dolomitizing solution, available surface area of the reactant, mineralogy of the reactant, and the presence of inhibitors or catalysts (Graf and Goldsmith, 1956; Land, 1967; Lippmann, 1973; Gaines, 1974, 1980; Katz and Matthews, 1977; Baker and Kastner, 1981; Sibley et al., 1987; Morrow and Ricketts, 1988; Sibley, 1990; Sibley et al., 1994; Kessels et al., 2000). Gaines (1974) reported that temperature, the solution $Mg^{2+}:Ca^{2+}$ ratio, and the type of reactant (calcite vs. aragonite) all have an effect on the rate of dolomitization. Land (1967), Katz and Matthews (1977), Gaines (1980), Sibley et al. (1987), Sibley (1990), and Kessels et al. (2000) showed that increasing solution $Mg^{2+}:Ca^{2+}$ ratios caused the reaction rate to increase. Gaines (1980) showed that the reaction rate increased when the $Mg^{2+}:Ca^{2+}$ was increase from 3 to 5, but decreased when the ratio was increased from 5 to 7. Sibley et al. (1987) argued that the decreasing reaction rate for $Mg^{2+}:Ca^{2+}$ ratios greater than 5 was likely due to the precipitation of magnesite.

Dolomitization rates in high-temperature experiments increase with reactant surface area (Katz and Matthews, 1977; Gaines, 1980; Sibley and Bartlett, 1987). More reactant surface area corresponds to more potential nucleation sites per unit mass of reactant. A greater reactant surface area also enhances the rate of dissolution of calcium carbonate, the source of carbonate anions for dolomite formation. Sibley and Bartlett (1987) showed that the rate of dolomitization was nearly three times faster in experiments where 1-10 μ m size calcite crystals were used as the reactant compared to experiments where 10-

40 μ m size calcite crystals were used. In their aragonite experiments, Sibley and Bartlett (1987) showed complete dolomitization took approximately 25 hours for 1-10 μ m calcite crystals and approximately 35 hours for 10-40 μ m calcite crystals.

Katz and Matthews (1977), Baker and Kastner (1981), and Sibley and Bartlett (1987) showed that aragonite is dolomitized much faster than calcite. Baker and Kastner (1981) showed that aragonite was completely converted to poorly ordered, Ca-rich dolomite in 48 hours whereas calcite experiments showed only minor amounts of nonideal dolomite after 48 hours at 200°C. Furthermore, aragonite was completely dolomitized in 112 hours, but calcite was only partially converted to nonideal dolomite after 112 hours. Sibley and Bartlett (1987) observed that aragonite was completely dolomitized in approximately 25 hours at 175°C, whereas calcite required nearly 65 hours.

Other experiments have indicated that certain additives may alter the way dolomitization takes place at high temperature. Baker and Kastner (1981) showed that dolomitization was suppressed in high-temperature experiments by the addition of sulfate. Gaines (1980) showed that the addition of 0.05 Li increased the reaction rate. Sibley (1990) observed that when N₂ and CO₂ gas were added to hydrothermal bombs, reaction rates increased. Morrow and Ricketts (1988) added HCO₃⁻ through NaHCO₃ to high-temperature experiments and recorded an increased reaction rate. Because calcite equilibrates relatively fast at high temperatures, Sibley et al. (1994) argued that it was unlikely that addition of NaCO₃ significantly increased the ion activity product of dolomitizing

solutions. Lippmann (1973) suggested that CO_3^{2-} might help dehydrate Mg^{2+} ions in solution, thus explaining the increased rate of MgCO_3 precipitation.

Sibley (1990) showed that the first products to form during dolomitization experiments exhibited a compositional dependence on the $\text{Mg}^{2+}:\text{Ca}^{2+}$ ratio in solution. When a solution $\text{Mg}^{2+}:\text{Ca}^{2+}$ ratio of 1 was used, the average composition of the initial products was approximately 60 mole% CaCO_3 . When the solution $\text{Mg}^{2+}:\text{Ca}^{2+}$ ratio was 0.66, initial products had an average composition of 65 mole% CaCO_3 . Sibley et al. (1994) also reported that solutions with higher initial $\text{Mg}^{2+}:\text{Ca}^{2+}$ ratios lead to more stoichiometric products. They reported the formation of very high magnesium calcite (VHMC, 35-40 mole% MgCO_3 with no ordering) when initial solutions had a $\text{Mg}^{2+}:\text{Ca}^{2+}$ ratio of 0.66 and nonstoichiometric dolomite (43-45 mole% MgCO_3) when initial solutions had a $\text{Mg}^{2+}:\text{Ca}^{2+}$ ratio of 1.2. Despite highly variable compositions and poor ordering in initial dolomite products, and the fact that no experiment has produced well-ordered stoichiometric (ideal) dolomite as an initial reaction product, all products tend towards well-ordered, stoichiometric (ideal) dolomite after all reactants have been consumed.

1.b. Ca-Enrichment in Natural Dolomite

Although ideal dolomite is the thermodynamically stable carbonate phase in seawater, a considerable fraction of sedimentary dolomite contains Ca in excess of the ideal 1:1 Mg:Ca ratio. The excess calcium content in natural dolomite is quite variable and can reach 9-10 mole% CaCO_3 (Graf and

Goldsmith, 1956; Füchtbauer and Goldschmidt, 1965; Lippmann, 1973; Lumsden, 1979; Lumsden and Chimahusky, 1980; Reeder, 1981, 1983; Wenk et al., 1983; Sperber et al., 1984; Gregg et al., 1992; Malone et al., 1994; Budd, 1997; Böttcher et al., 1998; Jones et al., 2001). In addition, calcium-rich dolomites exhibit a lower degree of cation order than their ideal counterparts.

Although Ca-enrichment in natural dolomite is a common phenomenon, the factors responsible for deviation from ideality are poorly understood. Goldsmith and Graf (1958) using X-ray diffraction were the first to report on the structural and compositional variations in natural Ca-rich and stoichiometric dolomites. Powder-mount and single crystal X-ray diffraction (XRD) data indicate expanded unit cell dimensions, attenuated superlattice reflections, and diffuse or bimodal basal plane reflections in Ca-rich dolomite. Dolomite diffraction peak intensities were shown to indicate differences in occupancies and scattering factors of the Ca and Mg atoms in the structurally nonequivalent A and B cation sites, respectively (Graf and Goldsmith, 1956). Therefore the occurrence of attenuated superlattice reflections suggested to Goldsmith and Graf (1958) that there was some degree of Ca-Mg disorder in the Ca-rich samples. They argued that some defect mechanism or alternate crystal structure was required in order to accommodate excess calcium. Graf et al. (1967) reported that cation substitution and/or mixed-layer disorder were necessary in order to produce the reflections reported by Goldsmith and Graf (1958). Recent refined single crystal X-ray diffraction studies have produced similar results (Reeder, 2000). Complete cation order is characteristic of most ancient

stoichiometric dolomites, whereas Ca-rich dolomite is most commonly associated with highly variable lattice parameters (Reeder, 1983; Miser et al., 1987; Reeder, 2000).

Navrotsky and Copobianco (1987) and Chai et al. (1995) studied the energetics of Ca-enrichment in natural sedimentary dolomites. Solution calorimetry experiments for a suite of sedimentary dolomites with 0-6 mole% excess calcium were used to show that enthalpies of formation increase in a near-linear manner with Ca-enrichment. This supports the widely recognized view that nonideal dolomite forms more easily than ideal dolomite because of kinetic reasons, as they are metastable and more soluble.

Although recent dolomites are characterized by being Ca-rich and having expanded unit cell dimensions, the structural description of these dolomites varies significantly from the ancient Ca-rich dolomites (Lippmann, 1973; Gregg et al., 1992; Mazzullo, 1992; Wenk et al., 1993). The XRD patterns of the recent deposits show that superlattice reflections are weak or absent. This is most likely because the Ca and Mg cations are distributed more randomly between the A and B sites. Other reflections are also broad and diffuse, which further suggests a low degree of structural order in the dolomite. Wenk et al. (1993), for example, observed a rhombohedral Ca-Mg carbonate with weak or no ordering reflections that contained approximately 30 mole% MgCO₃ in recent sediments from Abu Dhabi. In contrast, ancient nonideal dolomites, although typically calcium-rich, display a much greater degree of cation ordering than their Holocene counterparts.

Selected area electron diffraction (SAED) and transmission electron microscopy (TEM) have been used to demonstrate that Ca-rich dolomites are both structurally and compositionally heterogeneous in comparison to ideal dolomites (Barber, 1977; Reeder and Wenk, 1979; Reeder, 1981, 1983, 1992, 2000; Wenk et al., 1983; Van Tendello et al., 1985; Frisia, 1994; Schubel et al., 2000). These workers observed the occurrence of a heterogeneous microstructure in almost all pre-Holocene Ca-rich dolomites, including laminar-like structural modulations and superstructures. Modulation occurs as a regular, alternating dark/light wavy pattern in TEM images (Barber, 1977; Reeder and Wenk, 1979; Reeder, 1981, 1992, 2000; Schubel et al., 2000). Modulations can have sharp to diffuse boundaries and are observed in both brightfield and darkfield imaging (Barber, 1977; Reeder and Wenk, 1979; Reeder, 1981, 1992, 2000; Schubel et al., 2000). However, the greatest contrast occurs with the {104} reflection beam in darkfield imaging, which is concurrent with indices of the cleavage faces in dolomite (Reeder, 1981, 2000). More detailed work has shown that modulations are oriented subparallel to the growth direction and are therefore perpendicular to the dominant {104} faces (Reeder, 2000). Modulations are pervasive features throughout the dolomite crystal lattice (Reeder, 1981, 1992, 2000). Laminar-like modulations typically have wavelengths between ten and several tens of nanometers (Barber, 1977; Reeder and Wenk, 1979; Reeder, 1981, 1992, 2000; Schubel, 2000). Wenk et al. (1983) reported that although modulations were absent in some very recent nonideal dolomites, microstructures were heterogeneous.

Most ancient sedimentary dolomites with stoichiometric compositions and a high degree of cation order lack modulated microstructures and SAED superstructures (Wenk et al., 1983; Reeder, 1983, 1992). However, the most common structural defects in ideal dolomites are dislocations, which are observed in variable densities (Reeder, 1992). Although modulated microstructures have been observed in stoichiometric dolomite, the occurrence is relatively rare. Miser et al. (1987) reported on TEM observations of modulation-like features in a well-ordered, stoichiometric twinned dolomite crystal. Modulations were reported to be weaker and coarser than commonly reported for ancient calcian dolomites. Reeder (1992) reasoned that because modulations in stoichiometric dolomite are typically localized and volumetrically insignificant, the phenomenon seems to be the exception. In the only study of its kind, Rosen et al. (1989) reported observing modulations in a Mg-rich dolomite that exhibited poor ordering and a structure that was expanded in the c_0 direction and contracted in the a_0 direction relative to ideal dolomite.

SAED patterns used in conjunction with TEM imaging reveal the presence of weak and/or diffuse extra spots that coincide with small elongate domains that are seen with dark field imaging. High-resolution TEM (HRTEM) confirms that the domains have a different cation distribution from that of ideal dolomite. Modulated microstructures were therefore interpreted as strain contrasts within the crystal lattice that result from distinct chemical and/or structural domains (Barber, 1977; Reeder and Wenk, 1979; Reeder, 1981, 1992, 2000; Frisia, 1994; Schubel et al., 2000). TEM and SAED observations led a number of workers to

suggest that the relationship between stoichiometry and dolomite microstructure may be the result of distinct growth processes (Wenk et al., 1983; Reeder and Sheppard 1984; Reeder and Prosky, 1986; Miser et al, 1987). The occurrence of modulations that change orientation according to different growth sectors supports this hypothesis (*c.f.* Reeder, 2000). Fouke and Reeder (1992) reported that various levels of Ca-enrichment in dolomite were a function of surface structure and suggested that “the nature of [the] growth mechanism may be a important factor in controlling the range of Ca:Mg ratios observed in dolomite.”

1.c. Crystal Growth Mechanisms

Mononuclear, birth and spread, polynuclear, and spiral crystal growth models (Figure 2), all assume that crystal growth occurs by the addition of structural units (ions or molecules) to energetically favorable attachment sites on a crystal surface (Nielsen, 1964; Ohara and Reid, 1973). Because the rate of crystal growth is related to the crystal growth mechanism (Sunagawa, 1982, see Figure 3), crystal growth models are characterized according to differences in the rate of formation of surface nuclei versus the rate of lateral attachment to an already existing surface feature. Nucleation dependent models, like mononuclear growth, birth and spread, and polynuclear growth represent successively higher rates of nucleation relative to lateral growth. Because nucleation and crystal growth are energetically driven processes, theoretical models emphasize that different growth mechanisms dominate under different thermodynamic conditions. At conditions near equilibrium, no growth can occur

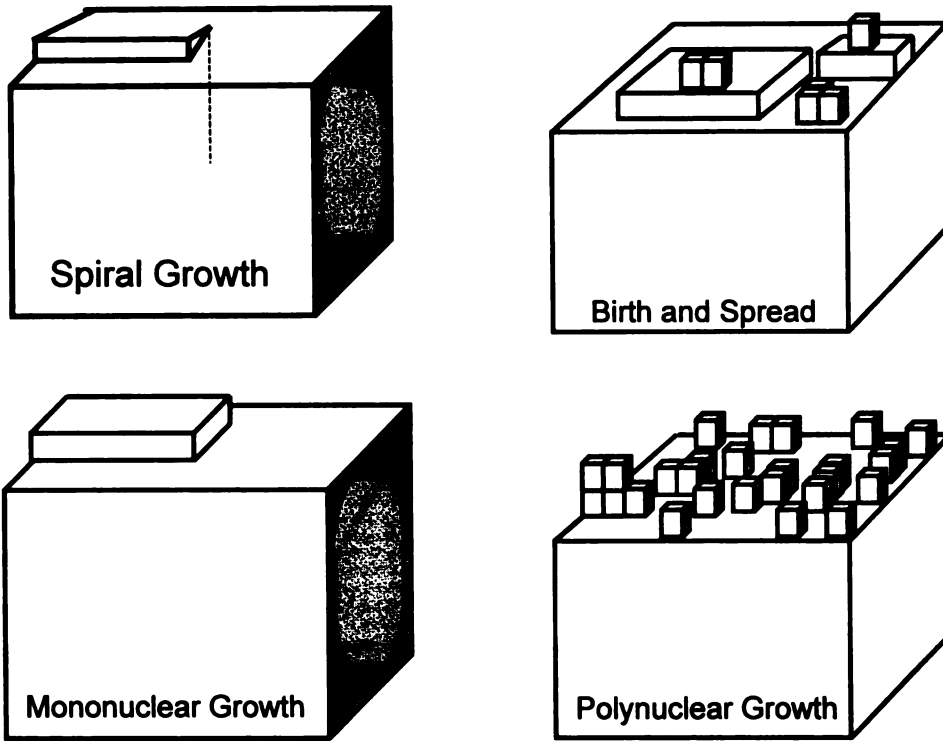


Figure 2. Surface expressions of some common crystal growth models.

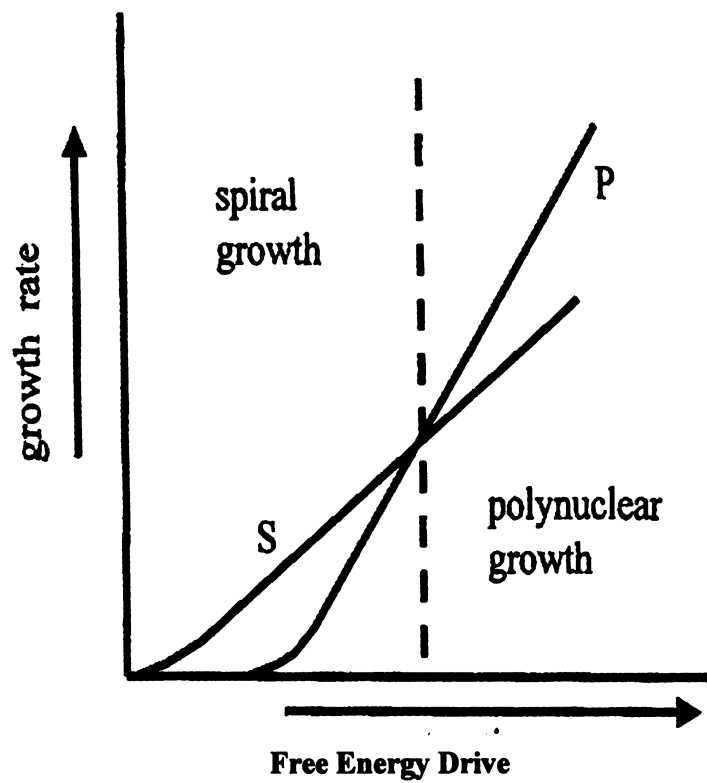


Figure 3. Diagram showing theoretical growth rates of spiral and polynuclear growth as a function of free energy (after Sunagawa, 1984).

on a crystal surface free from defects because a certain degree of supersaturation is required to form a critical nucleus. The critical nucleus is the minimum size a particle must attain to be stable in a supersaturated solution. Particles smaller than the critical nucleus dissolve back into solution. The size of the critical nucleus is directly related to the activation energy for nucleation. Nucleation on a crystal surface is difficult because there is an energy barrier associated with increasing the surface area and therefore the surface free energy of the crystal (Nielsen, 1964; Ohara and Reid, 1973; Kirkpatrick, 1981; Lasaga, 1990). Once this has occurred, however, crystal growth can proceed by attaching to the nucleus because there is not such a large increase in surface area.

Mononuclear crystal growth is characterized by the attachment of a single nucleus to a flat crystal surface followed by lateral growth along the periphery of the nucleus. Each additional growth layer requires a new nucleation event to occur. The nucleation rate is relatively slow compared to the rate of lateral growth in the mononuclear model. Because each successive growth layer requires the energetically difficult step of surface nucleation, mononuclear growth is considered to be an inefficient growth mechanism (Nielsen, 1964). At higher free energy drive, the birth and spread model is predicted by crystal growth theory. In the birth and spread model, crystal layers are generated in a manner similar to mononuclear growth, but instead of lateral growth occurring by attachment at a single nucleus per layer, growth proceeds by attachment along the periphery of multiple surface nuclei per layer. Similar to mononuclear growth, the birth and spread model is characterized by a lateral growth rate that is higher

than the nucleation rate. In conditions where the degree of supersaturation is sufficiently high, growth is predicted to occur in a manner consistent with the polynuclear growth model. Polynuclear growth proceeds as multiple nucleation events occur simultaneously on the crystal surface (Nielsen, 1964; Ohara and Reid, 1973; Sunagawa, 1984). Polynuclear growth differs from the birth and spread model in that the rate of surface nucleation is more rapid than the rate of lateral growth.

As opposed to the former models, crystal growth by a spiral mechanism does not require the energetically difficult step of surface nucleation. Instead, spiral growth takes advantage of crystalline defects, like screw dislocations, which create offsets on the crystal surface and in turn provide a continuous supply of energetically favorable growth sites (Burton et al., 1951). As a result, crystal growth can occur at conditions near equilibrium (Burton et al., 1951; Sunagawa, 1984). According to Sunagawa (1984), spiral growth is the most common crystal growth mechanism in nature.

Because different mechanisms add material to a growing crystal by distinctly different means (e.g., by lateral attachment to a spiral dislocation arm or surface nucleation), surface nanotopography is indicative of the dominant crystal growth mechanism. In fact, studies investigating crystal surface nanotopography have established a close relationship between the dominant crystal growth mechanism and the resulting expression of the crystal surface nanotopography. The most commonly observed surface nanotopographies are consistent with models that describe 1) spiral growth centered on a dislocation and 2) surface

nucleation followed by lateral growth (Sunagawa, 1984; Hochella et al., 1990; Hillner et al., 1992; Gratz et al., 1993; Hochella, 1990; Dove and Hochella, 1993; Bosbach and Rammensee, 1994; Pina et al., 1998; Bosbach et al., 1998; Maiwa et al., 1998; Kessels et al., 2000; Pina et al., 2000; Jiang et al., 2001a; Pina et al., 2004). Moreover, observations of crystal surface nanotopography are seemingly consistent with theoretical crystal growth models in that different growth mechanisms operate under the relative thermodynamic conditions for which they are predicted.

Dove and Hochella (1993) investigated *in situ* growth of calcite under varying degrees of supersaturation with scanning force microscopy (SFM) at 25°C and 0.96atm. They observed the formation of surface nuclei ~20-30nm wide and ~6-9 nanometers high in solutions with supersaturation $\Omega > 2$. At lower degrees of supersaturation, flat layers hundreds of nanometers across with 0.3 nanometer high steps were observed. Surface nuclei were reported to be rhombohedral in shape, except in experiments where orthophosphate (a growth inhibitor) was added, in which case nuclei were rounded in shape. After 10 minutes of continued growth in the solutions with orthophosphate, calcite nuclei coalesce into larger islands that were nearly 200 nm in diameter and up to 31 nm high. The overall growth surface was highly irregular and covered with rounded islands and small voids. After 1 hour of growth, Dove and Hochella (1993) observed that the calcite surface became flatter, which was interpreted as the result of coalescing islands (their Figure 3). Bosbach and Rammensee (1994) made *in situ* observations of the surfaces of gypsum with the atomic force

microscope (AFM). They observed layers with steps $>1000\mu\text{m}$ long and one to nine monolayers ($\sim 0.7\text{-}6.1\text{nm}$) high as well as a lack of surface nuclei for supersaturations less than 1.1. At higher degrees of gypsum supersaturation (>8), Bosbach et al. (1998) observed crystal growth proceeding by the formation of islands up to 300nm long, $<100\text{nm}$ wide and generally 0.7nm (1 monolayer) high. Bosbach et al. (1998) demonstrated that barite surface nanotopography was dominated by layers and spiral hillocks during crystal growth at low to moderate supersaturations ($\Omega < 5$). These features were interpreted to result from crystal growth by a spiral mechanism. At higher degrees of barite supersaturation, surface nucleation was observed to dominate during crystal growth. Island heights were equal to 0.35nm , consistent with the height of a BaSO_4 monolayer. Islands were euhedral in shape (their Figures 8, 10). After 5 minutes of growth islands spread and covered the entire surface resulting in a flat layer. With the addition of a crystal growth inhibitor (NTMP), Bosbach et al. (1996) observed that individual islands became rounded. Pina et al. (1998) demonstrated that surface nucleation and growth spirals could occur simultaneously during crystal growth in barite. Maiwa et al. (1998) observed growth islands, which were interpreted as 2-D nuclei on the surfaces of well-developed $\{111\}$ and $\{100\}$ faces of barium nitrate crystals. The islands were interpreted to form when crystals were exposed to brief periods of elevated supersaturation upon removal from the experimental solutions. The islands were circular to slightly elongated. Islands were $0.41\text{-}0.5\text{nm}$ high, consistent with the height of unit layers formed during spiral growth (their Figure 5). Upon continued

growth, nuclei coalesced with the adjacent layers formed earlier during spiral growth. Several layers of different height were observed and were interpreted as evidence for a birth and spread crystal growth mechanism. Pina et al. (2000) showed that barite growth occurred by the advancement of steps generated on screw dislocations when the degree of supersaturation was relatively low. In contrast, they observed that surface nucleation was the dominant growth mechanism at higher degrees of barite supersaturation. The degree of supersaturation was shown to be a function of the solid composition in the $(\text{Ba,Sr})\text{SO}_4$ solid solution series.

Kessels et al. (2000) reported a change in surface nanotopography on dolomite crystals when all calcite was depleted at the end of their high-temperature experiments. They observed that island nanotopography was present throughout most of the reaction, but after reactant depletion dolomite surface topography changed to broad flat layers. Round growth islands were reported to be 25 to 200nm wide and 2-50nm high. Jiang et al. (2001a) reported the occurrence of elliptical or irregular 2-D nuclei on the growth surfaces of Cadmium Mercury Thiocyanate Crystals (CMTC). The 2-D nuclei were described as having a height equal to the interplanar spacing for CMTC (0.81 nm). In a later paper, Jiang et al. (2001b) observed CMTC growth by layer advancement at low concentrations, whereas two-dimensional nuclei readily formed during experiments with relatively high degrees of supersaturation. These observations were interpreted as being consistent with the spiral and polynuclear growth models, respectively.

1.d. Chemical Etching

During the crystal growth process, surface features are continually covered as new material is deposited. As a result, growth features ultimately become part of a mineral's internal crystalline microstructure. Because solid-state diffusion is a relatively slow process, defect microstructures formed during growth are likely to remain unmodified long after the mineral initially forms (Reeder, 1992). It should therefore be possible to acquire information about the details of crystal growth by examining a mineral's microstructure. If surface material can be removed in a manner reverse to growth, it seems likely that imperfections created and utilized during growth can be detected (Sangwal, 1987a). In fact, workers were using chemical etching to detect defects in crystalline solids as early as the late 1800's (e.g., Becke, 1890). Since then, a number of workers have employed chemical etching as a means to reveal structural information concerning defects in crystalline materials (Horn, 1952; Vogel et al., 1953; Sangwal, 1987a; Brantley et al., 1986; Kirkland et al., 1999). Preferential dissolution occurs at imperfections because they are often associated with strain and increased reactivity. Because a variety of defects may occur during growth, the chemical reactivity of the crystal and the type of dissolution that occurs at the defect are highly dependent on the nature of the defect (Lasaga and Blum, 1986; Brantley et al., 1986; Sangwal, 1987a; Gratz et al., 1991).

Etch-pits, the most commonly documented dissolution feature, result from selective dissolution at the intersection of a defect and the crystal surface

(Johnston, 1962; Berner and Morse, 1974; Berner and Holdren, 1977; Berner, 1978, 1981; Lasaga and Blum, 1986; Brantley et al., 1986; Sunagawa, 1987; Pande and Vaderbade, 1990; Stipp et al., 1994). Etch pits are commonly polyhedral with a shape and orientation that is constrained by the structure of the crystalline material (Sunagawa, 1987; Blum et al., 1990). The geometry of the pit depends heavily on the nature of the lattice defect (Johnston 1962; Brantley et al., 1986, Sangwal, 1987a). In the case of dissolution at an extended line defect (e.g. screw dislocation), thermodynamic barriers to pit nucleation are overcome more easily because of the excess strain energy that is associated with a defect (Frank, 1951; Cabrera and Levine, 1956, Heimann 1982; Brantley et al, 1986; Lasaga and Blum, 1986; Sangwal, 1987a). The linear nature of a dislocation promotes continued dissolution at an angle to the crystal surface and the resulting etch pit will be deep (Joshi et al., 1970; MacInnis and Brantley, 1993). According to several reviews (e.g., Heimann, 1982; Brantley et al., 1986; Lasaga and Blum, 1986; Sangwal, 1987) the driving force for etch pit formation at dislocation outcrops is contingent on: 1) the strain energy associated with the dislocation, 2) surface free energy of the crystal, 3) impurities associated with the line defect, and 4) the degree of undersaturation of the solution.

In contrast, shallow etch pits generally form at point defects. Once pit nucleation at a point defect occurs, and the defect is eliminated, the energetic drive for dissolution in a direction normal to the crystal surface is removed (Brantley et al., 1986; Sangwal, 1987a). Most dissolution at point defects therefore takes place in the lateral direction, which results in a broad shallow pit

(perhaps only a few monolayers deep). Upon continued dissolution complete annihilation of the pit is likely (Johnston, 1962; Brantley et al., 1986; MacInnis and Brantley, 1993).

Berner and Holdren (1977) observed the formation of deep etch pits on natural feldspar crystals when etched in hydrofluoric acid (HF). They suggested that dissolution of the crystal occurred at etch pits that formed along dislocations. Lasaga and Blum (1986) used Monte Carlo simulations to model etch pit formation at dislocation outcrops. They noted that etch pit geometry was highly dependent on the degree of undersaturation, the degree of surface diffusion, and a number of other mineral-dependent parameters. Although the shape and size of etch pits in their simulations were related to the degree of undersaturation, all pits were relatively deep with relatively flat bottoms. Using TEM, Lin and Shen (1993) observed dislocations in willemite that corresponded to {0001} direction, consistent with the orientation of the observed etch pits that developed along the c-axis. The pits they observed were tens of microns in size after 120 minutes of dissolution. Etch pit density was about 10^4 - 10^5 cm⁻², which was consistent with the relatively low dislocation density observed in transmission electron microscopy (TEM) analysis. They interpreted these observations to indicate that etch pits formed primarily at dislocation outcrops.

Hillner et al. (1992) studied *in situ* calcite dissolution with AFM. They observed the formation of deep and shallow euhedral etch pits on calcite surfaces after exposure to undersaturated solutions. They interpreted the deep etch pits (40-90nm) to be dissolution at dislocations and the shallow pits (<5nm)

to be from dissolution at point defects. Gratz et al. (1991) used ex situ AFM observations to study etch pit formation in quartz crystals. Pits were relatively broad (1500nm wide, 20nm deep), but were interpreted as dissolution at dislocation outcrops. They reasoned that dissolution at point defects would not result in such deep pits (i.e. ~20nm) because the driving force for dissolution into the crystal would be eliminated after a point defect was dissolved. Using in situ AFM techniques, Liang et al. (1996) observed the dissolution surfaces of Iceland Spar calcite. They observed the formation of two distinct types of etch pits. Type 1 pits were shallow (~0.3nm, 1 atomic layer) and interpreted to form at point defects. Type 2 pits were deep (15nm, 40 atomic layers) and interpreted to indicate dissolution at dislocations. The orientation and shape of the type 2 (deep) pits were crystallographically controlled.

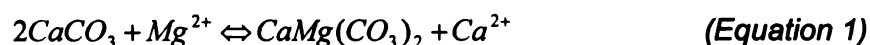
Empirical observations suggest that, although not all dislocations form deep etch-pits, there is good correlation between deep euhedral etch pits and dislocations. (Vogel et al., 1953; Gilman et al., 1958; Johnston, 1962; Patel et al., 1965; Joshi et al., 1970; Joshi and Paul, 1973; Heimann, 1975; McClay, 1977; Grandstaff, 1978; Reeder, 1982; Brantley et al., 1986; Lasaga and Blum, 1986; Sangwal, 1987a,b; Murphy, 1989; Meike, 1990a,b; Pande and Vaderbade, 1990; Blum et al., 1990; Gratz et al., 1991; Lin and Shen, 1993; MacInnis and Brantley, 1992; MacInnis and Brantley, 1993; Lin and Shen, 1995; Liang et al., 1996; Bosbach et al., 1998). An extended discussion on the energetics of etch pit formation can be found in reviews by Lasaga and Blum (1986), Brantley et al. (1986), and Sangwal (1987a).

Although less commonly observed than etch pits, etch hillocks (topographically high surface features) have also been identified as dissolution features during etching experiments (Lin and Shen, 1993; Zbik and Smart, 1998; Kirkland et al., 1999). The formation of etch hillocks has been attributed to many things, such as surface contaminations (Batterman, 1957), etch resistant point defects (Stadler, 1963), reaction products (Tuck, 1975), and gas bubbles attached to the crystal surface (Weyher and Van Enkevort, 1983). Although their interpretation is more ambiguous than etch pits, it is generally accepted that etch hillocks form due to suppressed dissolution on the crystal surface (Tuck, 1975).

2. METHODS

2.a. Dolomite Synthesis

Dolomite was synthesized according to equation 1 by combining a calcium carbonate reactant with $MgCl_2$ - $CaCl_2$ solutions in pre-weighed, Teflon-lined stainless steel reaction vessels (bombs).



All bombs initially contained 15 ml of a 1M $MgCl_2$ - $CaCl_2$ solution mixture and were heated to 218°C in a muffle furnace for various durations. Synthesis experiments started with solid reactants consisting of either 1) 0.1 g ground Iceland spar calcite (40-60µm size-fraction), or 2) a mixture of 0.05g Iceland spar calcite (40-60µm size-fraction) and 0.05g ground aragonite (12-22µm size-fraction). These experiments will be referred to herein as calcite reactant experiments and aragonite reactant experiments, respectively. Because the aragonite reactant experiments were originally designed to provide information only regarding dolomite surface nanotopography, a different size-fraction of aragonite was used than in the calcite reactant experiments. Reactant surface area was not determined for either reactant. Eight loaded reaction vessels were placed in the oven at a time and remained there for times that ranged from hours to weeks depending on the initial solution $Mg^{2+}:Ca^{2+}$ ratio. Reaction times were estimated based on findings from previous experimental work done by the

current author as well as other published high-temperature studies. Individual bombs were periodically removed from the oven and allowed to cool to room temperature. Teflon bombs were re-weighed and the contents were filtered, rinsed with distilled water, dried, and stored in a vacuum desiccator until analyses. Reaction vessels that lost more than 5% of the initial weight were not used in the analyses.

According to equation 1, the free energy drive with respect to dolomite is a function of the $\text{Ca}^{2+}:\text{Mg}^{2+}$ in solution (activity of products/activity of reactants). For the sake of simplicity, experimental solutions will be described herein by the initial $\text{Mg}^{2+}:\text{Ca}^{2+}$ ratio. This convention states that solutions with higher $\text{Mg}^{2+}:\text{Ca}^{2+}$ ratios have a higher free energy relative to solutions with lower $\text{Mg}^{2+}:\text{Ca}^{2+}$ ratios. The range of initial $\text{Mg}^{2+}:\text{Ca}^{2+}$ ratios used in the experiments (0.43, 0.50, 0.66, 0.79, 1.0, 1.14, 1.27, 1.50) were obtained by mixing different proportions of 1M $\text{CaCl}_2 \cdot 2\text{H}_2\text{O}$ and 1M $\text{MgCl}_2 \cdot 6\text{H}_2\text{O}$ solutions. Although exact $\text{Mg}^{2+}:\text{Ca}^{2+}$ activity ratios cannot be directly measured in the bombs, the assumption is made that $a\text{Mg}^{2+}:a\text{Ca}^{2+}$ ratios are directly proportional to the $\text{Mg}^{2+}:\text{Ca}^{2+}$ molar ratios in solution. Plotting the activity coefficients of calcium and magnesium using Pitzer's Equation demonstrates that the behavior of these ions in solution is similar at high ionic strengths under standard temperatures and pressures. However, there is not an accepted way to accurately extrapolate Ca^{2+} and Mg^{2+} activity coefficients for the high temperatures used in these experiments.

2.b. X-Ray Diffraction

The percent products, as well as product compositions (dolomite stoichiometry) and degree of cation order were determined by powder X-ray diffraction (XRD). X-ray diffraction analyses were conducted using $\text{CuK}\alpha$ radiation on a Rigaku Instruments Diffractometer. Powdered fluorite (CaF_2) was added as an internal standard to calibrate diffraction peak positions. Data were collected between $25\text{--}45^\circ 2\theta$ using a step size of 0.004° with a 1 second count time. Percent products provide a measure of reaction progress and were determined according to the peak-height ratio of the dolomite $d_{(104)}$ peak divided by the dolomite $d_{(104)}$ plus the calcite $d_{(104)}$ peak (Royce et al., 1971). Both tetragonal and hexagonal (i.e. three and four Miller-indices) conventions are commonly used in the literature when describing crystal planes in minerals, such as dolomite. Although both are equivalent nomenclatures, this paper will use the tetragonal system (i.e. three-Miller index) for internal consistency.

Dolomite stoichiometry was calculated according to the relative corrected position of the $d_{(104)}$ peak, consistent with the methods of Goldsmith and Graf (1958) and Lumsden and Chimahusky (1980). The 2-theta peak positions are a function of the interplanar d-spacing in carbonates. Smaller 2-theta diffraction angles correspond to larger interplanar d-spacings (measured in Angstroms). Therefore larger d-spacings indicate calcium enrichment in dolomite because larger calcium ions substitute for smaller magnesium ions. The relationship between dolomite stoichiometry and d-spacing is illustrated in equation 2 from Lumsden and Chimahusky (1980).

$$\text{Mole\% CaCO}_3 = [(333.33 \times d - \text{spacing}) - 911.99] \quad (\text{Equation 2})$$

This method assumes a linear relationship between dolomite composition and the position of the dolomite $d_{(104)}$ peak. Reeder and Sheppard (1984) argued that this could lead to inaccuracies of up to 2-3 mole% CaCO_3 , particularly at higher MgCO_3 contents. Therefore CaCO_3 mole% can vary up to 1% and 3% for Ca-rich and stoichiometric dolomites, respectively. According to Equation 2, dolomite samples with relatively small d-spacings (i.e. large 2-thetas) yield dolomite compositions enriched in magnesium. For example, a number of dolomite samples are characterized by a 31.0° 2-theta measurement, which corresponds to a d-spacing of 2.8824 Angstroms. This d-spacing corresponds to 48.8 mole% CaCO_3 according to Equation 2. Because Mg-enrichment is very rare in dolomite (Reeder, 2000) these dolomites are considered as stoichiometric. The X-ray determined $d_{(104)}$ peak position was reproducible to within 0.006° 2θ . This variation leads to an approximate compositional error of ± 0.33 mole % CaCO_3 . Because XRD measures all parameters in the bulk sample, heterogeneities in dolomite stoichiometry and degree of cation order are averaged. Furthermore, due to the resolution limits of powder X-ray diffraction, it is difficult to detect mineral phases that constitute less than approximately 5 weight% of the bulk sample. Therefore analyses reported as 100% (products or reactants) may contain impurities that are in abundances below the ~5% X-ray detection limit.

To discriminate between dolomite and calcite structures, dolomite superlattice reflections were used. Although this method is largely qualitative, the degree of cation order in the dolomite lattice is commonly reported relative to the ratio of the {015}:{110} reflection peaks (Fuchtbauer and Goldschmidt, 1965; Goldsmith and Graf, 1958). The {015} is a principle order reflection that is less pronounced for Ca-rich dolomites compared to ideal dolomites. The {110} is not a dolomite ordering reflection so it serves as a reference for changes in order intensity (Goldsmith and Graf, 1958). As a result, higher {015}:{110} ratios indicate a higher degree of cation order in dolomite.

Thirty natural dolomite samples analyzed in this study range from Ordovician to recent in age (Table 1). Compositions and degree of cation order were determined according to the same procedures for high-temperature synthetic dolomites. The natural dolomite samples represent a wide range of geographic locations, ages, and inferred formation conditions.

Sample ID	Age	Formation/ Group	2- theta	Mole% CaCO3	S/NS	Ordering	Pits/Islands
MH-2	Perm.	Hueco	31.00	50.00	S	1.13	pits
MH-6	Perm.	Hueco	31.034	50.00	S	1.08	pits
MH-10	Perm.	Hueco	31.022	50.00	S	1.08	pits
MH-11	Perm.	Hueco	31.026	50.00	S	1.07	pits
MH-20	Perm.	Hueco	31.034	50.00	S	1.11	pits
MH-52	Perm.	Hueco	31.038	50.00	S	1.22	pits
SAL 7-5	Ord.	Saluda	30.842	53.73	NS	0.82	islands
SAL 7-11	Ord.	Saluda	30.87	52.75	NS	0.67	islands
7-9-99-3	Ord.	Saluda	30.858	53.23	NS	0.54	islands
SB 42	Plio.	Seroe Domi, Bonaire	30.91	51.50	NS	0.60	islands
SC 10D	Plio.	Seroe Domi, Bonaire	30.872	52.75	NS	0.57	islands
SB 35	Plio.	Seroe Domi, Bonaire	30.878	52.67	NS	0.73	islands
RR 17	Ord.	Prarie DuChen	31	50.00	S	0.96	pits
RR 19	Ord.	Prarie DuChen	31.006	50.00	S	1.00	pits
PdC 1	Ord.	Prarie DuChen	31.046	50.00	S	1.33	pits
L2 91	Ord.	Prarie DuChen	31.034	50.00	S	0.97	pits
80-8-TS	Plio.	Seroe Domi, Aruba	30.85	53.37	NS	0.67	islands
80-8-17-1	Plio.	Seroe Domi, Aruba	30.85	53.37	NS	0.48	islands
Aruba Dol	Plio.	Seroe Domi, Aruba	30.846	53.43	NS	0.46	islands
8-9-84-5	Mio.	Spain	31	50.00	S	0.44	islands
8-9-84-3	Mio.	Spain	31.002	50.00	S	0.62	islands
13-4	Ord.	Galena	31.06	50.00	S	1.14	pits
16-8	Ord.	Galena	31.034	50.00	S	1.04	pits
S-1	Silur.	Lockport	31.034	50.00	S	1.07	pits
8-23-86-7	Silur.	Lockport	31.042	50.00	S	1.04	pits
DC37	Miss.	Burlington Keokuk	30.92	51.33	NS	0.68	islands
Niagara	Silur.	Niagara	31.046	48.80	S	1.00	pits
GWP287 120-130	Holo.	Abu Dhabi	31.022	50.00	S	0.67	islands
FC 2C	Miss.	Kentucky	30.878	52.67	NS	1.17	islands
7-22-02-3	Plio.	Bonaire	30.886	52.33	NS	0.56	islands

Table 1. Natural dolomite sample list and data table.

2.c. Atomic Force Microscopy

Atomic force microscopy was used to observe nanometer-scale features on the surfaces of natural and synthetic dolomite crystals. Flat-sided dolomite crystals were chosen with a binocular microscope for AFM analyses. Individual crystals as well as clusters of dolomite crystals were mounted on magnetic AFM disks using water-insoluble EM adhesive tabs. Synthetic dolomite crystal surfaces are assumed to correspond to the dominant {104} growth face because only the dominant rhombohedral form was observed. Natural dolomites were cleaved and ultrasonically cleaned in distilled water prior to analysis. All cleaved crystal surfaces are assumed to correspond to the dominant {104} cleavage plane.

The atomic force microscope is capable of resolving atomic-scale surface structures in air, under vacuum, and in liquids (Ohnesorge and Binnig, 1993). The AFM images surface features by measuring the changes between a rastered sample and a cantilever spring with a fine tip. The cantilever, which remains in constant contact with the sample, moves in the Z-direction as the surface topography changes. Cantilever movements are imaged by a laser-beam that is deflected onto a photodiode. In areas where the sample surface is relatively high the cantilever is deflected more, thus an increase in topography is recorded by the laser onto the photodiode. The entire system is linked in a feedback loop that keeps the cantilever in constant contact with the rastered sample.

AFM analyses were performed on a Digital Instruments Nanoscope III using constant force mode. Assuming the manufacture's reported spring

constant of 0.06, the average applied force for the crystal surfaces was 1-5nN. According to empirically determined force calibration procedures an actual average applied force of 5-20nN was more reasonable. Although the force between the sample and the cantilever was minimized as best as possible, cantilever-surface interaction in this force range can potentially alter crystal surface features (Kessels et al., 2000). Artifacts caused by cantilever-surface interaction were not observed in any of the analyses. Moreover, no change in dolomite surface nanotopography was observed for AFM scans of a single surface that lasted over 20 minutes. Typical scan durations were between 30 seconds and 2 minutes depending on the scanning frequency. Image artifacts may also arise during imaging due to irregularly shaped cantilevers, as well as irregular cantilever movement across the crystal surface. Artifacts were detected by sample rotation and/or changing cantilevers. All images reported in this study were reproduced and replicated on more than one crystal per sample using multiple cantilevers.

AFM images were acquired under atmospheric conditions using silicon nitride cantilevers (NP-20) with an average tip radius (reported as radius of curvature, ROC) of 20 nm. According to the manufacturer (Veeco Probes), 1 in 10 NP-20 tips have an average ROC of 5nm. Many times during the image collection process, numerous tips were discarded because of poor performance before images were collected with a tip that provided better resolution. Eggleston (1994) showed that the height and spacing of AFM resolvable steps could be calculated by using the following formula:

$$R = \frac{(H^2 + D^2)}{2D} \quad (\text{Equation 3})$$

where, R is the radius of the cantilever tip, H is the height of a step, and D is the distance between steps. This tip radius thus allows for near atomic-scale resolution. Sometimes cantilever tips may contain irregularities or imperfections that project outward from the tip that make the effective tip area in contact with the surface even smaller. This can further enhance the resolving power of the AFM.

The figures presented in this paper represent the highest-quality images of the type of surface feature, which it is intended to illustrate. Although all results were confirmed by observing numerous samples, changing AFM tips, as well as observing multiple areas on any one crystal, the features reported may not always represent the entire crystal. As a result, size ranges for the described surface features are reported. Determination of average sizes for the various surface features was not attempted here because it is impossible to demonstrate that the images are representative of the entire sample.

Some natural and synthetic dolomite crystals were etched prior to AFM analyses. Individual dolomite crystals were chemically etched in 0.5% H₂SO₄ solutions (Johnson, 1962) between 10-120 seconds at room temperature. Samples were then rinsed in distilled water and dried in a vacuum desiccator. Caution must be used during chemical etching experiments because dissolution features may reflect the chemistry of the etchant (Keith and Gilman, 1960; Johnson, 1962) as well as the mechanism of dissolution (Berner, 1981; Pande

and Vadrabade, 1990; Morse and Arvidson, 2002). Etched surface topography has been shown to be especially dependent on the rate of dissolution (Berner and Morse, 1974; Berner, 1978). Slow interface controlled dissolution that occurs near equilibrium, produces crystallographically controlled surface features, such as etch pits and etch hillocks, (Lasaga and Blum, 1986), whereas rapid dissolution may completely annihilate evidence of microstructure and leave the crystal with smooth faces and rounded corners (Berner and Morse, 1974; Berner, 1978; Sangwal, 1987). Folk et al. (1985) suggested that etching could provide a way to reverse the crystal growth process. The purpose of using chemical etching in this study is to accentuate crystalline microstructures that formed during crystal growth. Therefore, the methods used here are used to minimize artifacts caused by the etching process. The consistency of our results suggests that the features observed here are in fact real features rather than artifacts of etching procedures.

2.d. *Scanning Electron Microscopy*

Following AFM analysis, sample disks were adhered to conductive scanning electron microscopy (SEM) stubs using double-sided carbon tape and made electrically conductive with a 10-30nm gold coating. Some of the samples also contained calcite and aragonite so each crystal was analyzed using SEM Energy Dispersive Spectroscopy (EDS) following AFM analysis. Because most samples only contain one dolomite phase (as identified by XRD), the presence of magnesium peaks above background levels in EDS spectra were used to confirm

the presence of dolomite. SEM-EDS analyses were performed at 25kV on the JEOL JSM-6400V scanning electron microscope. Other synthetic and natural dolomite samples were prepared with a 2nm osmium coating and analyzed using the JEOL 6300 field emission SEM (FESEM). Operating conditions were 8mm working distance with an acceleration voltage of 10kV. All microscopic and EDS analyses were performed at the Michigan State University Center for Advanced Microscopy (MSU-CAM).

2.e. Crystal Size Distributions

Crystal size distributions (CSD) were determined for dolomites synthesized according to the procedures described above. The only difference being that CSD dolomite experiments used different size solid reactants. Some CSD experiments used reagent grade calcium carbonate with a solution $Mg^{2+}:Ca^{2+}$ ratio = 0.66 and others used Iceland Spar Calcite (140-160micron) with a solution $Mg^{2+}:Ca^{2+}$ = 1.0. Following sample preparation protocol, dolomite products were mounted on conductive SEM stubs with double-sided conductive carbon tape. CSD were then determined by measuring the long axis of flat dolomite rhombohedra along a linear traverse using scanning electron microscope images. Between 140 and 502 crystals were measured for each sample. Measuring protocol required dolomite rhombs to lay relatively flat on SEM mounts and have at least three well-formed corners to be eligible for CSD analysis.

3. RESULTS

3.a. Synthetic Dolomite Reaction

High-temperature dolomite synthesis experiments are characterized by a relatively long induction period in which no dolomite is detected for some time after the onset of experimental conditions. Once initial products begin to form, however, the carbonate precursor is rapidly replaced by poorly ordered nonideal dolomite. During the dolomite growth period, rapid replacement by products occurs at an increasing rate. As reactants become depleted, the reaction rate slows as the reaction approaches 100% dolomite. Near the point in which initial reactants are completely consumed (i.e., reactant depletion), ideal dolomite starts to form at the expense of nonideal dolomite. The overall dolomitization reaction creates a sigmoidal-shaped reaction curve (refer to Figure 1), characterized by an initial growth period that is relatively short compared to the induction period. After reactant depletion, all products are generally ordered stoichiometric dolomite.

Results from the dolomite synthesis experiments with calcite as the reactant are recorded in Table 2a. Aragonite synthesis experiment data are recorded in Table 2b.

Table 2a. Experimental results for high-temperature calcite experiments.

Solution Mg:Ca	Sample ID	Time (hrs.)	% Prod.	Mole% CaCO₃	2-theta	Ordering Ratio
0.43	6-17-04-D	594	0			
0.43	6-17-04-E	762	3	61.07	30.600	0.00
0.43	6-17-04-F	930	12	61.00	30.606	0.00
0.43	6-17-04-G	1122	66	61.07	30.600	
0.43	6-17-04-H	1362	31	61.07	30.600	0.00
0.5	4-9-04-A	219.5	6	60.33	30.618	0.00
0.5	4-9-04-B	259.75	6	60.67	30.612	0.00
0.5	4-9-04-D	315	17	60.33	30.618	0.00
0.66	4-8-05-A	60	0			0.00
0.66	4-8-05-B	61	30	59.93	30.640	0.00
0.66	4-8-05-C	62	11	60.13	30.630	0.00
0.66	4-8-05-D	63	3	60.13	30.630	0.00
0.66	4-8-05-E	63	0			0.00
0.66	4-8-05-F	64	55	59.53	30.650	0.10
0.66	4-8-05-G	65	51	60.07	30.634	0.08
0.66	4-8-05-H	66	32	60.00	30.638	0.00
0.66	8-23-04-A	96	54	60.13	30.630	0.00
0.66	8-23-04-B	100	36	60.13	30.630	0.00
0.66	8-23-04-D	145	69	60.00	30.638	0.09
0.66	8-23-04-E	168	88	59.67	30.646	0.27
0.66	8-23-04-F	194	96	59.53	30.650	0.36
0.66	8-23-04-G	217	100	50.00	30.970	0.70
0.66	8-23-04-H	241	100	59.53	30.650	0.45
0.66	10-3-04-A	288	100	50.00	31.000	0.65
0.66	10-3-04-B	309	100	50.00	31.000	0.77
0.66	10-3-04-C	334	100	50.00	31.000	0.73
0.66	10-3-04-D	356	100	50.00	31.000	0.88
0.79	4-15-05-B	46	0			
0.79	4-15-05-C	48	1	58.27	30.690	0.00
0.79	4-15-05-D	49	8	59.28	30.658	0.00
0.79	4-15-05-E	56	14	58.90	30.670	0.00
0.79	4-15-05-F	58	68	58.40	30.686	0.21
0.79	4-15-05-G	59	56	58.50	30.682	0.13
0.79	4-15-05-H	61	50	58.78	30.674	0.10
0.79	10-20-04-A	64	62	58.50	30.682	0.00
0.79	10-20-04-B	65	47	58.50	30.682	0.00
0.79	10-20-04-C	65	51	58.67	30.678	0.00
0.79	10-20-04-D	65	30	59.00	30.660	0.00
0.79	10-20-04-E	66	86	58.50	30.682	0.17
0.79	10-20-04-F	66	90	59.00	30.666	0.20
0.79	10-20-04-G	66	81	59.17	30.662	0.14
0.79	10-20-04-H	66	43	58.50	30.682	0.00
0.79	10-20-04-I	79	100	50.00	31.000	0.80

Solution Mg:Ca	Sample ID	Time (hrs.)	% Prod.	Mole% CaCO₃	2-theta	Ordering Ratio
1.0	10-18-04-C	33	0			
1.0	10-18-04-D	38	15	56.17	30.760	0.00
1.0	10-18-04-E	39	71	55.83	30.770	0.10
1.0	10-18-04-F	39	70	55.83	30.770	0.11
1.0	10-18-04-G	40	95	56.17	30.760	0.17
1.0	10-18-04-H	40	8	55.33	30.790	0.00
1.0	9-14-04-A	160	100	50.00	30.998	0.48
1.0	9-14-04-B	168	100	50.00	31.000	0.50
1.0	9-14-04-C	184	100	50.00	31.000	0.51
1.0	9-14-04-D	192	100	50.00	31.000	0.72
1.0	9-14-04-E	211	100	50.00	31.000	0.77
1.0	9-14-04-F	306	100	50.00	31.000	0.76
1.0	9-14-04G	336	100	50.00	31.000	0.76
1.0	9-14-04-H	361	100	50.00	31.000	0.82
1.14	4-12-05-A	30.5	0			0.00
1.14	4-12-05-B	31.5	0			0.00
1.14	4-12-05-C	32.5	0			0.00
1.14	4-12-05-D	33	3	53.23	30.858	0.00
1.14	4-12-05-E	33.5	0			0.00
1.14	4-12-05-F	34	4	53.97	30.830	0.00
1.14	4-12-05-G	34.5	76	54.73	30.806	0.25
1.14	4-12-05-H	49	99	54.13	30.826	0.36
1.14	10-13-04-E	35	47	53.63	30.838	0.00
1.14	10-13-04-F	37	75	53.67	30.840	0.10
1.14	10-13-04-G	38	79	53.73	30.842	0.11
1.14	10-13-04-H	41.5	47	54.17	30.822	0.00
1.27	4-6-05-A	29	0			0.00
1.27	4-6-05-B	29.5	15	52.33	30.886	0.00
1.27	4-6-05-C	30	44	52.33	30.886	0.00
1.27	4-6-05-D	30.25	68	52.75	30.870	0.22
1.27	4-6-05-E	31.25	98	51.83	30.900	0.20
1.27	4-6-05-F	32	32	52.67	30.878	0.00
1.27	4-6-05-G	48	100	51.13	30.926	0.33
1.27	4-6-05-H	53	95	53.77	30.846	0.30
1.27	10-5-04-E	30	6	52.00	30.894	0.00
1.27	10-5-04-F	31	67	52.00	30.894	0.09
1.27	10-5-04-G	32	85	52.33	30.888	0.14
1.27	10-5-04-H	33	17	51.67	30.906	0.00
1.27	9-28-04-A	38.5	97	52.00	30.894	0.30
1.27	9-28-04-B	40	94	52.67	30.876	0.18
1.27	9-28-04-C	40	96	52.33	30.886	0.25
1.27	9-28-04-D	45	96	52.67	30.878	0.23
1.27	9-28-04-E	48	99	51.33	30.922	0.39
1.27	9-28-04-F	62	100	50.00	30.986	0.54
1.27	9-28-04-G	117	100	50.00	31.000	0.69

Solution Mg:Ca	Sample ID	Time (hrs.)	% Prod.	Mole% CaCO₃	2-theta	Ordering Ratio
1.5	8-17-04-C	28.25	0			
1.5	9-4-04-A	28	14	50.00	31.000	0.00
1.5	9-4-04-B	28	11	50.00	31.000	0.00
1.5	9-4-04-C	30	14	50.00	31.000	0.00
1.5	9-4-04-D	32	9	50.00	30.986	0.00
1.5	9-4-04-E	33	16	50.00	30.958	0.00
1.5	9-4-04-F	34	65	50.00	30.962	0.08
1.5	9-4-04-G	35	100	50.00	31.000	0.40
1.5	9-4-04-H	36	93	51.33	30.918	0.31
1.5	8-17-04-D	39	55	50.00	31.000	0.00
1.5	8-13-04-A	77.5	100	50.00	31.000	0.42
1.5	8-13-04-B	91	100	50.00	31.000	0.39
1.5	8-13-04-C	91	100	50.00	31.000	0.37
1.5	8-13-04-D	115	100	50.00	31.000	0.55
1.5	8-13-04-E	149	100	50.00	31.000	0.59
1.5	8-13-04-F	236	100	50.00	31.000	0.65
1.5	8-13-04-G	236	100	50.00	31.000	0.67

Table 2b. Experimental results for high-temperature aragonite experiments.

Mg:Ca	Sample ID	Time (hrs)	% Prod.	Mole %CaCO₃	2-theta	Ordering Ratio
1.0	4-5-05-A	1.5	0			0.00
1.0	4-5-05-B	2.25	0			0.00
1.0	4-5-05-C	3.25	20	59.83	30.642	0.00
1.0	4-5-05-D	3.75	50	61.00	30.606	0.00
1.0	4-5-05-E	4.5	80	58.33	30.686	0.00
1.0	4-5-05-F	5.5	90	57.17	30.726	0.00
1.0	4-5-05-G	6.5	90	56.83	30.738	0.10
1.0	4-5-05-H	8	100	57.00	30.734	0.10
1.0	3-31-05-A	14	100	52.50	30.882	0.16
1.0	3-31-05-B	16	100	51.33	30.922	0.22
1.0	3-31-05-C	17.3	100	50.00	30.974	0.25
1.0	3-31-05-D	18.5	100	50.00	30.950	0.20
1.0	3-31-05-E	20	100	50.00	30.950	0.22
1.0	3-30-05-A	22	100	50.00	30.930	0.35
1.0	3-30-05-B	24	100	50.00	30.930	0.25
1.0	3-30-05-C	25	100	50.00	30.978	0.30
1.0	3-30-05-D	27	100	50.00	30.974	0.32
1.0	3-30-05-E	30	100	50.23	30.954	0.20
1.0	3-30-05-F	32	100	50.00	31.000	0.26
1.0	3-30-05-G	34	100	50.00	30.998	0.35
1.0	3-30-05-H	46	100	50.00	30.974	0.39

Table 2a. Experimental results for high-temperature calcite experiments. **2b.** Experimental results for high-temperature aragonite experiments.

3.b. Calcite Reactant Experiments

3.b.1. Reaction Rate: Figures 4-11 are plots of time after onset of experimental conditions versus the percent product (dolomite) for each solution $\text{Mg}^{2+}:\text{Ca}^{2+}$ ratios studied here (0.43, 0.50, 0.66, 0.79, 1.0, 1.14, 1.27, 1.50, respectively). The plots represent reaction curves for the individual calcite reactant experiments. Each point represents the analyzed contents from an individual reaction vessel. There is considerable scatter in the data that cannot be explained by error in laboratory techniques. Because some reaction vessels within a single experiment form dolomite faster than others, it appears as though percent product decreases with time. In addition, some plots are incomplete because certain reactions did not progress until complete depletion of reactants. This generally results from extremely long reaction times required by solutions with relatively low $\text{Mg}^{2+}:\text{Ca}^{2+}$ ratios (e.g. $\text{Mg}^{2+}:\text{Ca}^{2+} < 0.66$). As discussed in the introduction, many factors are responsible for variations in the rate of dolomitization in high-temperature experiments. Even in these seemingly well-controlled experiments there are still factors that can affect the system that have not been accounted for. Sibley (1990) suggested that discrepancies in high-temperature dolomitization experiments could be attributed to an inadequately controlled variable that led to variation in nucleation and/or growth rates. Because some of the more complete and well-constrained data sets presented here and in other high-temperature dolomitization studies are very consistent, generalizations have been made regarding the reaction curves for some of the experiments with more scatter.

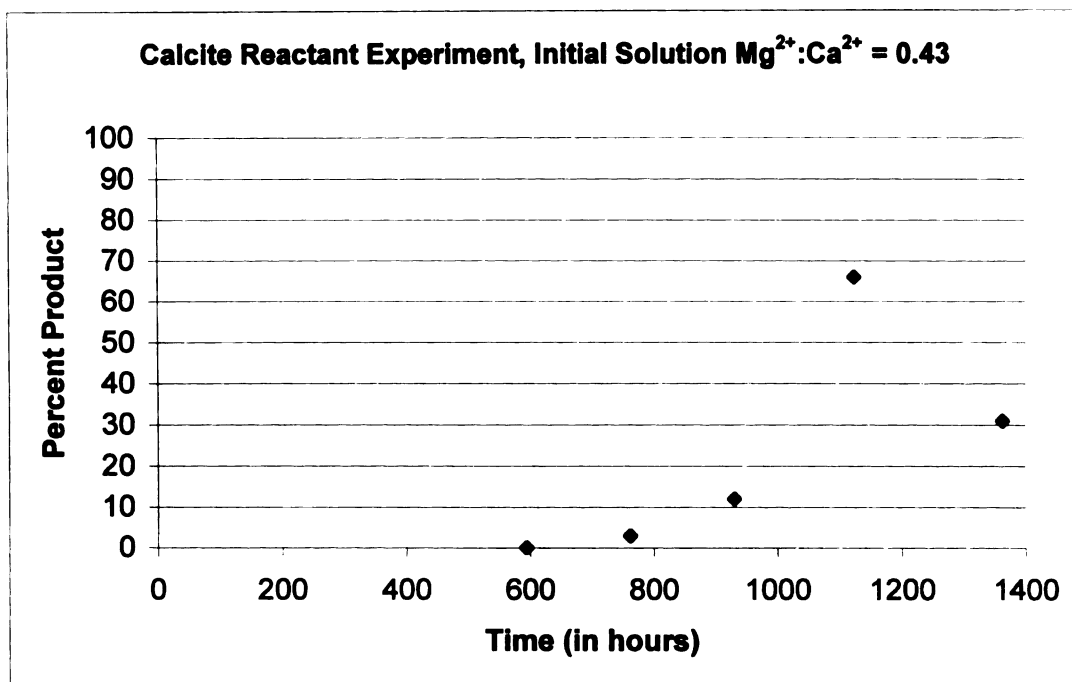


Figure 4. Percent product vs. time for calcite reactant experiment with initial solution $Mg^{2+}:Ca^{2+} = 0.429$.

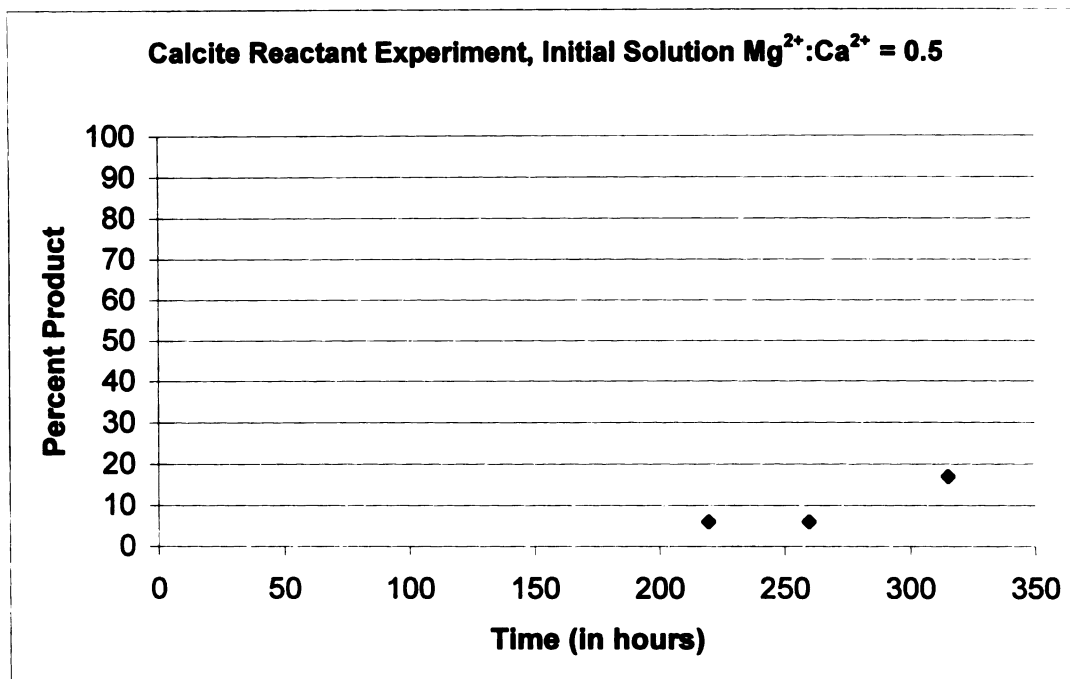


Figure 5. Percent product vs. time for calcite reactant experiment with initial solution $Mg^{2+}:Ca^{2+} = 0.50$.

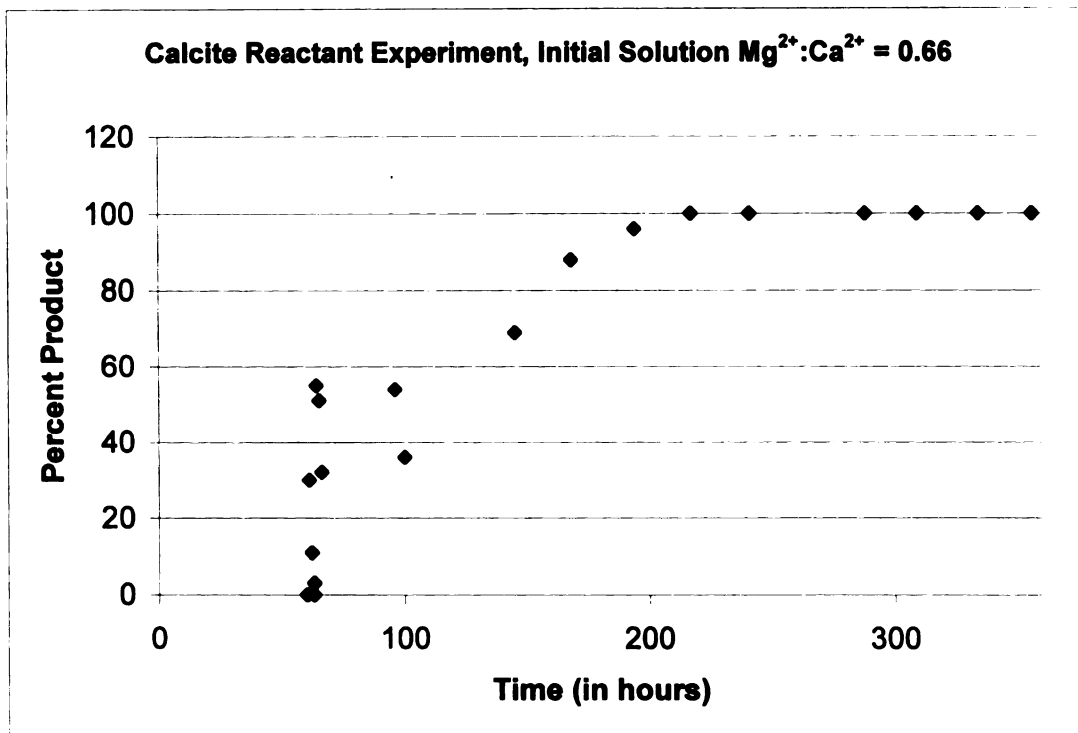


Figure 6. Percent product vs. time for calcite reactant experiment with initial solution $Mg^{2+}:Ca^{2+} = 0.66$.

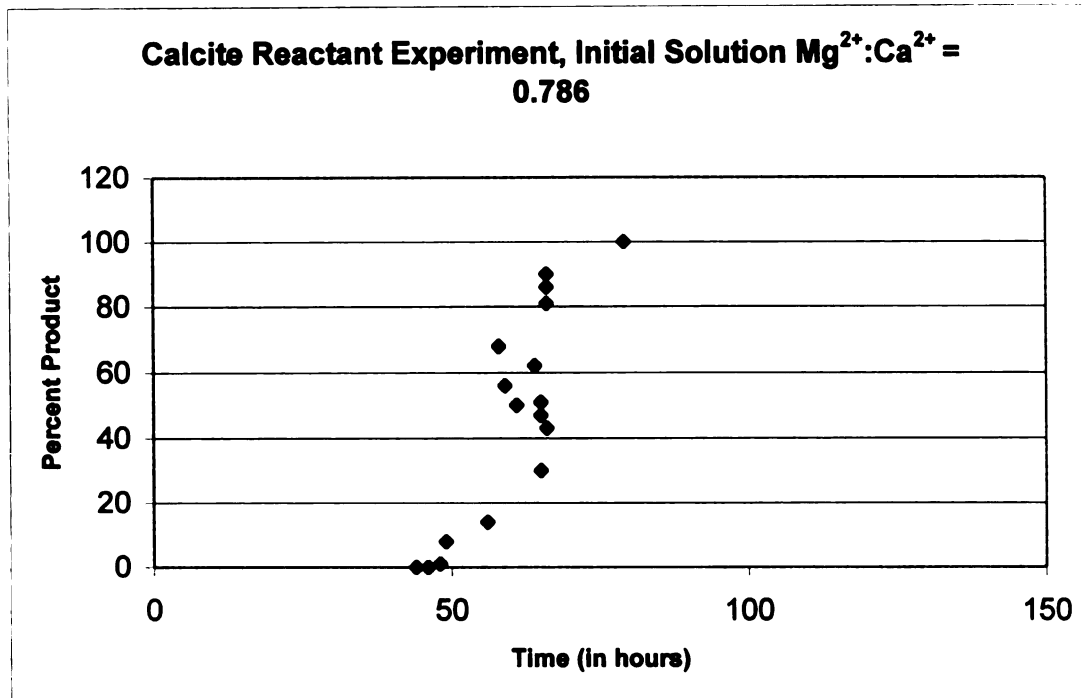


Figure 7. Percent product vs. time for calcite reactant experiment with initial solution $Mg^{2+}:Ca^{2+} = 0.786$.

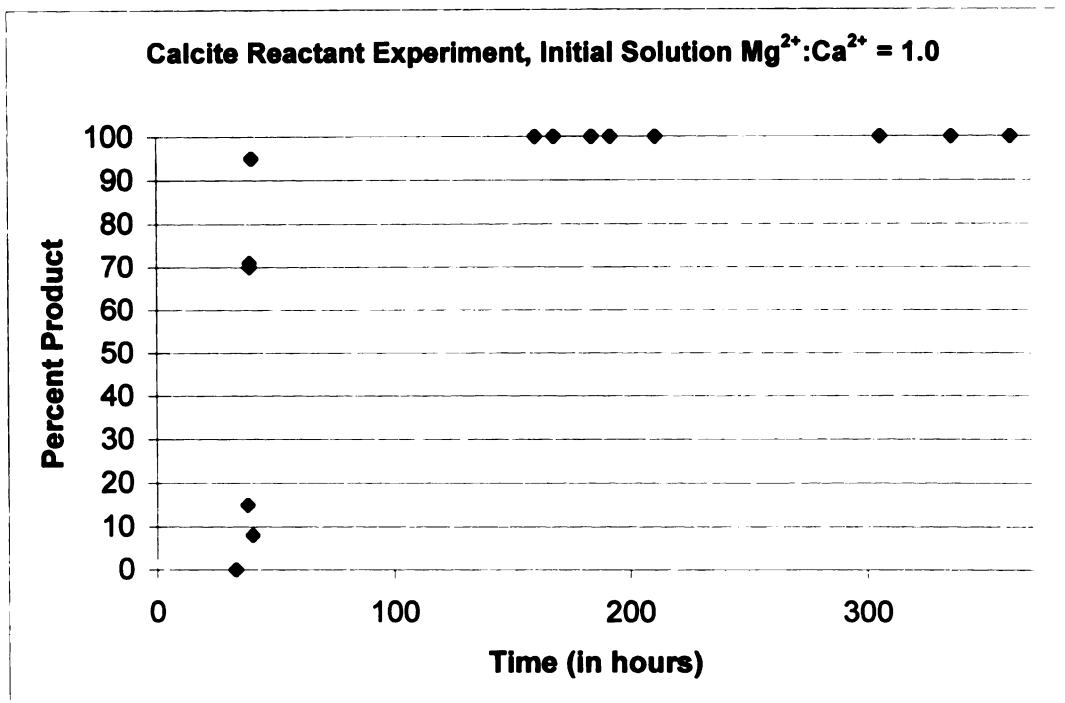


Figure 8. Percent product vs. time for calcite reactant experiment with initial solution $Mg^{2+}:Ca^{2+} = 1.0$.

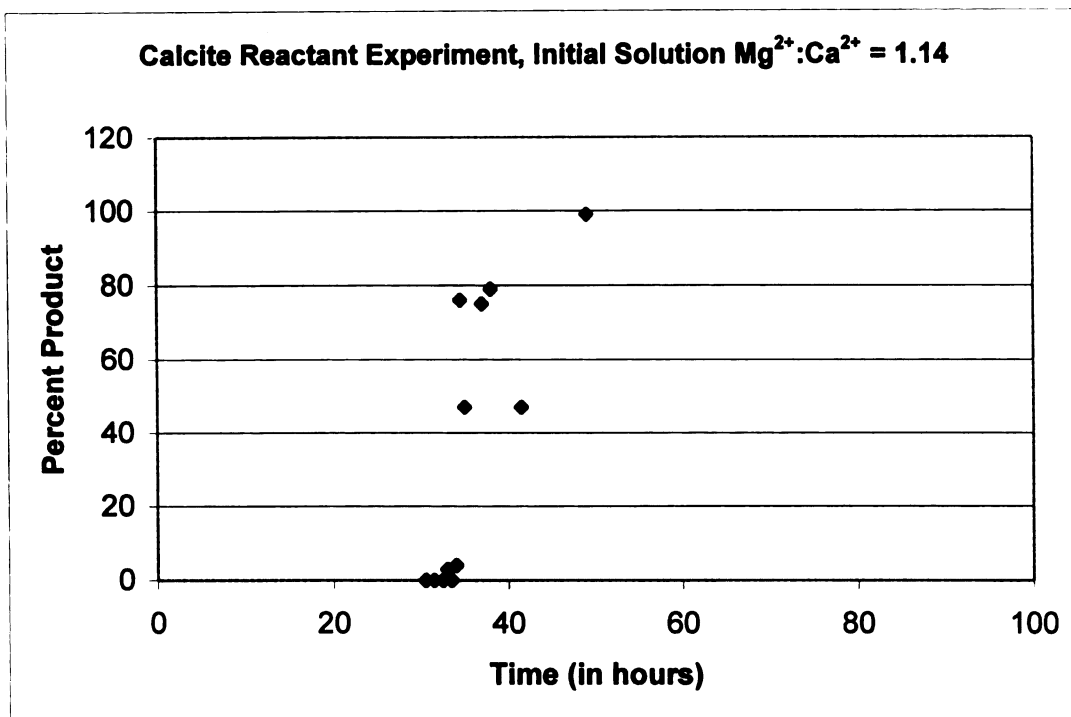


Figure 9. Percent product vs. time for calcite reactant experiment with initial solution $Mg^{2+}:Ca^{2+} = 1.14$.

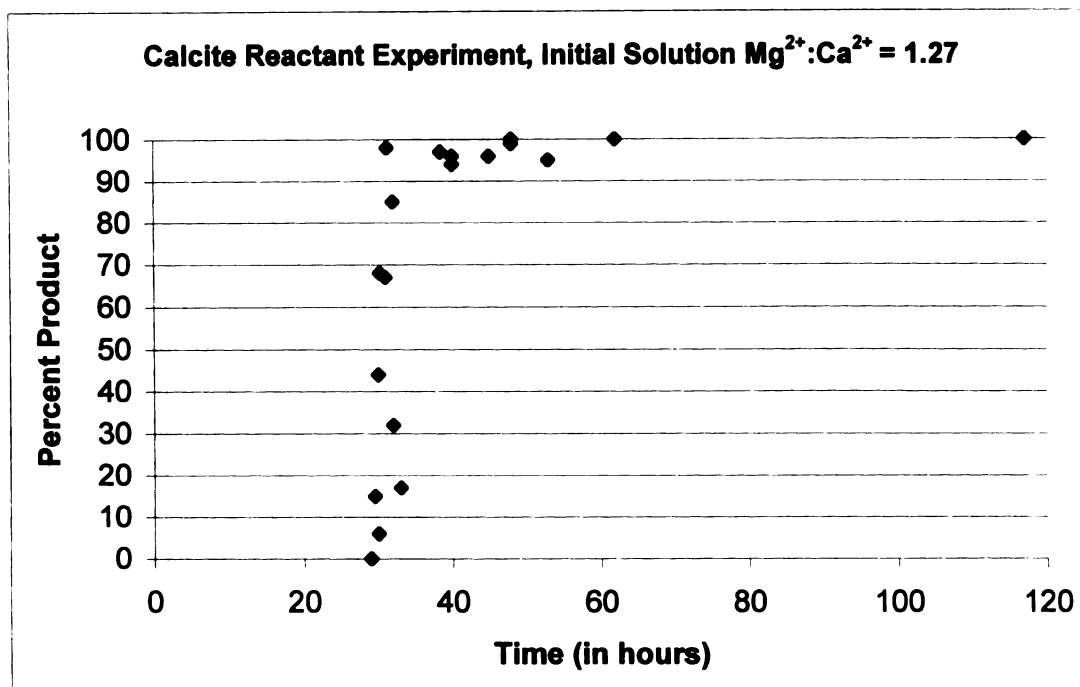


Figure 10. Percent product vs. time for calcite reactant experiment with initial solution $Mg^{2+}:Ca^{2+} = 1.27$.

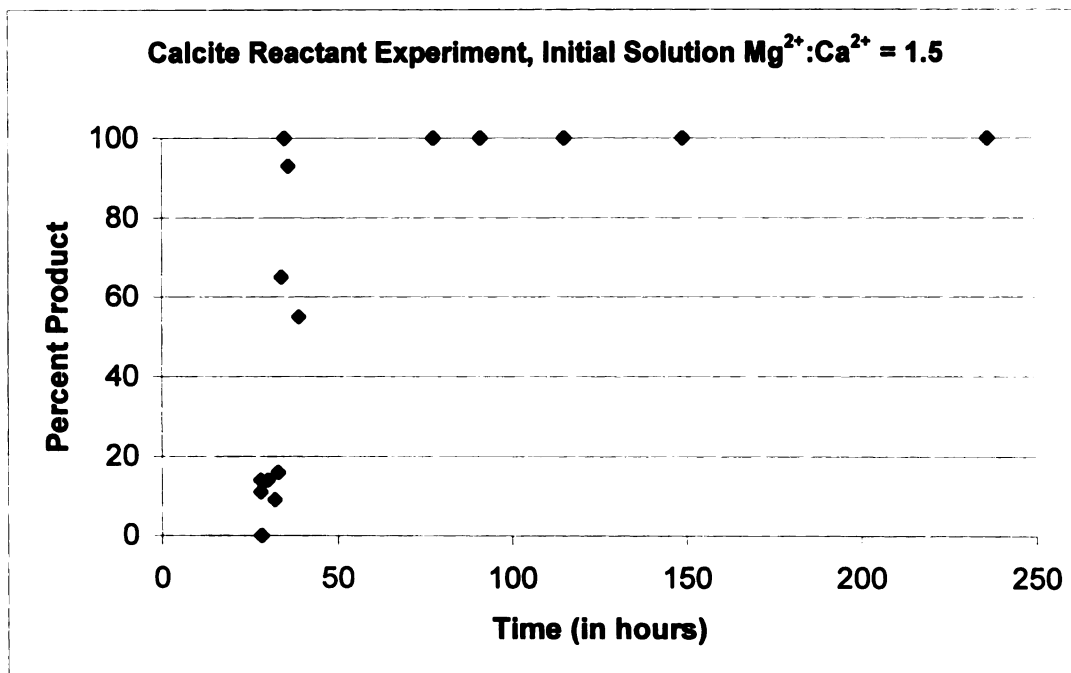


Figure 11. Percent product vs. time for calcite reactant experiment with initial solution $Mg^{2+}:Ca^{2+} = 1.5$.

One measure of reaction rate for an individual experiment is the length of the induction period. As illustrated in the reaction curves, the dolomitization rate is highest for experiments with relatively high solution $\text{Mg}^{2+}:\text{Ca}^{2+}$ ratios and lowest in experiments with relatively low solution $\text{Mg}^{2+}:\text{Ca}^{2+}$ ratios. Figure 12a plots length of the induction period (on a semi-log-scale) as a function of solution $\text{Mg}^{2+}:\text{Ca}^{2+}$ ratio. Induction period results for calcite reactant experiments are recorded in Table 3. Induction period data is also plotted on a linear scale in Figure 12b. The shortest induction period in the calcite experiments was approximately 28 hours, which was recorded for the experiment with an initial solution $\text{Mg}^{2+}:\text{Ca}^{2+} = 1.5$. Conversely, the longest induction period of 762 hours was recorded in the experiment with an initial solution $\text{Mg}^{2+}:\text{Ca}^{2+} = 0.43$. The relationship between the induction period and $\text{Mg}^{2+}:\text{Ca}^{2+}$ ratio in solution is not linear. When plotted on linear axes, the data are characterized by a curve that becomes nearly asymptotic to the axes of the plot at low and high solution $\text{Mg}^{2+}:\text{Ca}^{2+}$ ratios (Figure 12b). For solutions with $\text{Mg}^{2+}:\text{Ca}^{2+} \geq 1.0$, the length of the induction period is shortened only slightly with increasing $\text{Mg}^{2+}:\text{Ca}^{2+}$ ratios in solution. Conversely, for solutions with $\text{Mg}^{2+}:\text{Ca}^{2+} < 1.0$ the induction period is lengthened significantly by decreasing the solution $\text{Mg}^{2+}:\text{Ca}^{2+}$ ratio. For example, changing the solution $\text{Mg}^{2+}:\text{Ca}^{2+}$ ratio from 1.0 to 1.50 shortened the induction period from 35 hours to 28 hours, whereas changing the solution $\text{Mg}^{2+}:\text{Ca}^{2+}$ ratio from 0.43 to 0.50 reduced the induction period from approximately 762 hours to 220 hours.

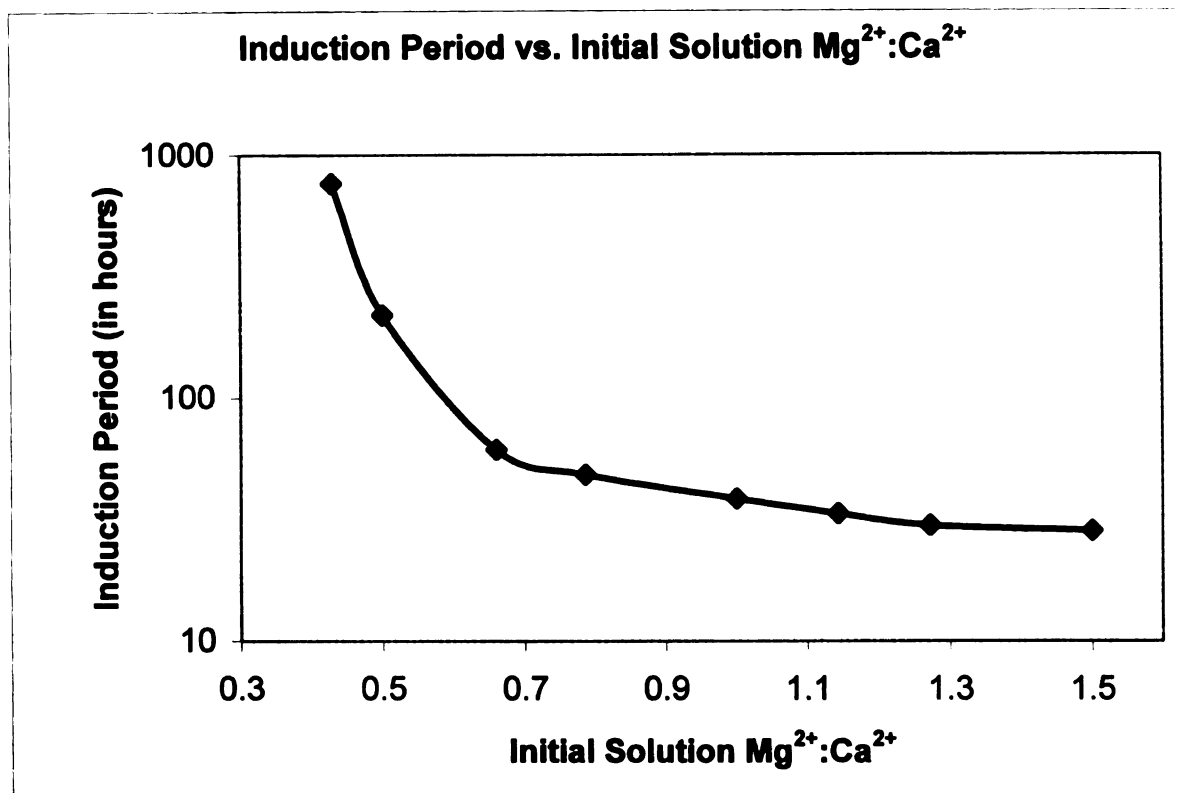


Figure 12a. Induction period (log-scale) vs. initial solution Mg²⁺:Ca²⁺ for calcite reactant experiments.

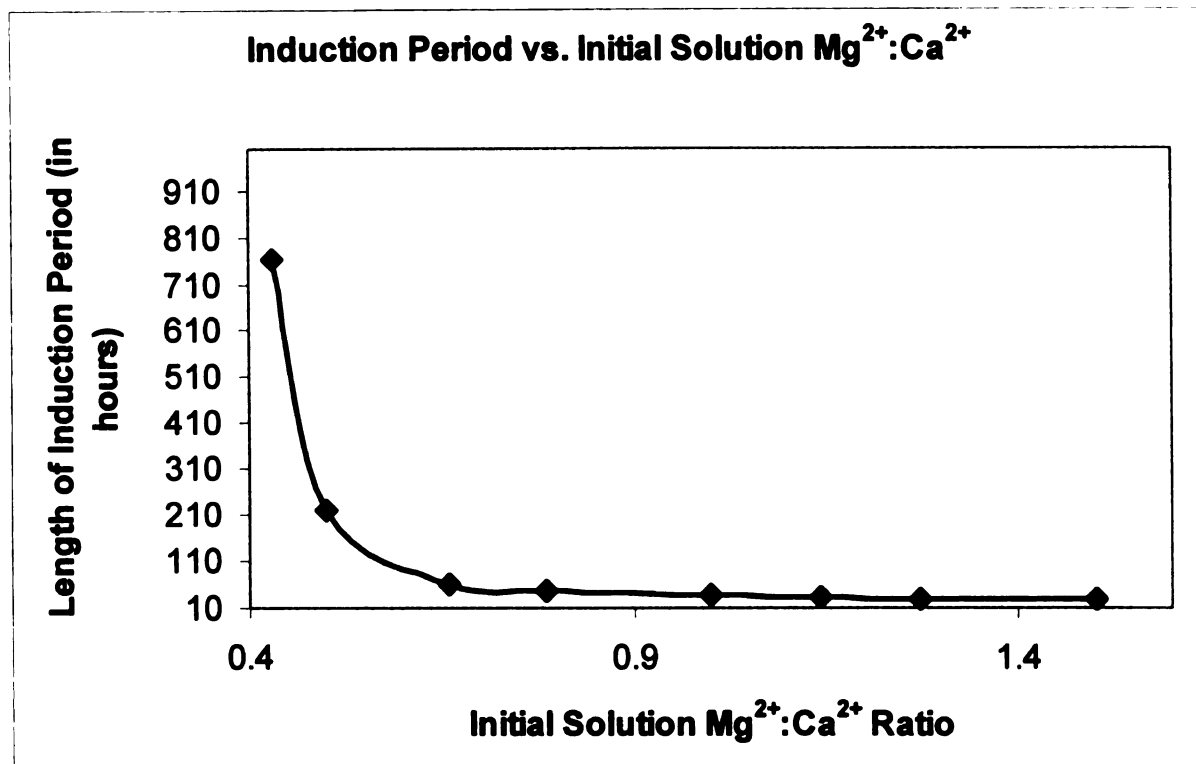


Figure 12b. Induction period (linear-scale) vs. initial solution Mg²⁺:Ca²⁺ for calcite reactant experiments.

Initial Solution Mg²⁺:Ca²⁺	Induction Period (in hours)
0.43	762
0.50	219.5
0.66	61
0.79	48
1.0	38
1.14	33
1.27	29.5
1.50	28

Table 3. Induction period times for calcite reactant experiments.

3.b.2. Dolomite Stoichiometry: Figure 13 indicates a strong relationship between dolomite stoichiometry for experiments ended prior to reactant depletion and the initial solution $\text{Mg}^{2+}:\text{Ca}^{2+}$ ratio ($R^2 = 0.97$). Experiments with a solution $\text{Mg}^{2+}:\text{Ca}^{2+}$ of 1.5, yield stoichiometric dolomite (50 mol% CaCO_3), whereas progressively lower solution $\text{Mg}^{2+}:\text{Ca}^{2+}$ ratios yield more calcium-rich compositions, respectively. For example, the experiment with an initial solution $\text{Mg}^{2+}:\text{Ca}^{2+}$ ratio of 0.43 produced the most Ca-rich dolomite with an average stoichiometry of 61 mole% CaCO_3 .

Prior to reactant depletion, overall dolomite stoichiometry does not appear to be related to percent product, which is shown in Figure 14 for all calcite reactant experiments ($R^2=0.023$). Dolomite stoichiometry also remains relatively constant prior to reactant depletion in each of the individual solution $\text{Mg}^{2+}:\text{Ca}^{2+}$ ratios. Figures 15 and 16 plot dolomite stoichiometry versus percent product for experiments with initial solution $\text{Mg}^{2+}:\text{Ca}^{2+}$ ratio = 0.79 ($R^2=0.0013$) and $\text{Mg}^{2+}:\text{Ca}^{2+}$ ratio = 1.27 ($R^2=0.0005$), respectively. The experiment with a solution $\text{Mg}^{2+}:\text{Ca}^{2+}$ ratio = 1.14 also has a very low correlation between percent product and dolomite stoichiometry ($R^2=0.0172$). Two other experiments had significantly higher correlations, namely the initial solution $\text{Mg}^{2+}:\text{Ca}^{2+} = 0.66$ experiment ($R^2=0.496$) and the initial solution $\text{Mg}^{2+}:\text{Ca}^{2+}$ ratio = 1.0 experiment ($R^2=0.212$). However, dolomite products from these experiments have very minor compositional ranges. The $\text{Mg}^{2+}:\text{Ca}^{2+} = 0.66$ solution experiment, for example, changed by only ~0.6 mole% CaCO_3 (60.13 to 59.53) and the $\text{Mg}^{2+}:\text{Ca}^{2+} = 1.0$ solution experiment changed by only ~0.8 mole% CaCO_3 (56.15 to 55.35). This

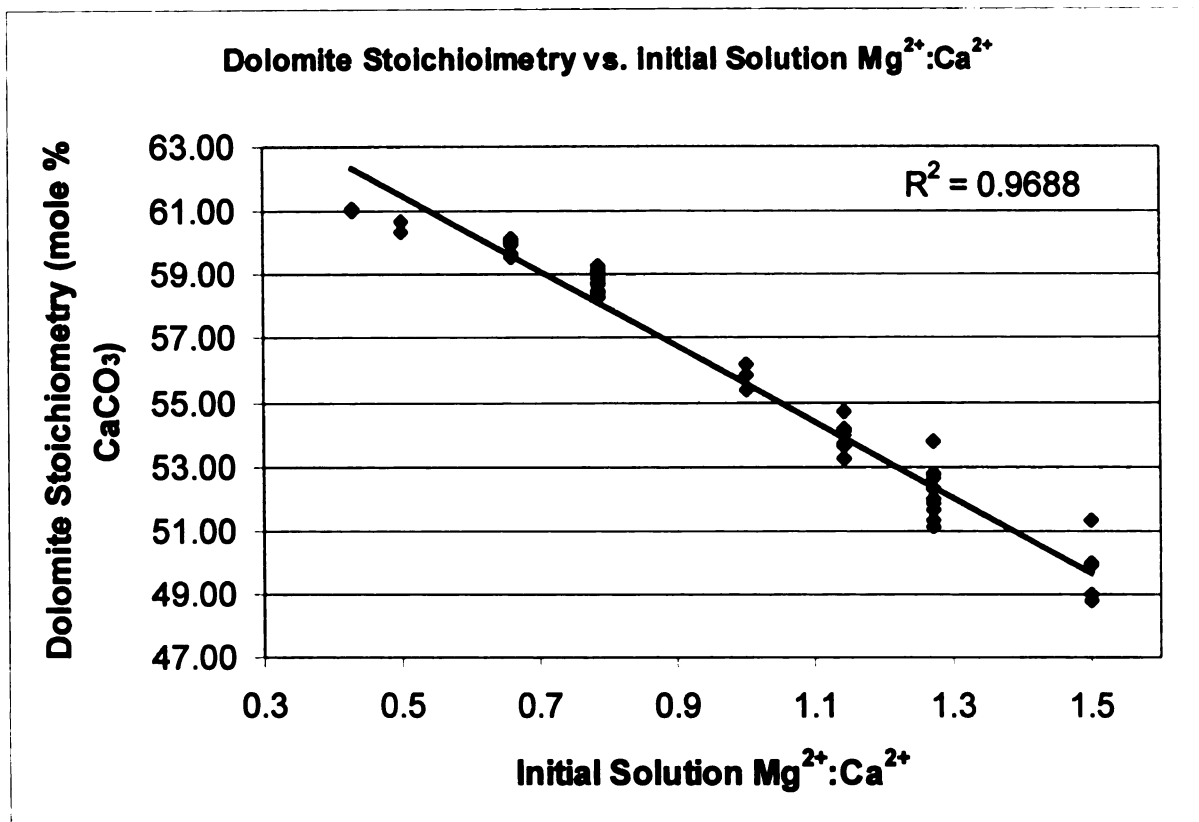


Figure 13. Dolomite stoichiometry vs. initial solution $Mg^{2+}:Ca^{2+}$ for all dolomites formed prior to calcite reactant depletion, calcite reactant experiments, $R^2=0.9688$, $N=69$.

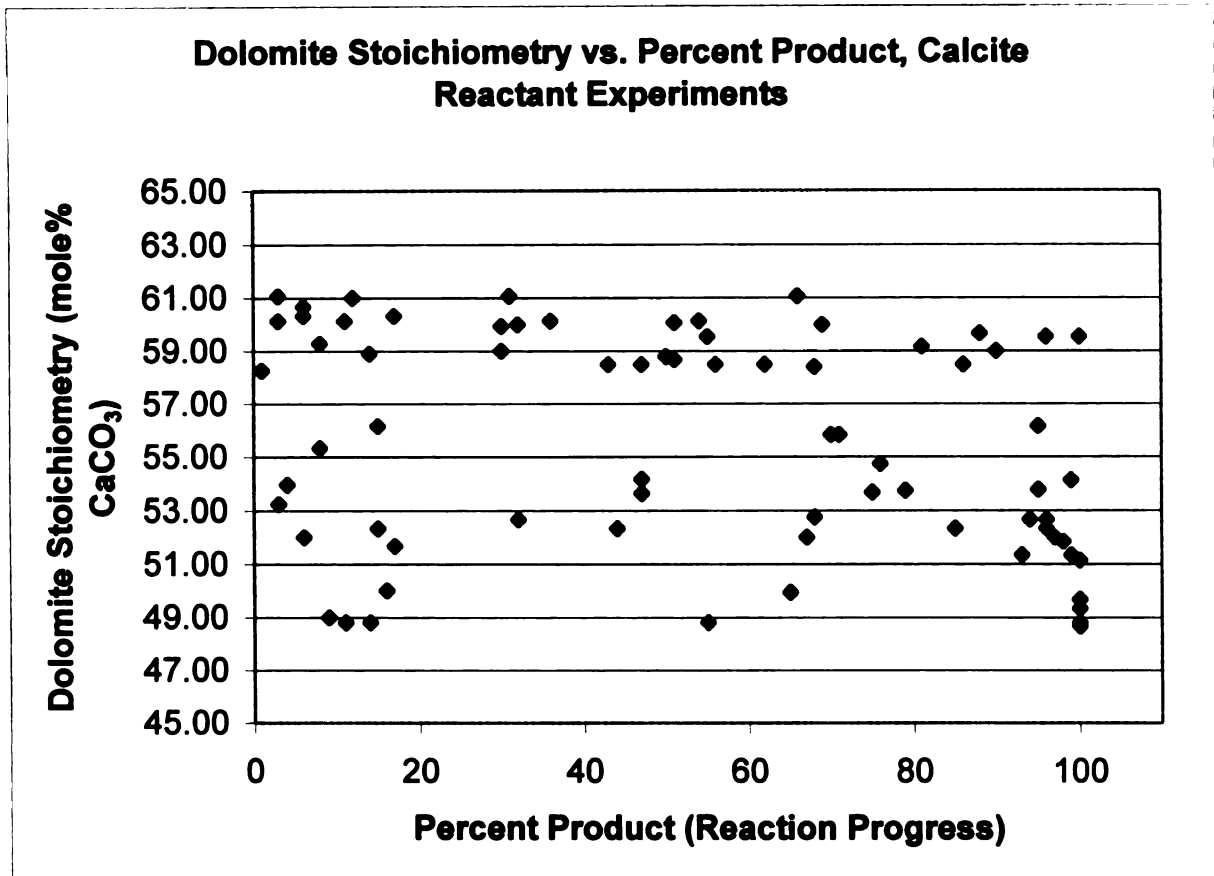


Figure 14. Dolomite stoichiometry vs. percent product for all dolomites formed prior to calcite reactant depletion, calcite reactant experiments, $R^2=0.023$, $N=69$.

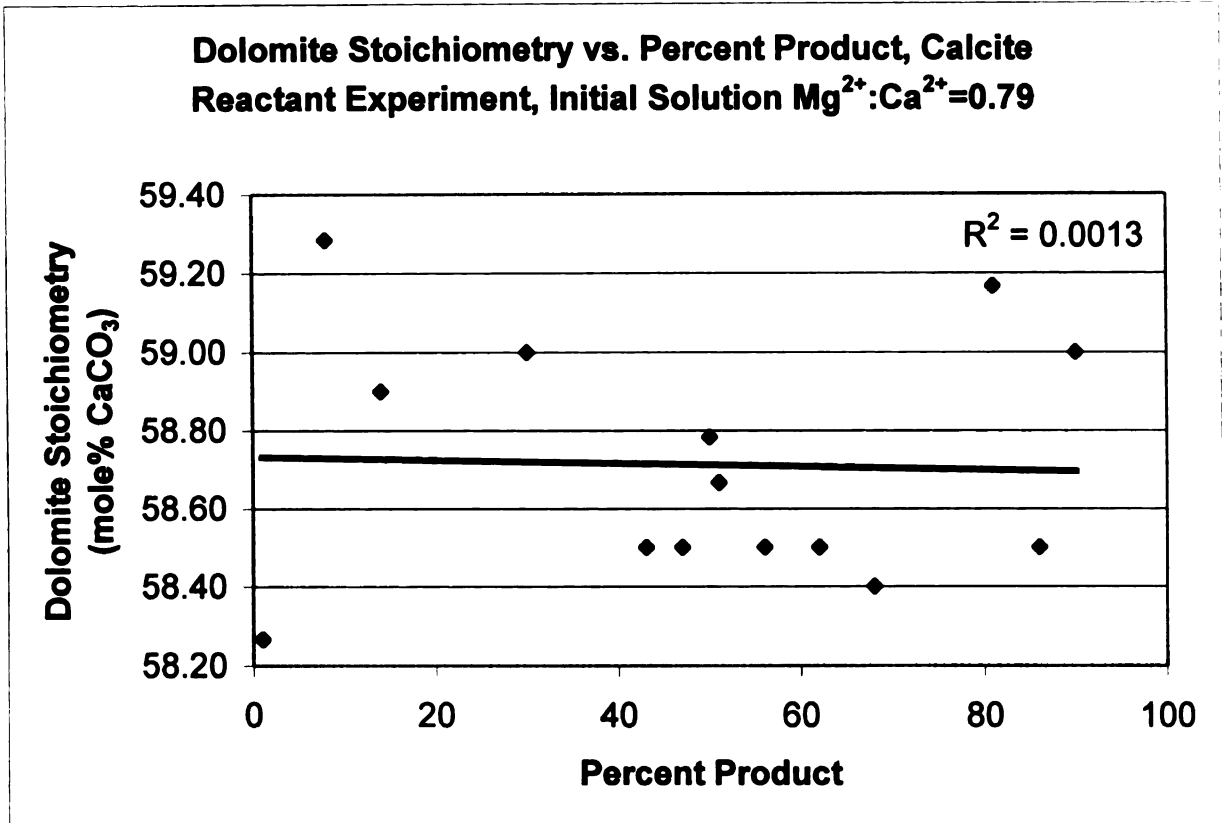


Figure 15. Dolomite stoichiometry vs. percent product for dolomites formed prior to calcite reactant depletion, calcite reactant experiment, initial solution $Mg^{2+}:Ca^{2+} = 0.79$, $R^2=0.0013$.

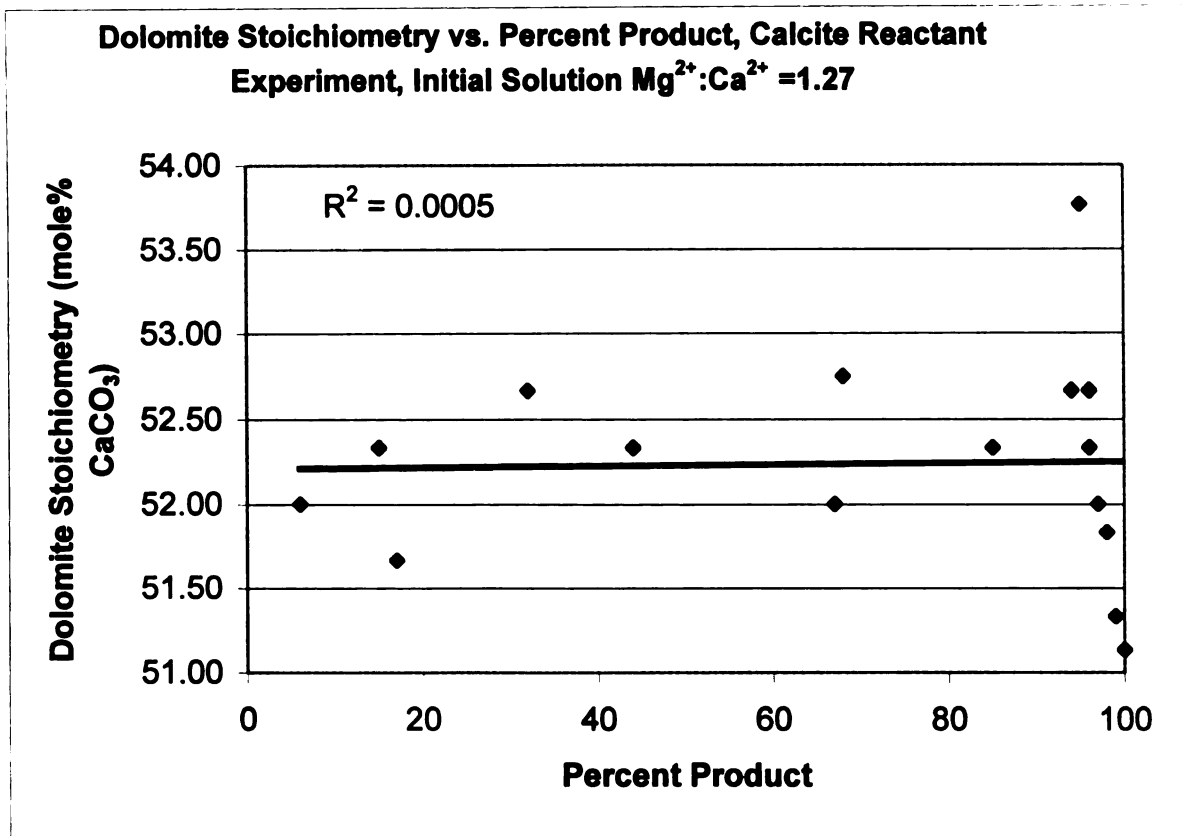


Figure 16. Dolomite stoichiometry vs. percent product for dolomites formed prior to calcite reactant depletion, calcite reactant experiment, initial solution $Mg^{2+}:Ca^{2+} = 1.27$, $R^2=0.0005$.

is in contrast to the dolomite products from the $\text{Mg}^{2+}:\text{Ca}^{2+} = 1.27$ calcite reactant experiment, which randomly varied in stoichiometry by approximately 2.5 mol% CaCO_3 ($R^2=0.005$). Such a small range in dolomite stoichiometry (< 1 mole% CaCO_3) is also near the XRD instrumental error of ± 0.33 mole% CaCO_3 . Moreover, by removing the highest percent product data point (96% dolomite), the correlation coefficient drops considerably to from 0.496 to 0.33. Experimental runs with initial solution ratios below 0.66 were not plotted because these experiments did not proceed to reactant depletion and there was insufficient data. Although dolomite stoichiometry remains relatively stable prior calcite reactant depletion, dolomite stoichiometry must increase rapidly because shortly after reactants are depleted all products are stoichiometric dolomite regardless of 1) the initial solution $\text{Mg}^{2+}:\text{Ca}^{2+}$ ratio, and 2) the composition of the dolomite first formed in the bombs.

The data also show that no correlation exists between the stoichiometry of dolomite formed prior to calcite reactant depletion and time after the onset of experimental conditions. Figures 17 and 18 plot dolomite composition as a function of time for the solution $\text{Mg}^{2+}:\text{Ca}^{2+} = 0.79$ ($R^2=0.003$) and 1.27 ($R^2=0.0097$) experiments, respectively. These plots exhibit the lowest correlation between dolomite stoichiometry and time. Although relatively minor, other calcite reactant experiments, particularly $\text{Mg}^{2+}:\text{Ca}^{2+} = 0.66$ ($R^2=0.275$), $\text{Mg}^{2+}:\text{Ca}^{2+} = 1.0$ ($R^2=0.218$), and $\text{Mg}^{2+}:\text{Ca}^{2+} = 1.14$ ($R^2=0.079$) may indicate a potential correlation between dolomite stoichiometry and reaction progress. Again, small ranges in dolomite product compositions in the experiments with higher correlation

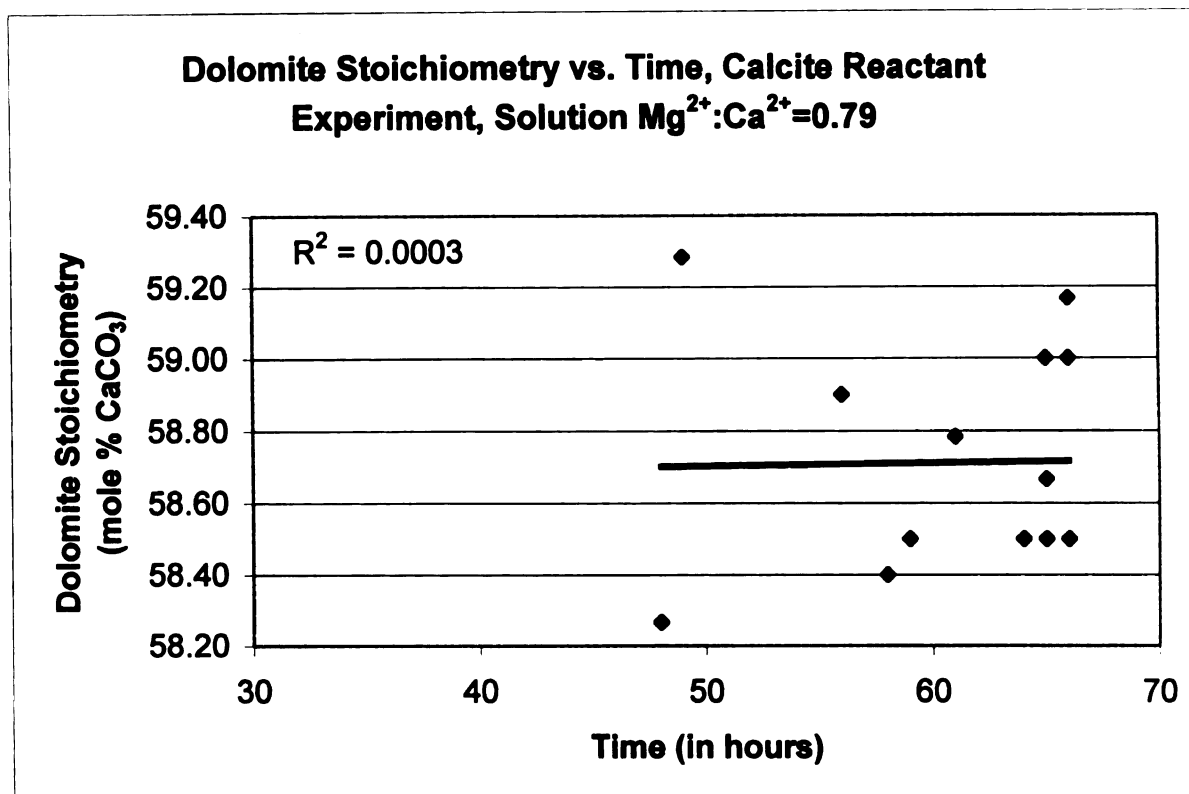


Figure 17. Dolomite stoichiometry vs. time for dolomite formed prior to calcite reactant depletion, calcite reactant experiment, initial solution $Mg^{2+}:Ca^{2+} = 0.79$, $R^2=0.0003$.

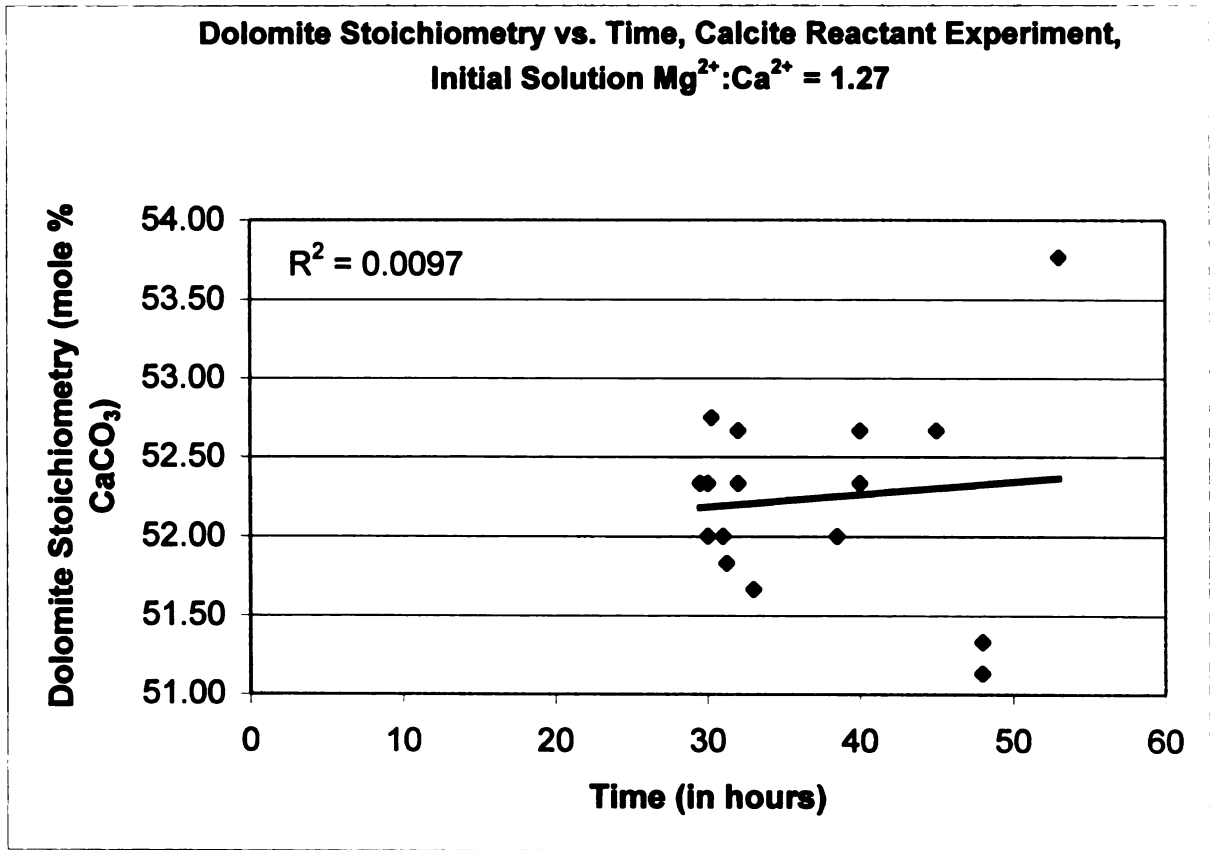


Figure 18. Dolomite stoichiometry vs. time for dolomites formed prior to calcite reactant depletion, calcite reactant experiment, initial solution $Mg^{2+}:Ca^{2+} = 1.27$, $R^2=0.0097$.

coefficients make it difficult to adequately assess the importance of the trend.

3.b.3. Cation Order: Dolomite ordering reflections first appear in XRD patterns when initial products compose more than approximately 30% of the bulk sample. Initial ordering reflections are attenuated, broadened, and shifted relative to ideal superlattice peaks for dolomite. Samples with less than 30% products exhibit no ordering peaks. Sibley (1990) argued that absence of ordering peaks may not indicate lack of order because the small abundance of products below 30% may result in low relative peak intensities that are not detected. The first dolomite ordering reflection peak to appear in X-ray diffraction patterns is at 33.5 degrees 2-theta. This is consistent with the observations of Sibley (1990) and Kessels et al. (2000) who also reported the same observation. The 33.5° ordering peak becomes increasingly visible as percent dolomite increases from 30% to 100%. Additional ordering reflections are detected as percent dolomite increases. For samples with greater than approximately 50% products, the ratio of the $d\{105\}$ and $d\{110\}$ peaks is used as a measure of the degree of cation order (Goldsmith and Graf, 1958; Fuchtbauer and Goldschmidt, 1965). The $d\{105\}$ peak is absent in samples with less than about 50% products. As a result, samples with less than ~50% product have no $\{105\}:\{110\}$ ordering ratios reported (refer to table 1). The $\{105\}:\{110\}$ ordering ratio and thus the degree of cation order increases with time. Dolomites formed prior to reactant depletion have ordering ratios that range from 0.0 to 0.45. These dolomites are considered relatively poorly ordered and are therefore referred to herein as nonideal synthetic dolomites. In some experiments, the degree of cation order

increases relatively fast as calcite is replaced by nonideal dolomite, but appears to slow after reactant depletion. This is illustrated in Figures 19 and 20, which show the relationship between cation ordering and time for the calcite reactant experiments with solution $Mg^{2+}:Ca^{2+}$ ratios of 1.0 and 1.5, respectively. The slope in each of these curves shallows considerably after consumption of the reactant, when dolomite products are stoichiometric. Other experiments do not exhibit a change in slope after reactant depletion. This can be seen in Figure 21 for the calcite reactant experiment with a solution $Mg^{2+}:Ca^{2+}$ ratio of 0.66. A linear relationship ($R^2=0.926$) is shown between the ordering ratio and time. Following reactant depletion, all contents of the reaction vessels, regardless of the initial solution $Mg^{2+}:Ca^{2+}$ ratio, are stoichiometric dolomite with ordering ratios that range from 0.50 to 0.88. Because these dolomites are stoichiometric and relatively well-ordered they are referred to herein as ideal synthetic dolomites.

Figure 22 shows little covariance between the degree of cation order (ordering ratio) and the stoichiometry of nonideal dolomite formed prior to reactant depletion ($R^2= 0.0342$). Furthermore, cation order appears to be independent of the initial solution $Mg^{2+}:Ca^{2+}$ ratio. For example, sample 8-13-04-G from the solution ratio $Mg^{2+}:Ca^{2+} = 1.5$ experiment had an ordering ratio of 0.67 after 236 hours, whereas sample 10-20-04-I from solution ratio $Mg^{2+}:Ca^{2+} = 0.79$ had an ordering ratio of 0.8 after only 79 hours.

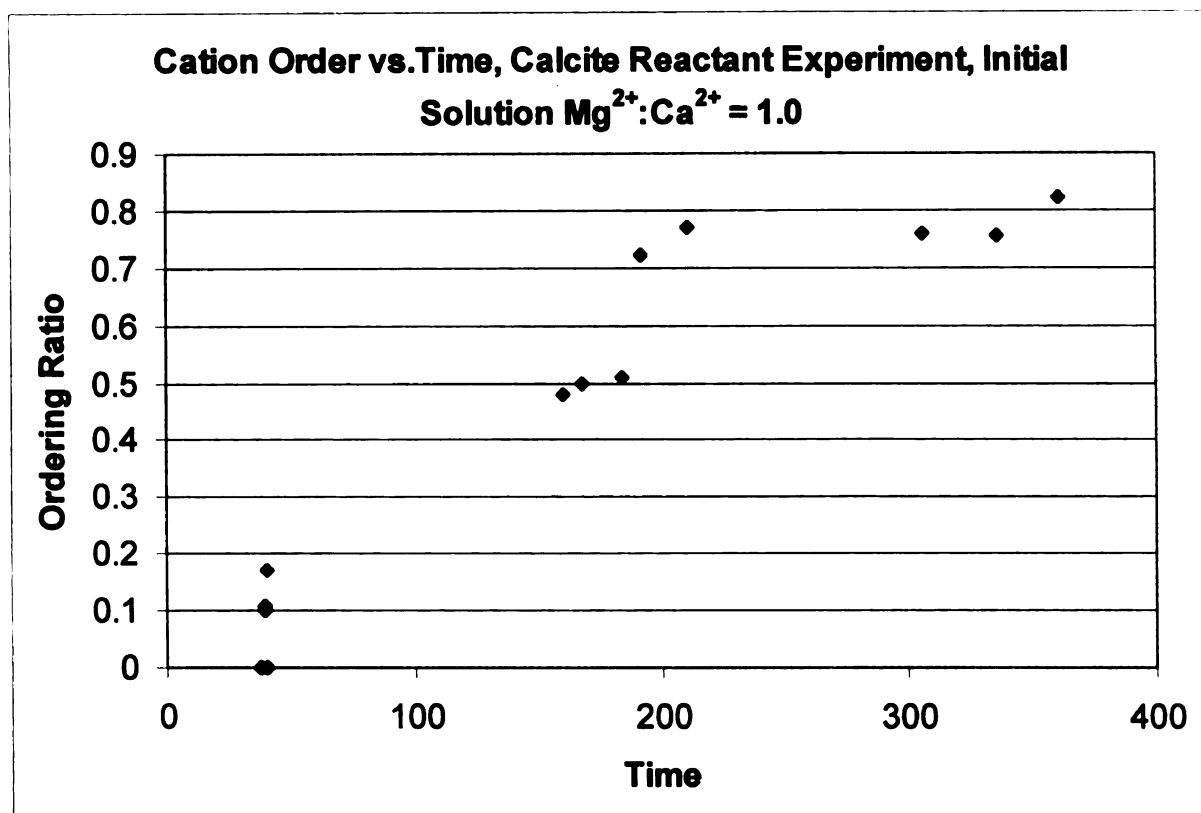


Figure 19. Cation order vs. time for calcite reactant experiment, initial solution $Mg^{2+}:Ca^{2+} = 1.0$. Reactant depletion occurs after ~160 hours.

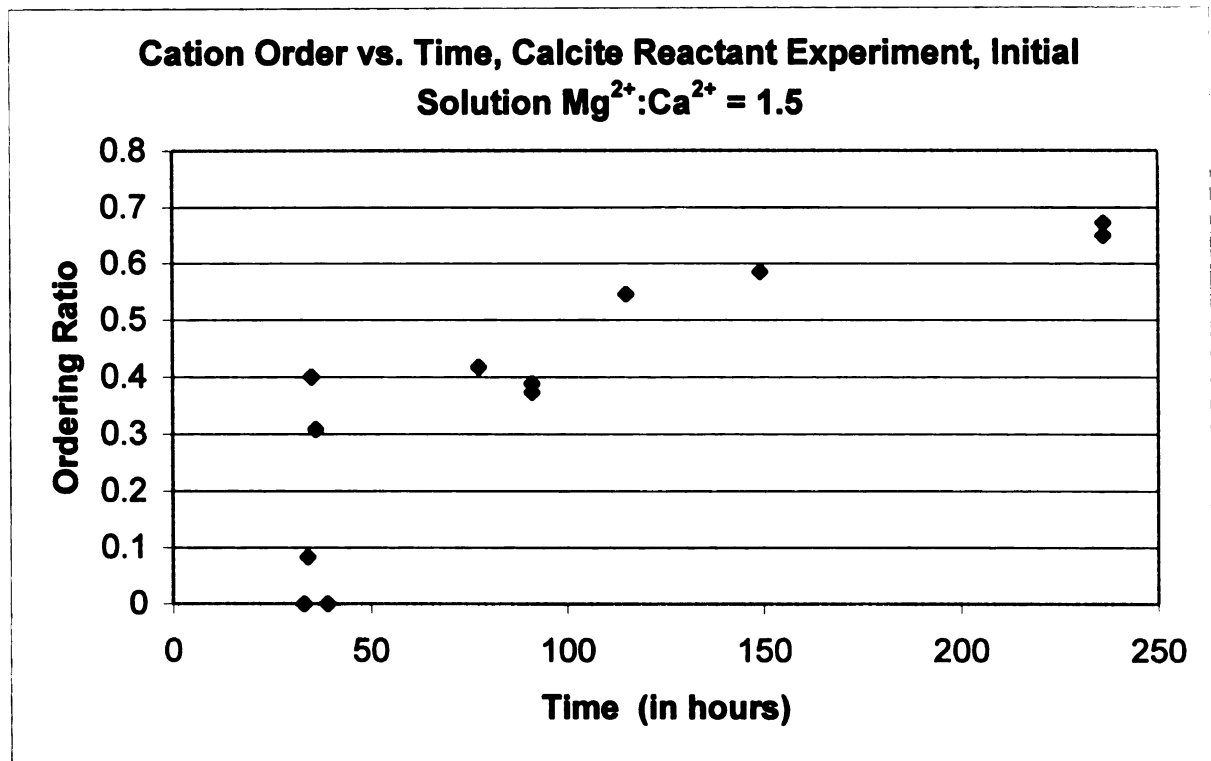


Figure 20. Cation order vs. time for calcite reactant experiment, initial solution $Mg^{2+}:Ca^{2+} = 1.5$. Reactant depletion occurs between 35 and 77 hours.

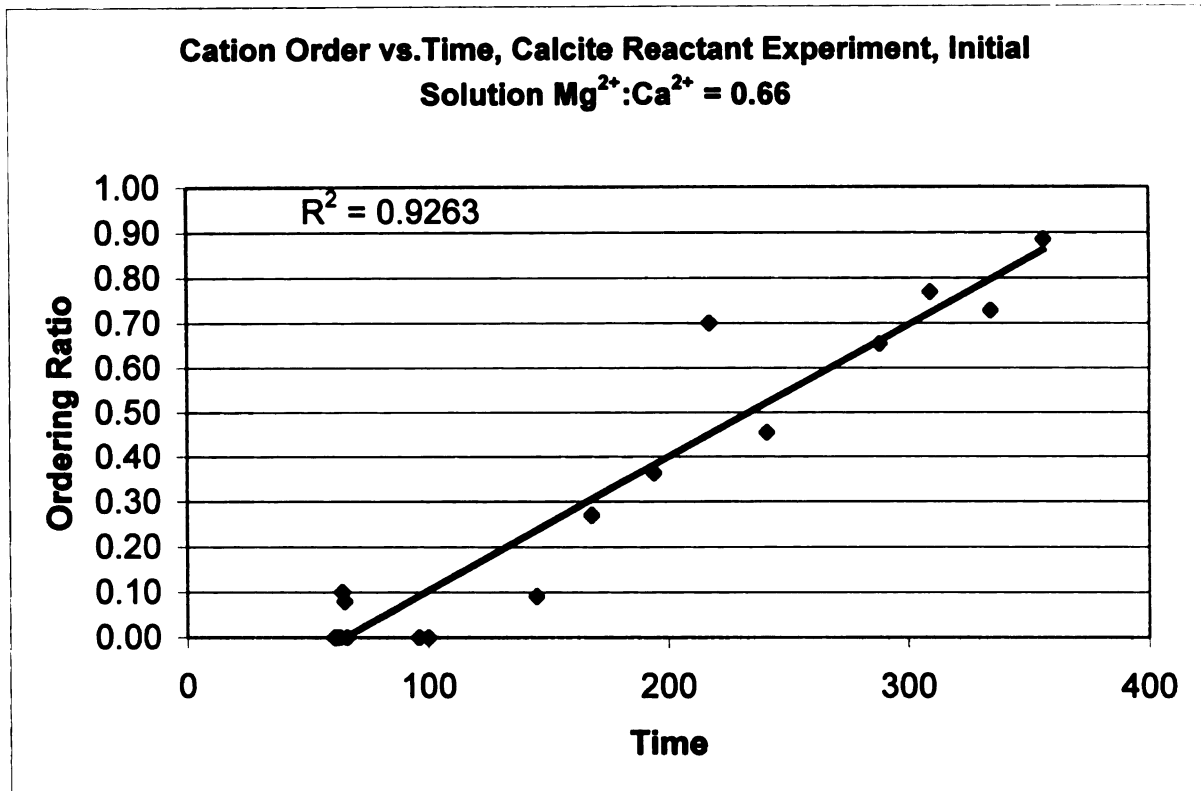


Figure 21. Cation order vs. time for calcite reactant experiment, initial solution $Mg^{2+}:Ca^{2+} = 0.66$. Reactant depletion occurs at ~217 hours.

3.b.4. Solution Chemistry: Solution chemistry changes considerably as dolomite replaces calcite in the high-temperature bombs. The $Mg^{2+}:Ca^{2+}$ ratio in solution is systematically lowered because magnesium is sequestered by dolomite and calcium is liberated into solution from dissolving calcite. Table 4 illustrates these effects as a function of dolomite composition and reaction progress for 50% product and 100% product. When 50% of the calcite has been replaced, solution $Mg^{2+}:Ca^{2+}$ ratios are 10-13 percent lower than initial values when the experiment started. And depending on the initial solution ratio, $Mg^{2+}:Ca^{2+}$ ratios are further reduced by approximately 20-24 percent after reactant depletion.

Initial Solution Mg²⁺:Ca²⁺	% Products	Mole% CaCO₃ in dolomite	Final solution Mg²⁺:Ca²⁺	% Change
0.429	50.0	61.00	0.377	-11.94
0.500	50.0	60.25	0.443	-11.47
0.667	50.0	60.00	0.596	-10.64
0.786	50.0	58.00	0.701	-10.82
1.000	50.0	56.00	0.889	-11.08
1.143	50.0	54.00	1.011	-11.56
1.273	50.0	52.00	1.119	-12.11
1.500	50.0	50.00	1.308	-12.82
Initial Solution Mg²⁺:Ca²⁺	% Products	Mole% CaCO₃ in dolomite	Final solution Mg²⁺:Ca²⁺	% Change
0.429	100.0	61.00	0.330	-23.05
0.500	100.0	60.25	0.390	-22.09
0.667	100.0	60.00	0.531	-20.41
0.786	100.0	58.00	0.623	-20.66
1.000	100.0	56.00	0.790	-21.00
1.143	100.0	54.00	0.894	-21.78
1.273	100.0	52.00	0.984	-22.68
1.500	100.0	50.00	1.143	-23.81

Table 4. Changes in solution Mg²⁺:Ca²⁺ chemistry at 50% products and 100% products. Column three is the average dolomite stoichiometry observed in the experiments for the initial solution Mg²⁺:Ca²⁺ in column one.

3.c. Aragonite Reactant Experiments

3.c.1. Reaction Rate: The induction period is shorter for aragonite reactant experiments than calcite reactant experiments. The induction period for aragonite reactant experiments (solution $Mg^{2+}:Ca^{2+} = 1.0$) is 3.25 hours (Figure 23), whereas products are first detected 38 hours into calcite reactant experiments with the same solution $Mg^{2+}:Ca^{2+}$ ratio (refer to Figure 8). After all aragonite is consumed at approximately 8 hours, all initial calcite, which comprises half of the starting solid reactants, still remains. In calcite reactant experiments, it takes longer than 40 hours to dolomitize half the calcite reactants. Polarizing light microscope (PLM), SEM, and XRD analyses indicate that dolomite selectively replaces aragonite when calcite and aragonite are present (Figure 24a). Calcite grains are generally not affected by dissolution as evidenced by sharp corners and edges. Conversely, aragonite grains are rounded and have pitted surfaces. Randomly oriented dolomite rhombs (Figure 24b) often form preferentially on the corners, edges, and steps of the aragonite crystals. X-ray diffraction data further indicate that aragonite is preferentially consumed during the aragonite reactant experiments. Samples from bombs with progressively longer reaction times yield weakened aragonite diffraction peak intensities, without a change in calcite peak intensities. Although it is theoretically possible to determine an apparent change in the growth rate between the calcite and calcite/aragonite experiments, the slopes of the reaction curves are too steep and the data is not constrained well enough to compare the reaction curves with any level of confidence.

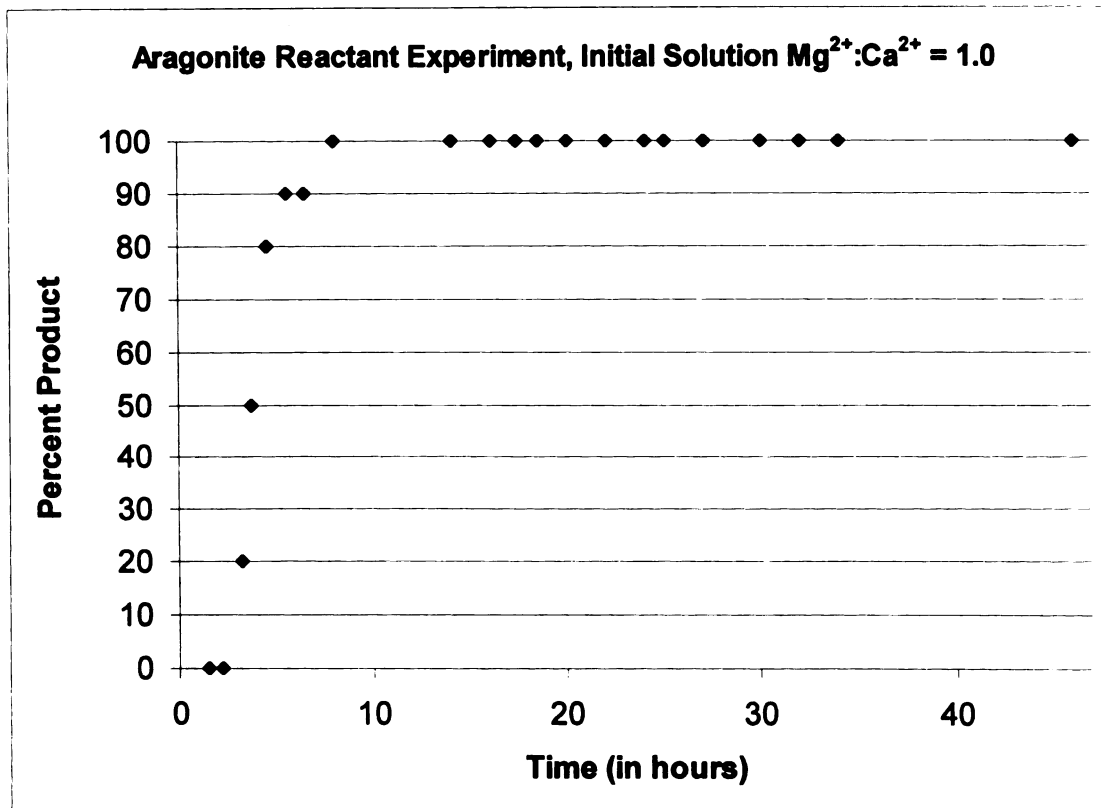


Figure 23. Percent product vs. time for aragonite reactant experiment with initial solution $Mg^{2+}:Ca^{2+} = 1.0$.

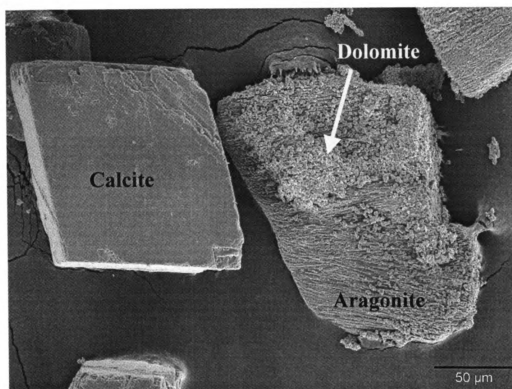


Figure 24a. SEM photomicrograph showing selective dolomitization of aragonite when both calcite and aragonite are present.

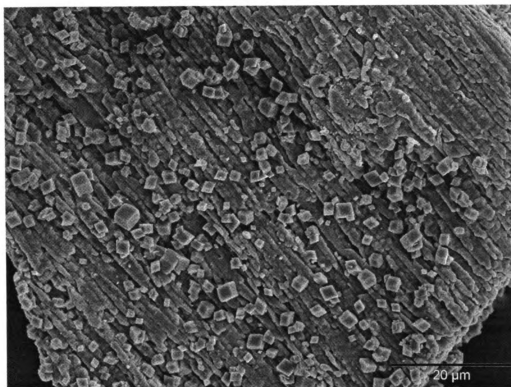


Figure 24b. SEM photomicrograph showing randomly oriented dolomite rhombs on an aragonite substrate.

3.c.2. Dolomite Stoichiometry: Dolomite from aragonite reactant

experiments is more Ca-rich than dolomite from calcite reactant experiments with the same solution $Mg^{2+}:Ca^{2+}$ ratio. Calcite reactant experiments with solution $Mg^{2+}:Ca^{2+}$ ratio = 1.0 generated dolomites with an average mole% $CaCO_3$ of 56, whereas the aragonite reactant experiments produced dolomite with 57-61 mole% $CaCO_3$. Unlike the calcite reactant experiments, dolomite products formed prior to aragonite depletion became more stoichiometric with time (Figure 25; $R^2=0.939$). In addition, dolomite products from aragonite experiments remain slightly Ca-rich after aragonite reactant depletion. For example, aragonite was completely consumed in about 8 hours, but it took over 17 hours before stoichiometric dolomite was detected in the aragonite reactant experiments. Therefore it took nearly twice the reactant depletion time before dolomite stoichiometric was detected. Because of short dolomitization times for aragonite and long dolomitization times for calcite, all aragonite reactant experiments were terminated prior to reaching calcite depletion. As a result no data was obtained regarding the time to calcite depletion in these experiments.

3.c.3. Cation Order: Dolomite ordering ratios increase with time for aragonite reactant experiments ($R^2 = 0.83$; Figure 26). Cation order in dolomite products from aragonite reactant runs, was however, significantly lower than in calcite reactant experiments. Furthermore, ordering ratios were not observed

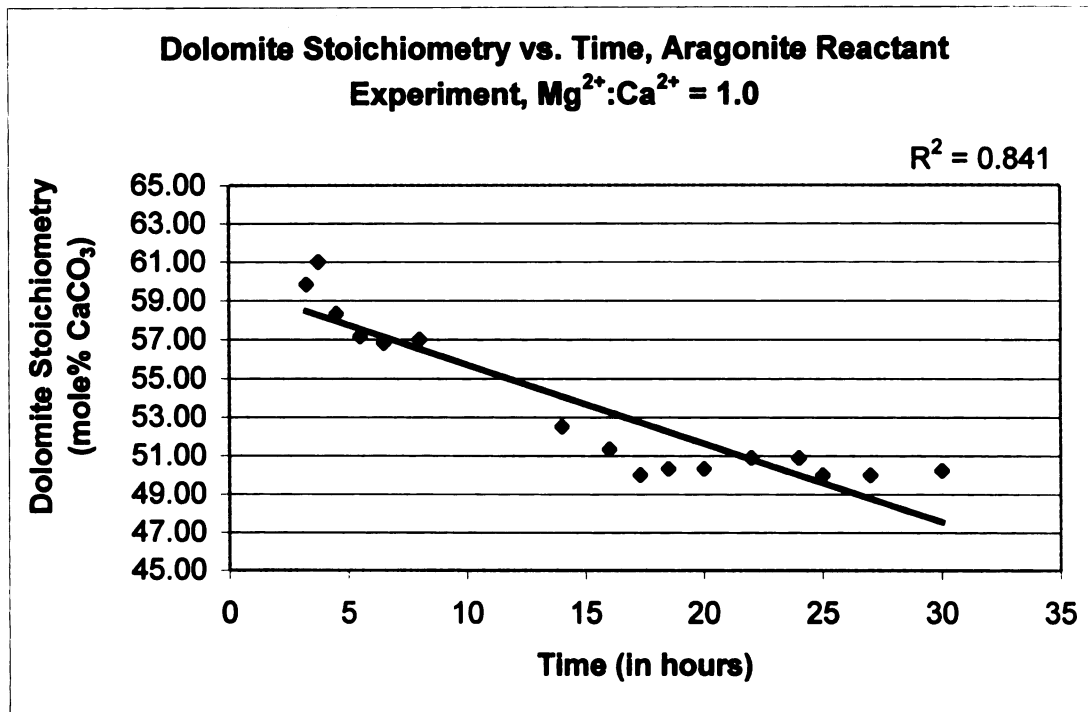


Figure 25. Dolomite stoichiometry vs. time for dolomite formed up to 30 hours after the onset of experimental conditions, aragonite reactant experiment, initial solution $Mg^{2+}:Ca^{2+} = 1.0$, $R^2=0.841$.

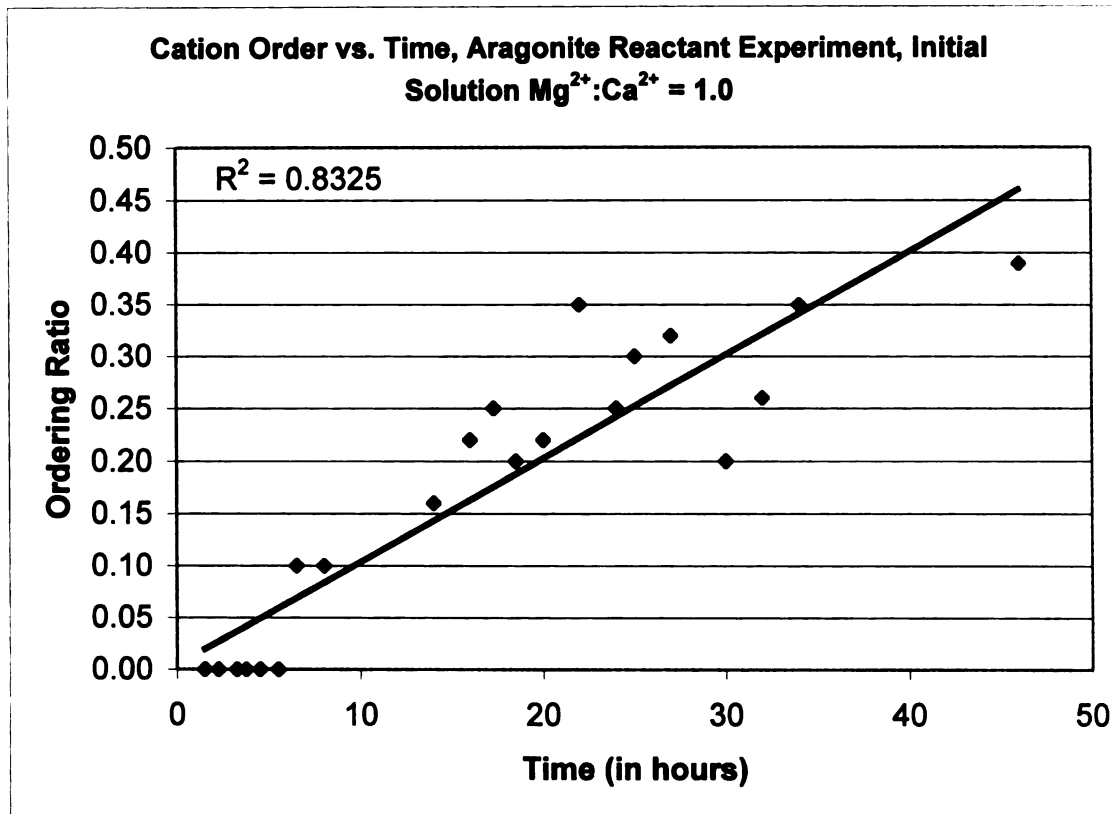


Figure 26. Cation order vs. time for aragonite reactant experiments, initial solution $Mg^{2+}:Ca^{2+} = 1.0$, $R^2=0.8325$.

until almost all aragonite was consumed (~90% products), whereas ordering ratios are first detected at approximately 50% products in the calcite reactant experiments. Dolomites formed after reactant depletion in aragonite reactant experiments with initial solution $Mg^{2+}:Ca^{2+}$ ratios of 1.0, have ordering ratios between 0.1 and 0.39. For calcite reactant experiments with solution $Mg^{2+}:Ca^{2+}$ ratios of 1.0, dolomites formed after reactant depletion have significantly higher ordering ratios between 0.48 and 0.82.

3.d. Synthetic Dolomite Crystal Size Distributions

The crystal size distributions (CSD) for five different synthetic dolomite samples are reported in Figures 27-31. Each histogram is characterized by a coarse-skewed crystal size distribution. The number of dolomite grains that were counted for each sample (N), as well as mean grain size of the sample (\bar{X}) is reported on the individual histograms.

3.e. Synthetic Dolomite Surface Nanotopography, AFM

3.e.1. Calcite Reactant Experiments: *Ex situ* AFM observations of synthetic dolomite growth surfaces reveal two principal features, described herein as islands and layers. Islands are rounded positive relief features that measure approximately 10-200nm in diameter and 1-20nm high (Figures 32 and 33). Islands occur pervasively on the growth surfaces of all nonideal dolomites formed prior to reactant depletion. Individual islands are generally round in shape without preferred orientation. Island topography is irregular in that the

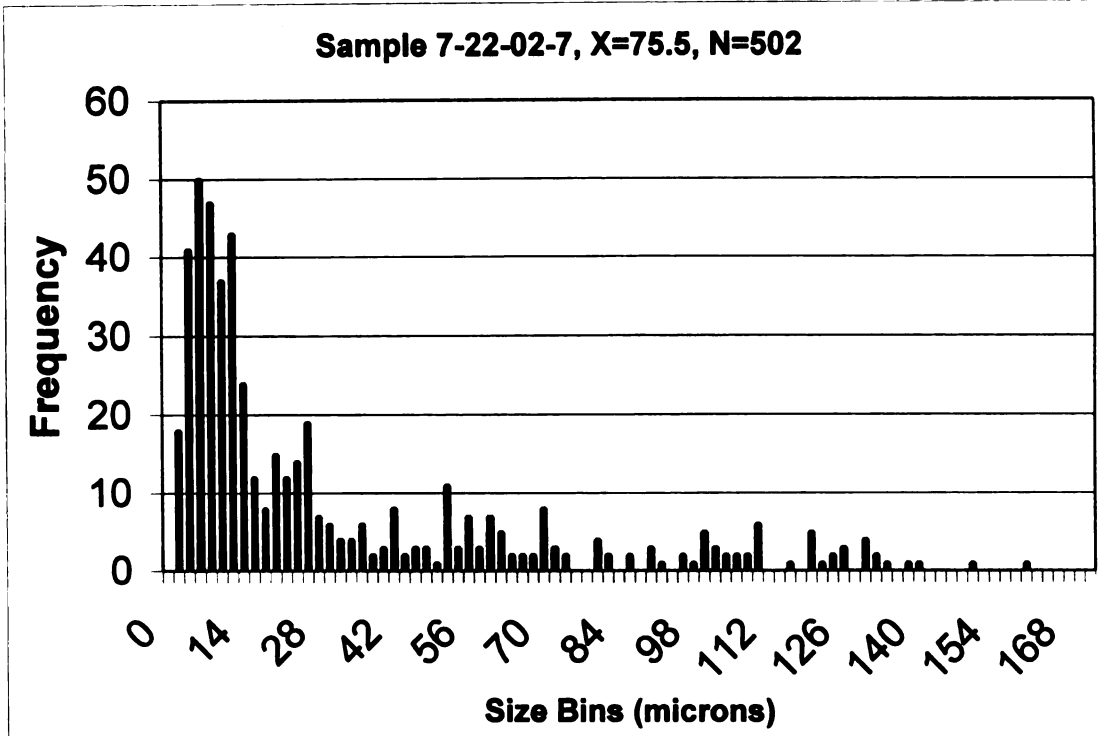


Figure 27. Coarse skewed CSD, sample 7-22-02-7. Reactant: 140-160 micron size Iceland spar calcite.

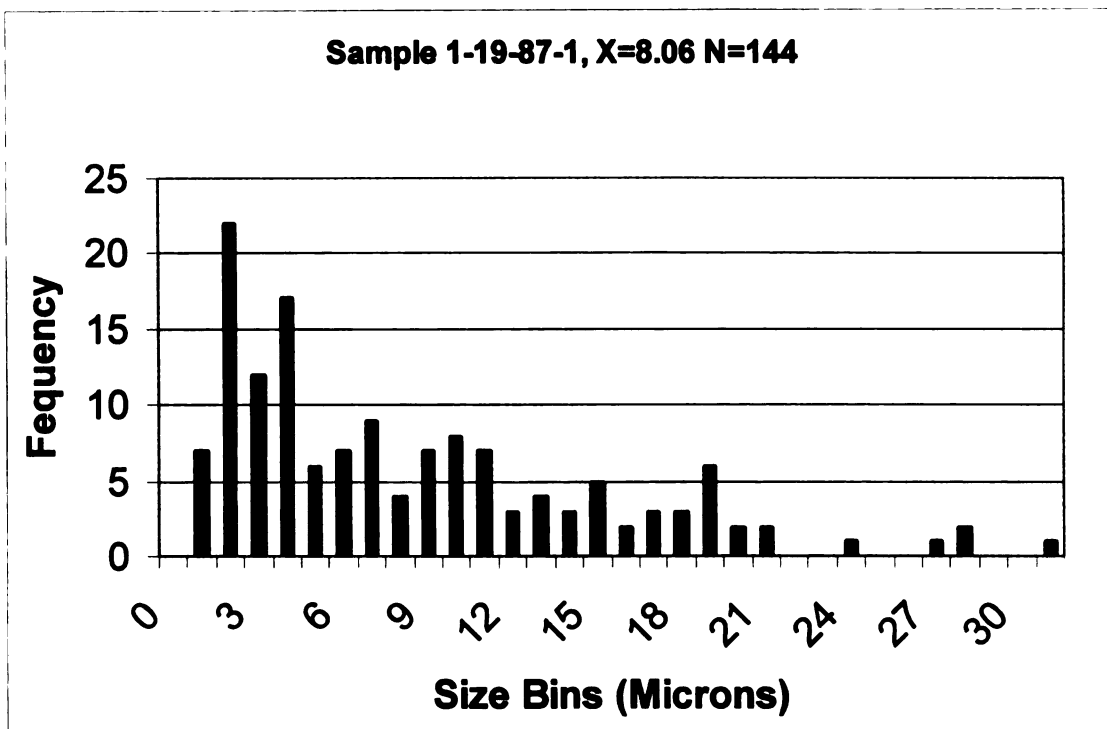


Figure 28. Coarse skewed CSD, sample 1-19-87-1. Reactant: reagent grade calcium carbonate.

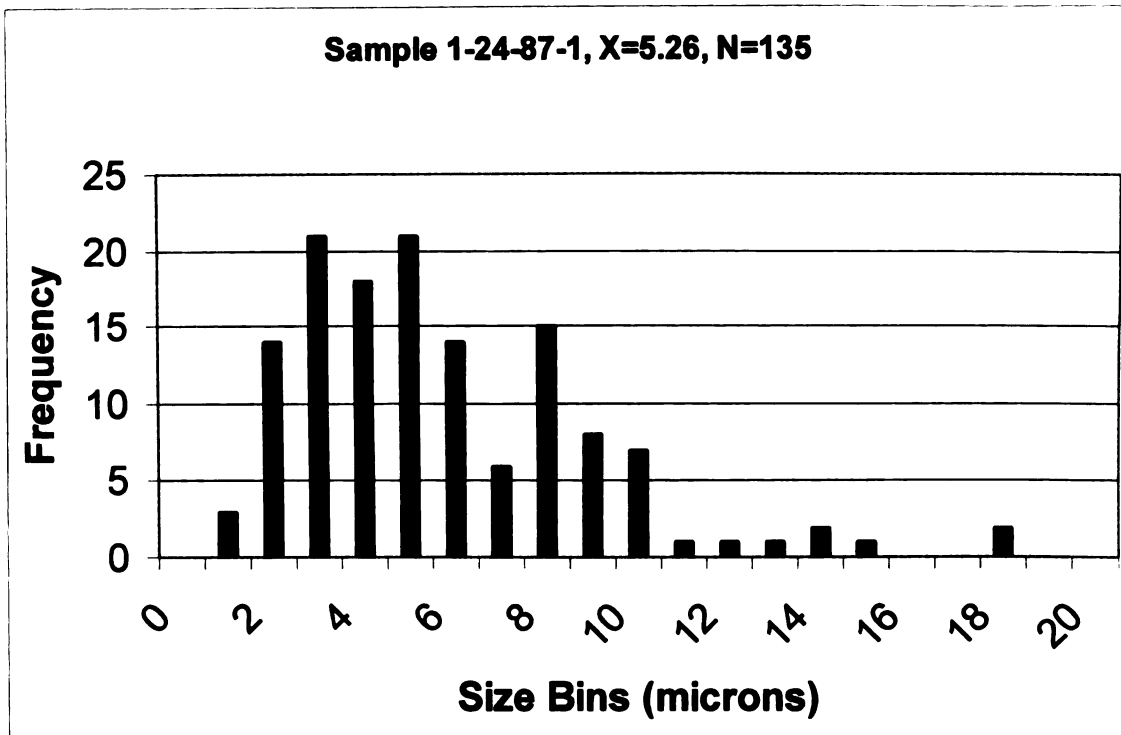


Figure 29. Coarse skewed CSD, sample 1-24-87-1. Reactant: reagent grade calcium carbonate.

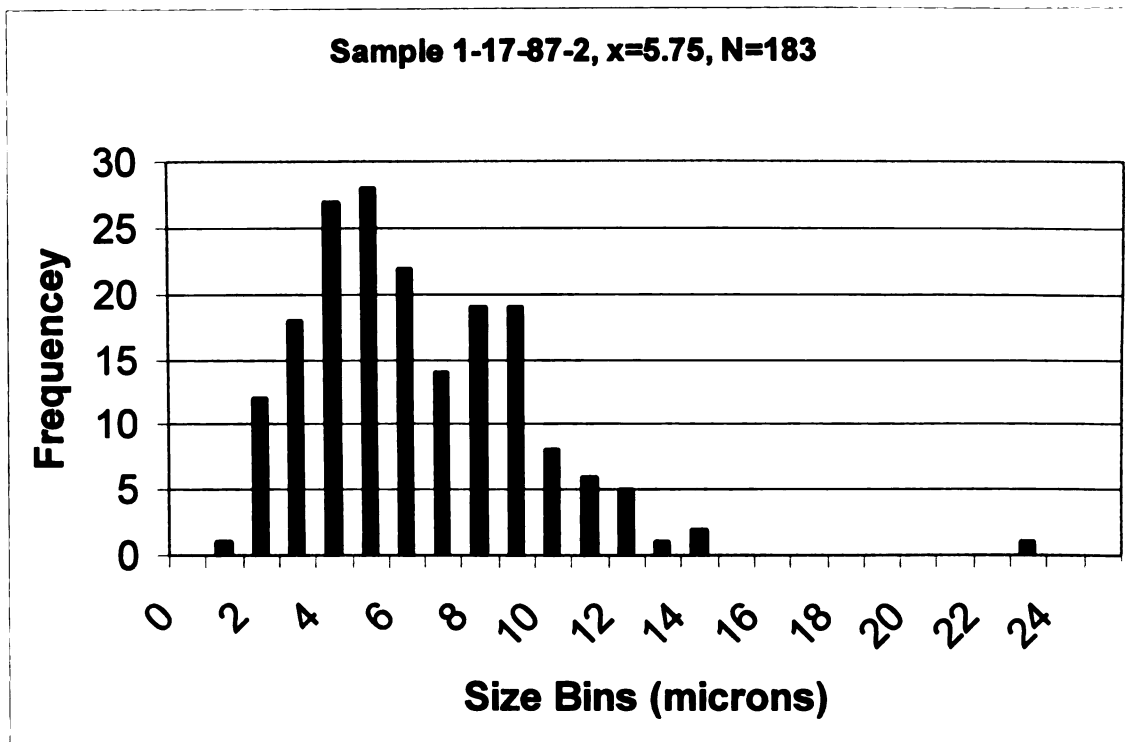


Figure 30. Coarse skewed CSD, sample 1-17-87-2. Reactant: reagent grade calcium carbonate.

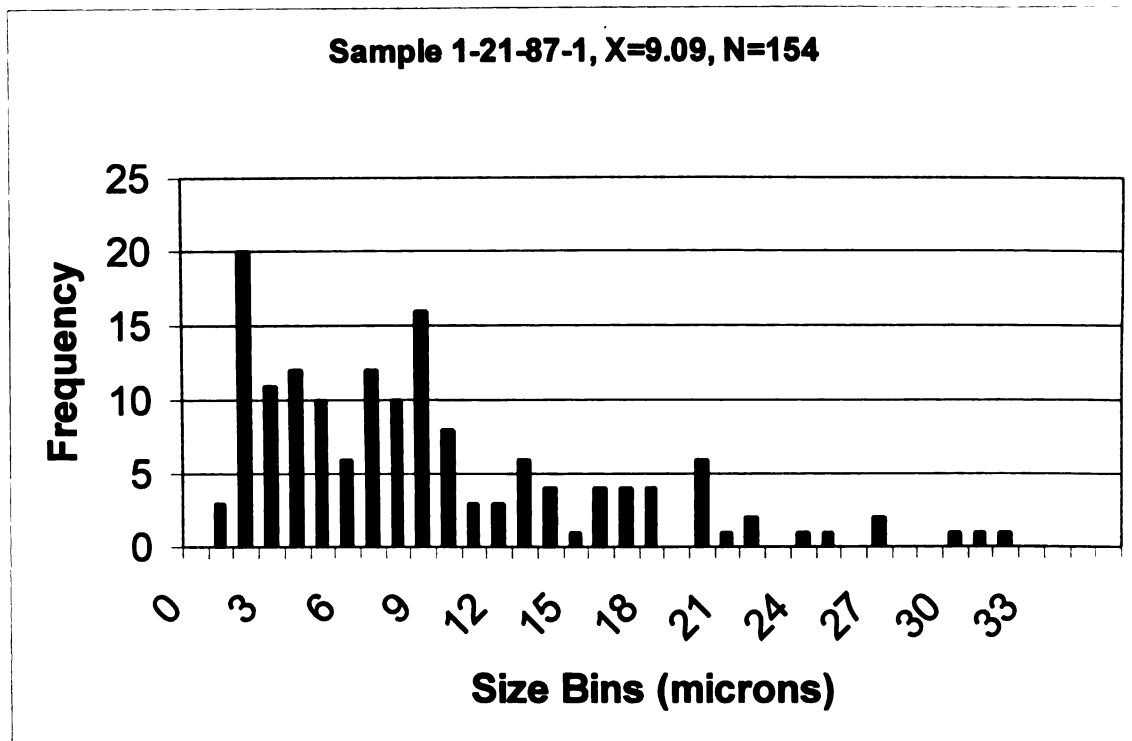
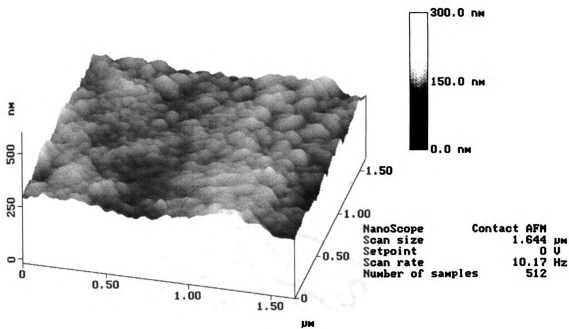


Figure 31. Coarse skewed CSD, sample 1-21-87-1. Reactant: reagent grade calcium carbonate.



10201505.001

Figure 32. AFM image of a nonideal synthetic dolomite growth surface showing pervasive island nanotopography. Calcite reactant experiment, solution $Mg^{2+}:Ca^{2+} = 1.0$.

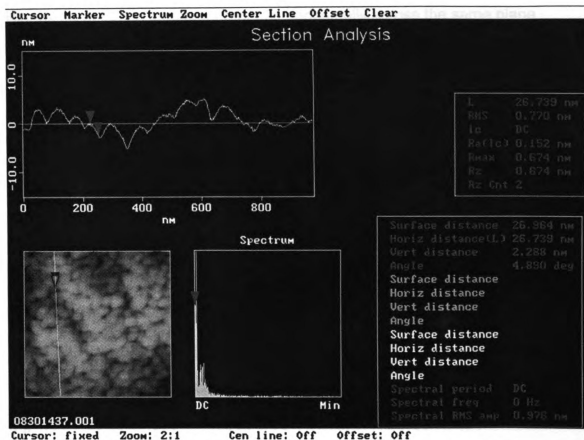
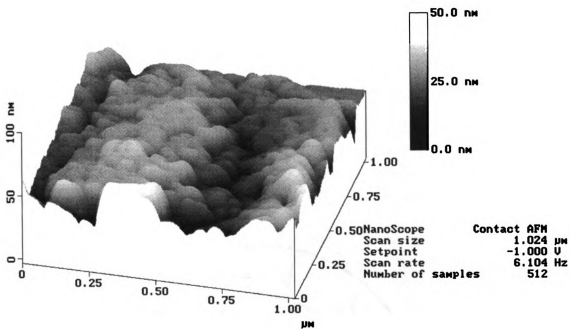


Figure 33. AFM image of a nonideal synthetic dolomite showing cross-section of island-covered growth surface. Calcite reactant experiment, solution $Mg^{2+}:Ca^{2+} = 0.66$.

islands on dolomite surfaces do not lie horizontally across the same plane. Instead, islands compose crystal surfaces that are uneven and hummocky (Figure 34). Generally speaking, no pits or flat layers are observed between individual islands except for an occasional irregularly shaped topographic depression. Adjacent islands touch and are ubiquitous across the dolomite crystal surface. Individual islands do not coalesce with other islands during growth to form flat layers. Islands are observed on dolomites from samples in which only a small amount of product has formed as well as samples that are nearly 100% dolomite. Islands appear equally on dolomites from solutions with high $Mg^{2+}:Ca^{2+}$ and low $Mg^{2+}:Ca^{2+}$ ratios. For example, islands were observed on a 30% dolomite with a composition of 61 mole% $CaCO_3$ from a 0.429 $Mg^{2+}:Ca^{2+}$ solution ratio as well as a 93% stoichiometric dolomite from a 1.5 $Mg^{2+}:Ca^{2+}$ solution ratio experiment. Islands are observed on all nonideal dolomites prior to reactant depletion despite highly variable solution $Mg^{2+}:Ca^{2+}$ ratios, product compositions, and reaction rates. Furthermore, no measurable geometric differences were observed for islands with different compositions, solution chemistries, or reaction progress.

Islands were also observed on a few samples that had progressed passed reactant depletion. These samples were removed from the oven at approximately the time when all calcite was consumed. Therefore they may contain a small amount of calcite that is below the XRD detection limit.

After reactant depletion, products are stoichiometric and relatively well-ordered (ideal) dolomite. Ideal dolomite crystal surfaces display flat, laterally



09040833.001

Figure 34. AFM image of a nonideal synthetic dolomite growth surface showing variable nanotopography caused by islands. Calcite reactant experiment, solution $Mg^{2+}:Ca^{2+} = 1.5$.

extensive layers with steps (Figure 35) that measure a few tenths ($\sim 0.221\text{nm}$) to tens of nanometers high. With an approximate error of $\pm 0.06\text{nm}$ (Kessels et al., 2000) in the step height measurement, 0.221nm layers are similar to the d-spacing for $d\{104\}$ dolomite plane = $\sim 0.3\text{nm}$ (1-monolayer). Due to the relatively large error, it cannot be ruled out that the measured layers are $\frac{1}{2}$ of a dolomite monolayer (i.e. either a calcite-like layer or a magnesite-like layer). Layer surfaces are extremely flat and do not have islands on top of them. Some layers are separated by straight-sided edges and steps (Figure 35), whereas others are defined by more wavy edges and steps (Figure 36). Despite variability in layer geometry, edges and steps generally run parallel to one another. Although classic multi-layer, helical growth spirals are not observed on dolomite surfaces, individual layers are observed to emerge from flat crystal surfaces as predicted by the spiral growth model. Figure 37a shows a flat surface with an emerging step (towards the top of the image), which measures approximately 0.2 nm near the offset. Figure 37b shows that the step completely disappears on the opposite side of the emerging surface layer (towards the bottom of the image).

3.e.2. Aragonite Reactant Experiments: Dolomite formed in aragonite reactant experiments have surfaces covered with islands (Figure 38). Islands are present on dolomite surfaces throughout the reaction. Dolomite growth islands in the aragonite reactant experiments are the same in size and shape as those described for dolomite from calcite reactant experiments.

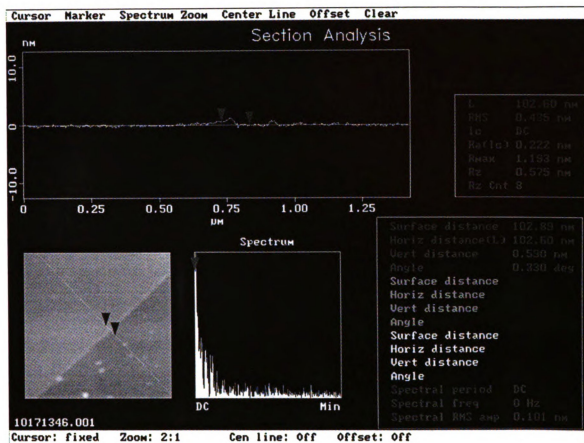


Figure 35. AFM image of an ideal synthetic dolomite growth surface showing straight-sided steps. Calcite reactant experiment, solution $Mg^{2+}:Ca^{2+} = 1.0$.

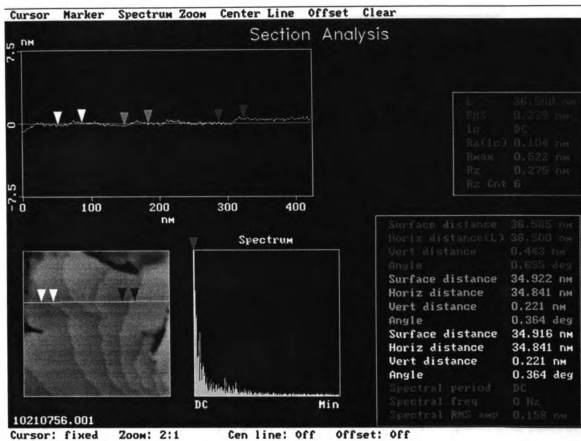


Figure 36. AFM image of an ideal synthetic dolomite growth surface showing multiple layers with curved steps. Calcite reactant experiment, solution $Mg^{2+}:Ca^{2+} = 1.5$.

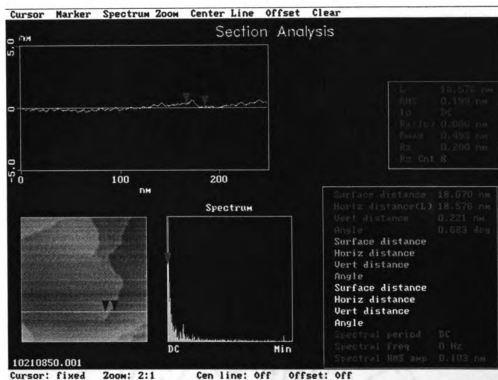


Figure 37a. AFM image and cross-section of an ideal synthetic dolomite growth surface showing an emerging growth layer. Calcite reactant experiment, solution $Mg^{2+}:Ca^{2+} = 0.66$.

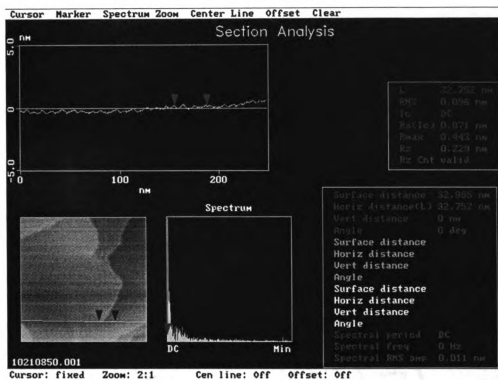


Figure 37b. AFM image and cross-section of an ideal synthetic dolomite showing the emerging growth layer disappears into the surface.

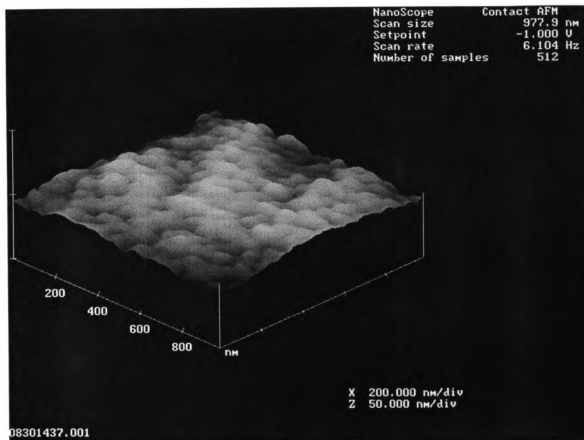


Figure 38. AFM image of a nonideal synthetic dolomite showing pervasive island nanotopography. Aragonite reactant experiment, solution $\text{Mg}^{2+}:\text{Ca}^{2+} = 1.0$.

3.f. Synthetic Dolomite Surface Nanotopography, SEM

3.f.1. Calcite Reactant Experiments: Dolomite rhombs form preferentially at edges and corners in crystallographic continuity with the dissolving calcite substrate (Figure 39). Figure 40 demonstrates the presence of euhedral etch pits on the calcite substrate that form as a result of dissolution. As the dolomitization reaction progresses, calcite becomes totally encrusted in dolomite rhombs (Figure 41). After this occurs, individual dolomite rhombs continue to nucleate on dolomite surfaces (Figure 42).

Nonideal synthetic dolomites are characterized by crystal surfaces with what appears to be relatively flat areas separated by jagged and irregular ledges. Figures 43a, and 43b are FESEM images, which show nonideal surface features are generally irregular with rounded topographic highs and edges. The rounded topographic features are on the order of tens to hundreds of nanometers in diameter, consistent with the island topography observed with AFM in Figures 32-34.

The surfaces of ideal synthetic dolomite, on the other hand, generally have flatter surfaces that are separated by straight-sided steps and ledges. The areas in between layers are more flat. Edges and steps are more angular than observed in nonideal dolomites. Figures 44a and 44b are FESEM images of ideal dolomite crystal surfaces taken at the same magnifications used in figures 43a and 43b, respectively). Straight-sided steps appear to form from the intergrowth of individual dolomite crystals and/or growth layers. The flat surfaces with straight-sided steps are comparable to AFM observed steps in figures 35-37.

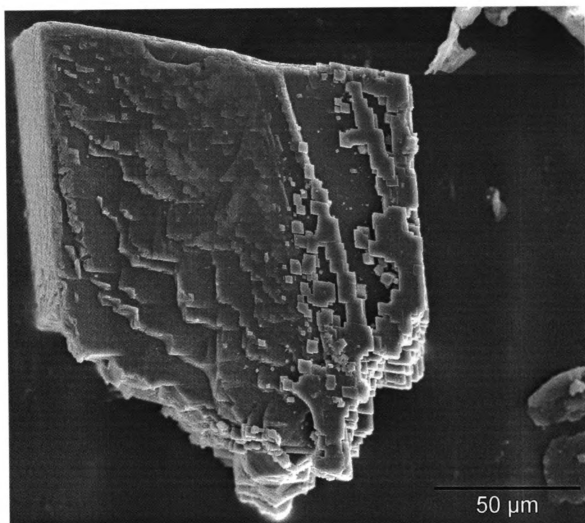


Figure 39. SEM photomicrograph showing crystallographically oriented dolomite rhombs on the edges and corners of the calcite substrate.

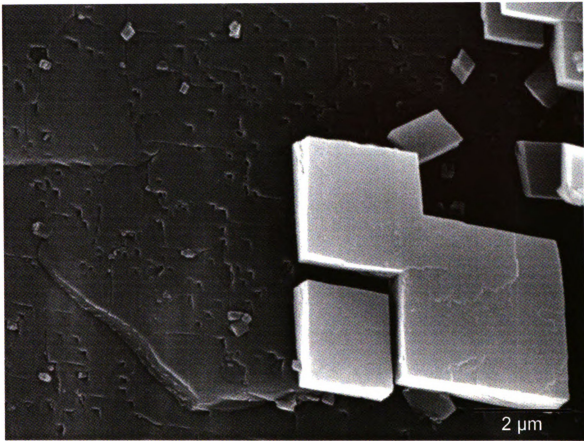


Figure 40. SEM photomicrograph showing dolomite growth rhombs on a pitted calcite surface that has been dissolved.

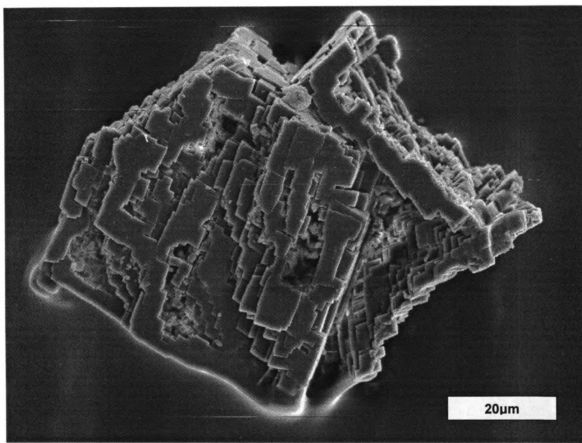


Figure 41. SEM photomicrograph showing a dolomite encrusted calcite grain.

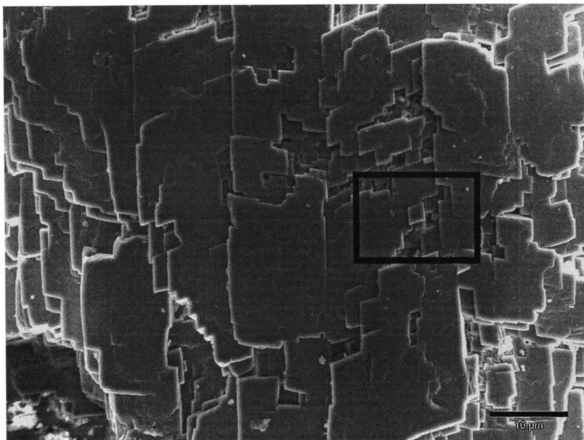


Figure 42. SEM photomicrograph of a small dolomite rhomb on a dolomite surface.

*Calibration bar = 10 micrometers .

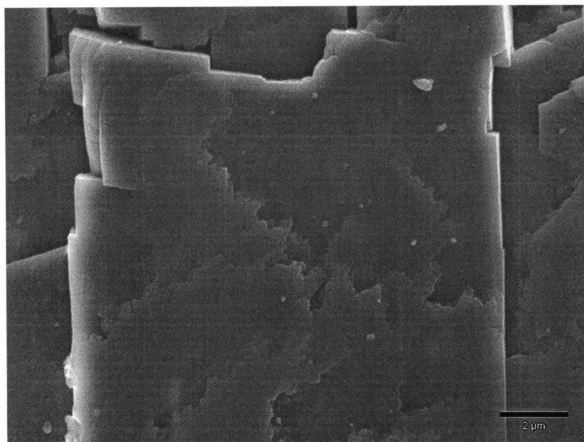


Figure 43a. SEM photomicrograph of a nonideal synthetic dolomite surface showing irregular growth nanotopography.

*Calibration bar = 2 micrometers

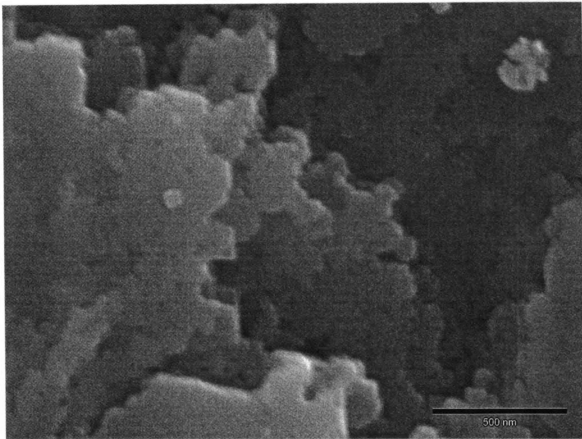


Figure 43b. SEM photomicrograph of the same nonideal synthetic dolomite growth surface at higher magnification showing rounded topographic highs and wavy ledges.

*Calibration bar = 500 nanometers

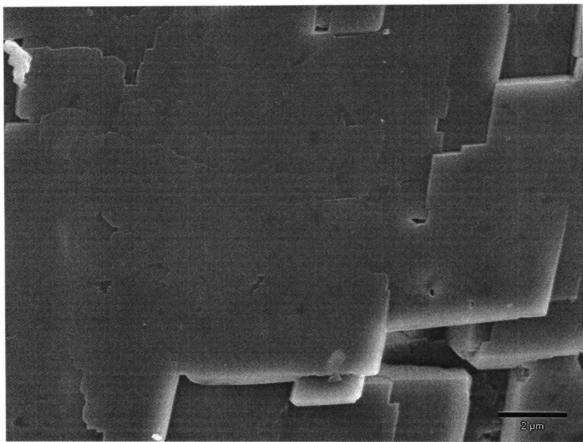


Figure 44a. SEM photomicrograph of an ideal synthetic dolomite showing relatively flat growth surfaces.

Calibration bar = 2 micrometers

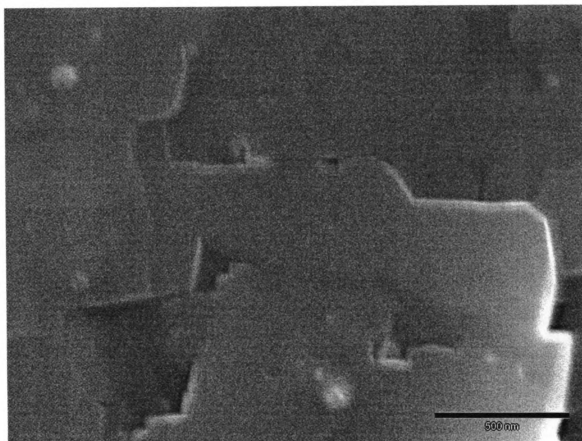


Figure 44b. SEM photomicrograph of the same ideal synthetic dolomite at higher magnification showing flat growth surfaces separated by straight-sided steps.

*Calibration bar = 500 nanometers

The nanometer-scale surface features described above were observed on samples coated with 2nm of osmium. Samples coated with 10-30nm of gold did not reveal such differences between ideal and nonideal dolomite. The gold coating, as shown in Figure 45, was too thick and covered up most nanometer-scale surface features.

3.f.2. Aragonite Reactant Experiments: Dolomite forms preferentially on aragonite when both aragonite and calcite are present (refer to Figure 27a). Dolomite grains have random orientation and nucleate on edges, steps and corners (refer to Figure 27b). Calcite remains in the reaction vessels after aragonite is consumed, but showed no signs of dolomitization.

3.g. Etched Synthetic Dolomite Surface Nanotopography, AFM

The surfaces of synthetic dolomite crystals chemically etched in dilute acid are characterized by two distinct surface nanotopographies – dissolution islands and euhedral etch pits on relatively flat layers. Dissolution islands are observed on nonideal synthetic dolomites that formed prior to reactant depletion whereas euhedral etch pits are observed on the surfaces of ideal synthetic dolomites that formed after reactant depletion. Dissolution islands observed on the surfaces of nonideal synthetic dolomite are indistinguishable from the growth islands previously described. Dolomite growth islands shown in Figures 32-34 are comparable to the dissolution islands in Figure 46. Dissolution islands occur pervasively across the crystal surface and generally measure 10-200nm in diameter and 1-20nm high. The sizes and shapes of individual islands are

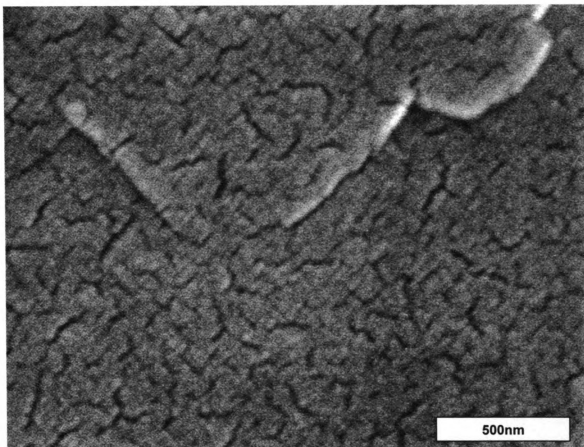
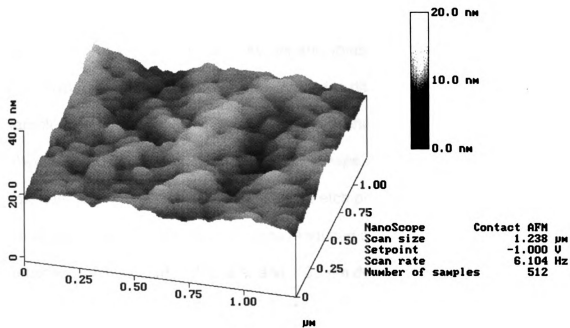


Figure 45. SEM photomicrograph showing gold coating on a synthetic dolomite grain.



08301452.001

Figure 46. AFM image of an etched synthetic nonideal dolomite showing a pervasive island dissolution surface. Calcite reactant experiment, solution $\text{Mg}^{2+}:\text{Ca}^{2+} = 0.66$.

variable and islands are not observed to have preferred orientation. Adjacent dissolution islands are in contact with one another, but remain distinct features. Occasionally, relatively large depressions and voids occur on dissolution island.

Synthetic ideal dolomite crystals etched in dilute acid have surfaces characterized by relatively flat layers with deep euhedral etch pits (Figure 47). Euhedral etch pits are commonly rhombic in shape and adjacent pits have consistent shape and orientation. Therefore etch pits are inferred to be crystallographically controlled. Etch pits produced on synthetic ideal dolomites are between 30-200 nm in diameter and 1-30 nm deep. In cross section, etch pits are asymmetric and have pointed bottoms (Figures 48 and 49). Etch pit densities are highly variable between samples. More interesting, however, is that the distribution of etch pits is very heterogeneous in a single sample. Some areas on the crystal surface are completely free of etch pits. This makes any attempt at determining accurate etch pit density extremely difficult. Etch pits become deeper and wider with increased exposure to etching solutions. Occasionally, longer etching times resulted in islands being observed on some of the etched ideal dolomites. These islands are also very similar to those previously described for growth and dissolution surfaces of nonideal synthetic dolomite. Uncovering islands during etching was more common on ideal dolomites with moderately low ordering ratios from experiments that had recently proceeded to reactant depletion than on ideal dolomites with higher ordering that had long since proceeded to reactant depletion.

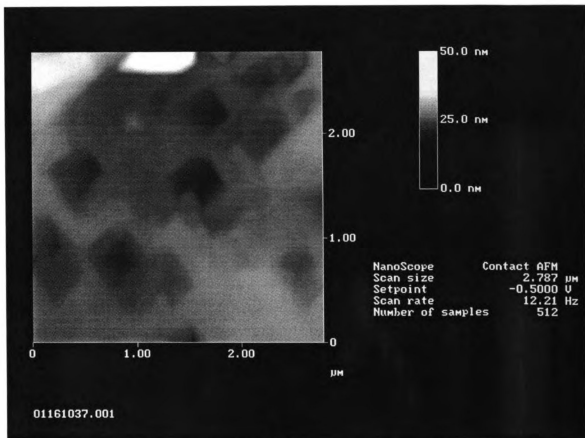


Figure 47. AFM image of an etched ideal synthetic dolomite showing euhedral etch pits. Calcite reactant experiment, solution $Mg^{2+}:Ca^{2+} = 0.66$.

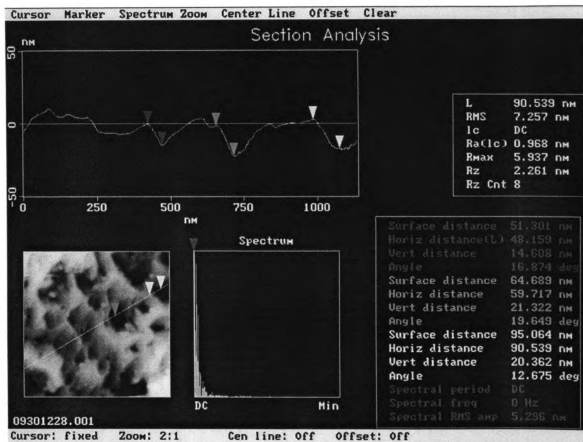


Figure 48. AFM image of an etched ideal synthetic dolomite showing a high density of euhedral etch pits. Calcite reactant experiment, solution $Mg^{2+}:Ca^{2+} = 1.5$.

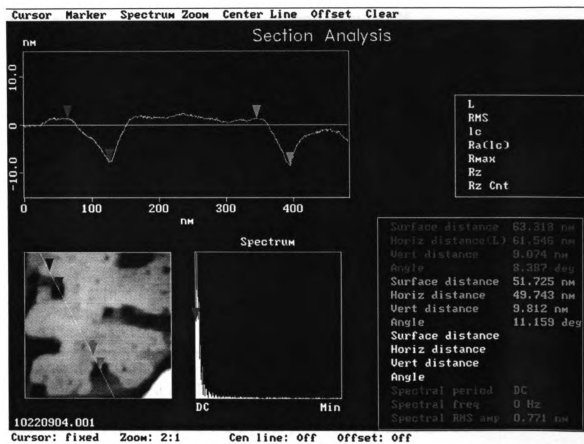


Figure 49. AFM image of an etched ideal synthetic dolomite showing euhedral etch pits and relatively flat inter-pit surfaces. Calcite reactant experiment, solution $Mg^{2+}:Ca^{2+} = 1.27$.

3.h. Natural Dolomite Surface Nanotopography, AFM

Chemically etched natural dolomite crystal surfaces are also characterized by the presence of islands and flat layers with euhedral etch pits. Islands occur on the surfaces of all chemically etched natural nonstoichiometric dolomites as well as stoichiometric dolomites with relatively low (<0.67) degrees of cation order (i.e. nonideal). Natural dolomite dissolution islands are pervasive across the crystal surface (Figure 50). Individual islands are rounded topographical highs that measure 20 to 300 nm in diameter (average ~ 60 -80nm) and of 1 to 20 nm high (Figure 51). Island-covered natural dolomite surfaces have areas of lower topography, but euhedral etch pits and flat layers with steps are absent (Figure 52). Dissolution islands on natural dolomites are very similar to those observed on synthetic dolomite crystal growth and dissolution surfaces.

The chemically etched surfaces of ideal natural dolomite exhibit euhedral etch pits with flat inter-pit layers separated by steps (Figure 53). Steps are generally straight-sided and when layers stacked on one another, steps are roughly parallel to one another. Euhedral etch pits are commonly rhombic or near rhombic in shape with sharp edges (Figures 54 and 55). Near-by etch pits have the same shape and orientation, which suggests that they are crystallographically controlled. Individual pits are 20 to 500 nm wide and 5 to 90 nm deep with pointed bottoms (Figure 56). Etch pit densities on natural dolomite are highly variable. Some areas have no observable etch pits, only flat faces. In addition, the distribution of etch pits is very heterogeneous in most samples. As stated previously, this makes reporting etch pit densities rather ambiguous.

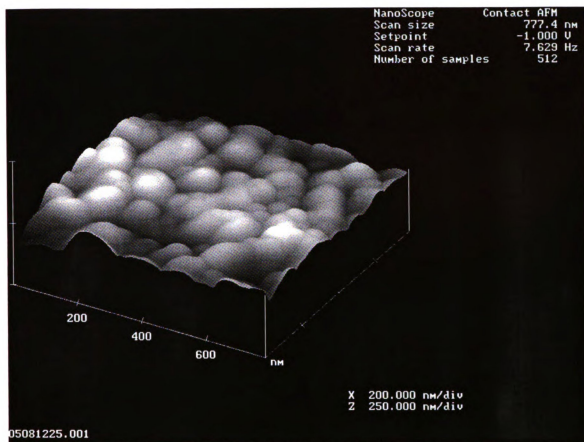


Figure 50. AFM image of an etched natural nonideal dolomite showing pervasive island-covered surface.

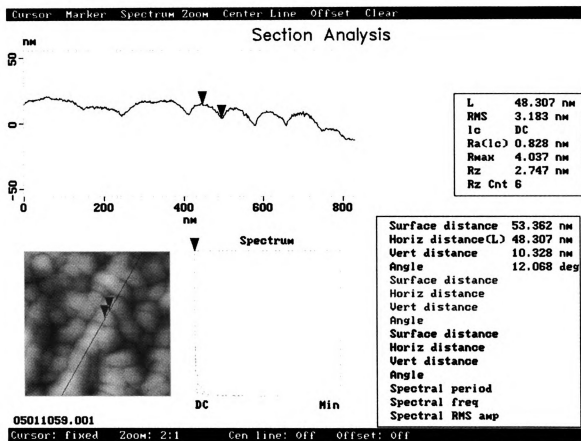


Figure 51. AFM image and cross-section of an etched natural nonideal dolomite showing dissolution island nanopopography.

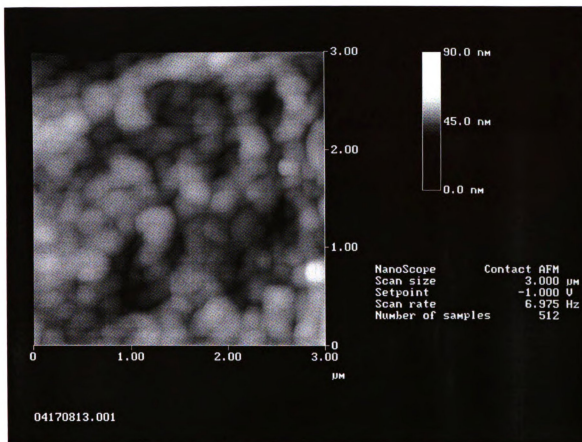


Figure 52. AFM image of an etched natural nonideal dolomite showing an island-covered surface with voids and depressions.

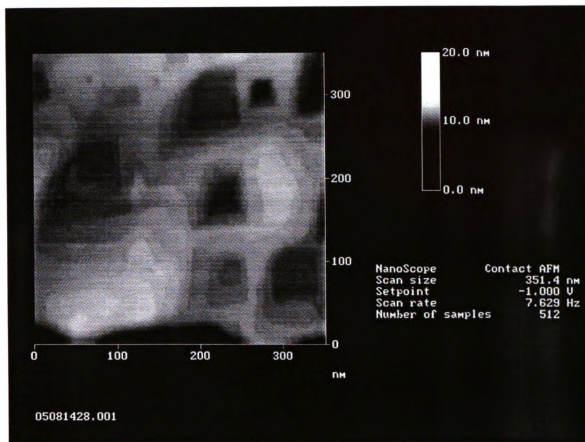


Figure 53. AFM image of an etched natural ideal dolomite showing euhedral etch pits with flat inter-pit layers.

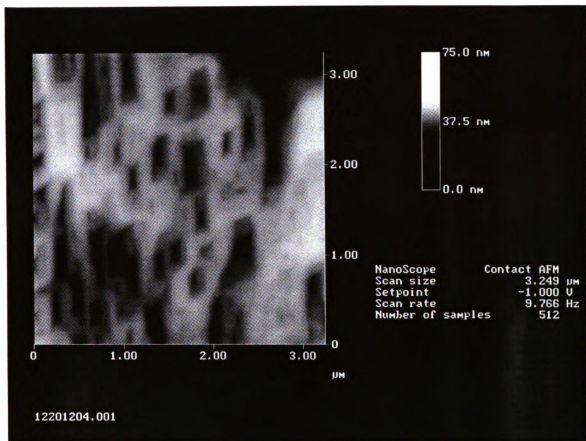


Figure 54. AFM image of an etched natural ideal dolomite showing crystallographically oriented rhombic etch pits.

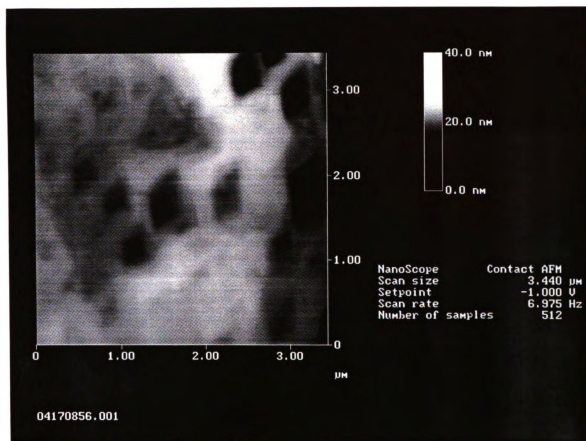


Figure 55. AFM image of an etched natural ideal dolomite showing euhedral etch pits with rhombic shape.

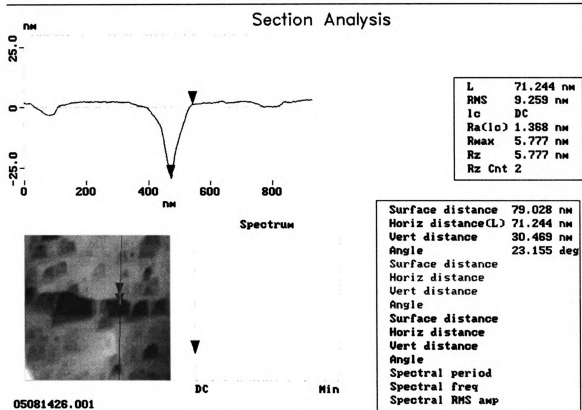


Figure 56. AFM image and cross-section of an etched natural ideal dolomite showing euhedral etch pits with pointed bottoms.

Upon continued dissolution, the surfaces of ideal dolomite are covered with wider, deeper etch pits.

3.i. *Natural Dolomite Surface Nanotopography, SEM*

Unetched natural dolomite surfaces observed with SEM are characterized by a variety of features including cleavage fractures, variously shaped voids, relatively flat surfaces, steps, and debris. This is demonstrated in the SEM image of an ideal dolomite crystal shown in Figure 57. Ultrasonic cleaning and brief periods (30-60 seconds) of chemical etching in 0.5% sulfuric acid removes most surface debris, but doesn't otherwise affect the overall surface topography. Ideal and nonideal dolomites with short etching times exhibit very similar surface features even when viewed at high magnification. Ideal dolomites have relatively flat surfaces with steps and voids. Nonideal dolomites also have relatively flat surfaces with steps and voids (Figure 58). SEM observed dolomite surfaces are highly irregular, yet the commonly observed surface features occur equally on all samples. Longer periods of chemical etching (2-15 minutes) did not accentuate ideal and nonideal dolomite surface nanotopography. In general, dolomite surfaces become much more irregular and pitted over longer etching times. Most dissolution voids observed with SEM are irregular and anhedral in shape, although occasionally some do have straight edges. However, none of the dissolution voids are euhedral like the AFM observed etch pits. For longer etching times (e.g., 10 minutes) some dolomites maintain flat surfaces with a low density of voids, whereas some nonideal dolomite surfaces become highly

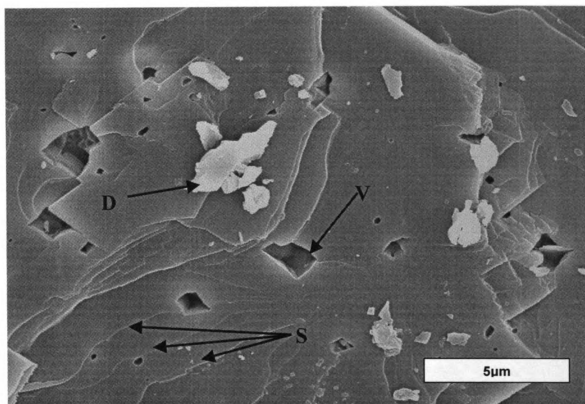


Figure 57. SEM photomicrograph of an unetched natural dolomite surface showing voids (V), steps (S), and debris (D).

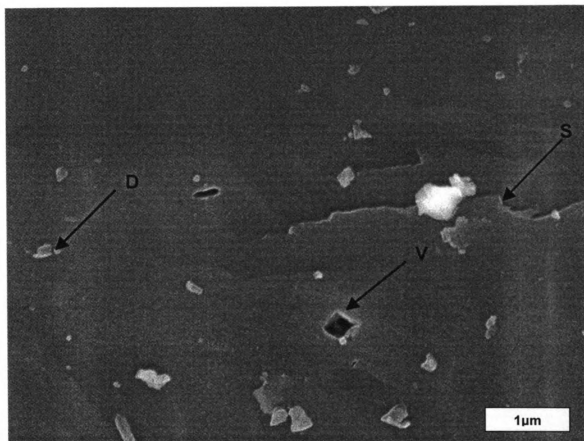


Figure 58. SEM photomicrograph of an etched natural nonideal dolomite surface. Arrows mark voids (V), steps (S), and debris (D).

irregular with many voids (Figure 59). Some dolomite crystals tend to dissolve much more rapidly at the center relative to the outer edges. The SEM observations described here are highly variable and as a result, provide no definitive way of distinguishing between ideal and nonideal dolomite surfaces.

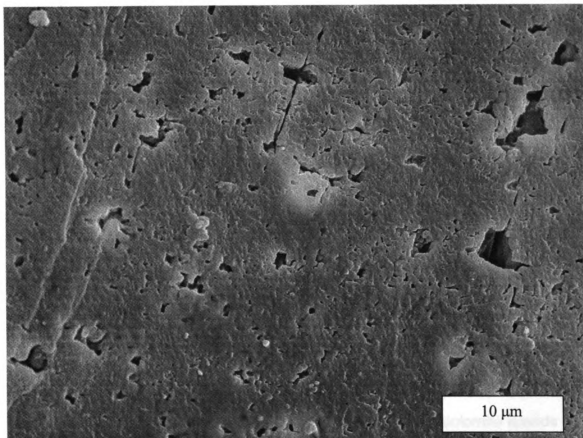


Figure 59. SEM photomicrograph of a natural ideal dolomite showing a highly irregular and dissolved surface after 10 minutes of etching in dilute acid.

4. DISCUSSION

4.a. Islands and Layers Are Growth Features:

The islands and layers observed on the surfaces of synthetic dolomite crystals are interpreted to form during crystal growth, despite the experimental design permitting the possibility that they form by dissolution. Because dolomite, like other carbonate minerals, has retrograde solubility (Nordeng and Sibley, 1994; Langmuir, 1997), dissolution may occur as high-temperature experimental conditions are terminated as bombs are removed from the oven. Prior to reactant depletion, however, solution chemistry is likely buffered by the faster dissolving calcite and/or aragonite reactants (Busenberg and Plummer, 1982). Using the AFM fluid-cell, Kessels et al. (2000) observed that dolomite islands remained stable, whereas adjacent calcite surfaces became covered with dissolution pits as distilled water flowed over the surfaces. This suggests that dolomite growth surfaces are more stable than calcite surfaces in experimental solutions undersaturated with respect to the two minerals. The empirical etching results also indicate that upon dissolution, nonideal dolomites remain covered by islands. This suggests that islands are pervasive throughout the dolomite crystals and are not only formed as a surface feature as reaction vessels cool. Furthermore, the development of euhedral etch pits on etched surfaces of synthetic ideal dolomites demonstrates that islands do not form by dissolution of growth layers.

It is also possible to initially interpret islands as an amorphous precipitate that forms upon cooling of the reaction vessels. Not only are the synthesis experiments carried out within the thermodynamic stability field of dolomite, but amorphous phases would likely have a higher solubility than the underlying crystalline dolomite. As a result, any amorphous phases on the surface would easily dissolve during chemical etching experiments and therefore reveal the underlying dolomite surface growth topography. Again, the chemical etching experiments demonstrate that island nanotopography persists after continued dissolution, further suggesting that islands are pervasive throughout the dolomite crystals and are not superficial precipitates that form when experimental conditions are ended.

Due to the limited resolution of the AFM, growth islands may actually be growth spirals with steps too small to be resolved. However, if mounds are centered on defects (e.g., spiral dislocations), chemical etching should result in etch pit formation at the center of the mound where the defect would be located, because these are areas of enhanced dissolution. Etching of island-covered surfaces uncovers additional islands, whereas etch pits do not form on any of the etched nonideal dolomites.

Layers on the surfaces of ideal synthetic dolomite are observed only in calcite reactant experiments in which all reactants have been consumed. Following reactant depletion, dissolution of ideal synthetic dolomites is not buffered by the presence of calcite, therefore ideal dolomites are even more susceptible to dissolution than nonideal dolomites once experimental conditions

are terminated. Two factors argue against the idea that layers form as a result of dissolution however: 1) The ideal dolomite formed after reactant depletion is considerably more stable than nonideal dolomite because of its stoichiometric composition and relatively high degree of cation order, and 2) Flat layers without etch pits are inconsistent with models of interface-controlled dissolution.

Busenberg and Plummer (1982) showed that dolomite dissolution rates were independent of advection rates under the experimental conditions pH 0-10, 1.5-65°C, P_{CO_2} 0-1atm. Furthermore, the chemical etching results clearly demonstrate that euhedral etch pits form upon dissolution of ideal dolomite. Both observations suggest that over a wide range of conditions, dolomite dissolution is an interface-controlled phenomenon. It can also be reasoned that because 1) chemical etching leads to the development of etch pits on ideal dolomite surfaces, and 2) no euhedral etch pits are observed on layer surfaces during the growth experiments, any dissolution during the growth experiments is insignificant.

4.b. Polynuclear Growth

The growth islands observed on sedimentary minerals like calcite, gypsum, barite, dolomite, and other crystalline materials, are commonly used as evidence for polynuclear crystal growth (Hillner et al., 1992; Dove and Hochella, 1993; Bosbach and Rammensee, 1994; Bosbach et al., 1994, 1998; Pina et al., 1998; Heraty, 1998; Pina et al., 2000; Kessels et al., 2000; Jiang et al., 2001a,b; Pina et al., 2004). During polynuclear growth, simultaneous nucleation events

out-pace lateral attachment to already existing surface features (Nielsen, 1964; Ohara and Reid, 1973). Because nucleation is the most energetically demanding step in the crystal growth process, polynuclear growth is associated with crystal growth in solutions where the degree of supersaturation is relatively high (Nielsen, 1964; Ohara and Reid, 1973; Kirkpatrick, 1981; Sunagawa, 1984; Lasaga, 1990). In supersaturated solutions, small critical nuclei (r^*) are continuously deposited on the crystal surface. Some nuclei attain critical size ($\geq r^*$) and are therefore stable, whereas other nuclei $< r^*$ dissolve back into solution. The size of the critical nucleus (r^*) is dependent on the activation energy of nucleation, which is a function of the supersaturation of the solution and the surface free energy of the nucleus (Nielsen, 1964; Walton, 1969; Ohara and Reid, 1973). Once a nucleus of critical size is deposited on a crystal surface, it may have material attach to its periphery or it may be covered by subsequent nucleation events. As a result, surfaces created during polynuclear growth may be characterized by the presence of growth islands with highly variable sizes.

To establish the similarities between dolomite growth islands observed here and those previously observed on the surfaces of other minerals that have been interpreted as polynuclear growth, it is necessary to outline and review some of the observations that are pertinent to such a comparison, like the size, shape, behavior, and conditions under which growth islands generally occur.

Dove and Hochella (1993) reported that rhombohedral growth islands, which measured 6-9 nm high formed during calcite growth experiments at

relatively high degrees of supersaturation ($\Omega < 2$). Upon continued growth, islands coalesced into even larger islands that measured approximately 200nm in diameter and up to 31nm high. Based on theoretical growth models, Dove and Hochella (1993) interpreted calcite islands as evidence of a polynuclear growth mechanism. They also observed that growth islands were rounded and less euhedral in growth experiments in which a growth inhibitor was used. They suggested that the added growth inhibitor disrupted growth processes, thus resulting in a compromised crystal form. Using *in situ* AFM techniques, Pina et al. (1998) observed the formation of euhedral growth islands on barite surfaces under relatively high degrees of supersaturation ($\Omega = 12$). Islands had straight edges that were oriented in crystallographic continuity with barite crystal faces. Growth islands measured one monolayer high and up to hundreds of nanometers wide. Pina et al. (1998) interpreted islands to be surface nuclei that formed during a polynuclear growth mechanism. Heraty (1998) observed the formation of large calcite growth islands during crystal growth experiments. She observed the formation of growth islands in solutions that were highly supersaturated with respect to calcite ($\Omega = 1.6$ to 10.5). Islands were greater than 50nm high and up to hundreds of nanometers in diameter. Heraty (1998) also demonstrated that the addition of sulfate and phosphate changed growth island morphology from euhedral to round and anhedral (Figure 60). Bosbach et al. (1998) reported the appearance of barite islands nearly 1 μ m in diameter during growth experiments at relatively high degrees of supersaturation. Growth islands were interpreted as evidence of crystal growth by surface nucleation (i.e., polynuclear growth). In

addition, Bosbach et al. (1998) observed that nucleation rates were reduced and island morphology changed dramatically after the addition of a growth inhibitor to barite growth experiments. Comparison of the two island morphologies revealed that inhibitor-free environments exhibited sector-zoned (euhedral) islands, whereas islands grown in solutions with a growth inhibitor had rounded islands without euhedral edges. Porsche et al. (1998) observed the formation rounded “quantum islands” measuring approximately 50-100 nm in diameter and 4-18 nm high that occurred pervasively across the crystal surfaces of synthetic InP and GaInP during growth experiments. Venegues et al. (1998) studied GaN growth on sapphire crystals. TEM cross-sections showed that growth islands with a pyramidal shape were 50nm to 600nm in diameter and 30nm to 250nm high. Kessels et al. (2000) observed rounded growth islands on the surface of high-temperature synthetic dolomite growth surfaces Individual islands measured <20nm high and <200nm wide. Astilleros et al. (2002) observed rounded growth islands forming on calcite surfaces that were tens to hundreds of nanometers in diameter and formed pervasively across crystal surfaces in the presence of Mn, a proposed growth inhibitor. Astilleros et al. (2002) reported a transition from layers to islands on freshly cleaved calcite crystal after changing the concentration of Mn solution. Nuclei were rounded relief features tens to hundred of nanometers in diameter and 1 monolayer in height. Upon continued growth, islands became broader and the surface density of islands increased. Islands eventually coalesced to form layers.

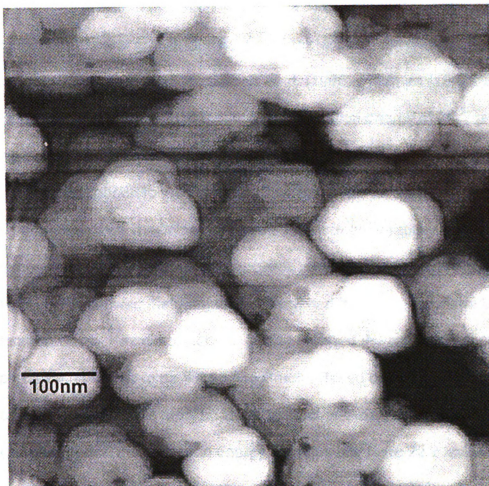


Figure 60. AFM image from Heraty (1998) showing amorphous growth islands on a calcite surface in phosphate-doped experiments.

If magnesium hydration acts as a growth inhibitor to dolomite growth, rounded, anhedral growth islands are consistent with the findings from many other crystal growth studies. Garrels et al. (1960), Hartman (1982), and Lippmann (1973) all argued that the high hydration energy of Mg^{2+} is a kinetic inhibitor of dolomite formation. In order for dolomite to form, Ca^{2+} and Mg^{2+} cations must attach to the crystal surface followed by dehydration and carbonation of each. Calcite has been shown to grow rapidly at relatively low temperatures (Dove and Hochella, 1993), whereas the findings of Sayles and Fyfe (1973) showed that magnesite was very difficult to grow in the lab at low temperatures. Kazmierczak et al. (1982) reported the activation energy for precipitating calcite to be $9.4 \pm 0.9 \text{ kcal mol}^{-1}$. Based on the assumption that calcite and magnesite grow by identical mechanisms, Arvidson and Mackenzie (2000) reported the activation energy of magnesite to be $22.2 \text{ kcal mol}^{-1}$ based on experimental data from Lippmann (1973). This is a difference of $12.8 \text{ kcal mol}^{-1}$ higher than the value for calcite. Arvidson and Mackenzie (2000) argued that if dolomite formation is viewed as a process of creating alternating layers of calcite and magnesite, then the rate of dolomitization is controlled by the formation of the magnesite layer. Because excess calcium increases the free energy of dolomite (Navrotsky and Capobianco, 1987; Chai et al., 1995) calcium will be incorporated if at the given conditions, dehydration of calcium requires less energy than does the dehydration of magnesium (Arvidson and Mackenzie, 2000). Because the activation energy of dolomite is nearly twice that of magnesite based on data from Arvidson and Mackenzie (1997, 2000), cation

ordering, as well as dehydration and carbonation of the Mg^{2+} cation could both be rate-limiting steps in dolomite formation.

A common observation from the calcite, gypsum, and barite growth experiments is that after continued growth, islands often coalesce to form layers (Hillner et al., 1992; Dove and Hochella, 1993; Bosbach and Rammensee, 1994; Bosbach et al., 1994, 1998; Pina et al., 1998; Astilleros et al., 2002). Although layers are observed on dolomite growth surfaces, they appear only after reactant depletion when islands cease to form. These layers are interpreted to form by spiral growth and not from coalescing islands. Individual dolomite islands are much greater than monolayers high and are highly variable in size. If two adjacent islands have slightly different chemical composition or cation order, it would be energetically difficult for the islands to completely grow together because the interface between the islands would have an associated free energy. This would be analogous to soap bubbles that are situated adjacent to one another. The bubbles may collide, but maintain their individuality due to the associated surface tension. Islands may also not form layers, like other minerals, because bombs are removed from the oven in while rapid surface nucleation is still occurring. The dolomite reaction curves show that once dolomite begins to form, it replaces reactants very rapidly. Because of this, islands are constantly being formed on the surface, which may prevent the formation of flat layers. Before multiple islands coalesced to form a flat layer, continued nucleation is likely to occur and deposit more islands on the surface, therefore covering up a flat layer. This is interesting because, upon cooling, the saturation state of

dolomite is increased and conditions tend toward equilibrium. Thus one would expect that the potential for layers to form at the end of an experiment is greater as the chemical conditions change. This is not the case, however; layers are never observed on the surfaces of nonideal dolomites, which form prior to reactant depletion. Heraty (1998) observed island nanotopography in calcite growth experiments persisted during extended periods of growth in the presence of a phosphate growth inhibitor. After two hours of growth at a high degree of supersaturation, the sample was covered with rounded calcite growth islands. Layers from coalescing islands were never observed, but a highly variable surface topography due to different patches of growth islands (figure 69) with variable lateral dimensions and vertical relief was reported as being common.

The observation that synthetic dolomite islands remain the dominant surface feature during chemical etching also supports the interpretation that islands remain pervasive and distinct throughout the crystal. Following this idea, one can also infer that because polynuclear growth occurs throughout the formation of nonideal dolomite and a defect microstructure results from the mismatch between individual islands. This is consistent with the observations of Penn and Banfield (1998), who reported on the formation of dislocations at the interfaces between differently oriented TiO_2 (titania) growth nanoparticles. Nanoparticles measured 5 to 6nm in diameter according to x-ray diffraction peak broadening analysis and HRTEM. Penn and Banfield (1998) showed that during crystal growth, individual titania nanocrystals attached to the crystal growth surface with slight differences in orientation. Dislocations were subsequently

observed to form at these interfaces when adjacent particles were not anatomically aligned. Banfield et al. (2000) suggested that defects between nanoparticles could fundamentally alter the way crystals grow by creating growth-related spiral dislocations for example. The observed nanoparticles may be comparable to the growth islands observed on dolomite surfaces. If there were no mismatch between islands then there would be no energetic drive for dissolution to occur in between individual islands.

Because dolomite islands are consistent in size, shape, and behavior to other previously observed growth islands, they are interpreted in a manner consistent with these studies, as evidence for a polynuclear growth mechanism.

4.c. Spiral Growth

The layers observed on the surfaces of ideal synthetic dolomite crystals are consistent with a number of theoretical growth models. Crystal growth theory predicts that spiral growth dominates at conditions where the free energy drive is relatively low because energy barriers to surface nucleation are circumvented by lateral attachment of growth units to the arm of a screw dislocation. As pointed out by Sunagawa (1977, 1981), spiral growth is the most common growth mechanism found in nature. The most commonly cited feature used as evidence for spiral growth is a multi-layer helical spiral, which occurs on a crystal growth surface (Hillner et al., 1992; Gratz et al., 1993; Dove and Hochella, 1993; Bosbach and Rammensee, 1994; Bosbach et al., 1994, 1998; Pina et al., 1998, 2004; Jiang et al., 2001a). Although layers occur on ideal synthetic dolomite

surfaces after all calcite reactants have been depleted, no multi-layer helical spirals were observed. However, individual layers were observed to merge into crystal surfaces (refer to figures 37a and 37b), thus producing a surface feature geometry that is consistent with an emerging screw dislocation (see figure 2). The emerging layers on dolomite growth surfaces are consistent with those observed at spiral dislocation outcrops on other crystalline solids (De Yoreo et al., 1997; Maiwa et al., 1998; Pina et al., 1998; Jiang et al., 2001). Pina et al. (1998) observed that emerging layers on the surfaces of barite later became the sites of developing multi-layer growth spirals after further growth in conditions at relatively low supersaturation. In the case of synthetic dolomite, multi-layer growth spirals may not be as common as in other minerals, for numerous reasons. Individual layers produced at growth spirals may converge before a large helical feature is produced. Additionally, the Burgers vector of the dislocation may be very small, which could cause spirals to be more laterally extensive and less vertically prominent. Paquette and Reeder (1990, 1995) both showed that at low to moderate degrees of supersaturation, single growth spirals on calcite commonly spread laterally for hundreds of micrometers, but may rise less than 5 microns above the crystal surface. Assuming calcite and dolomite are similar in this respect, it would be impossible to image laterally extensive dolomite growth spirals in their entirety because the scan sizes used in AFM would not be large enough.

Layers are also consistent with the mononuclear growth model. Recall, however, that mononuclear growth is predicted to be operational at conditions in

which the degree of free energy drive is relatively low, yet the mechanism requires the energetically difficult step of surface nucleation for each new layer that forms on a crystal surface. According to Nielsen (1964), surface nucleation is extremely difficult at conditions near equilibrium and as a result, mononuclear growth is a relatively inefficient growth mechanism. Furthermore, the observation that multiple dolomite growth layers with roughly parallel steps that are stacked on top of one another is inconsistent with the mononuclear growth model. The model is developed on the premise that only one nucleation event occurs per layer (hence the term mononuclear) because it is far easier to continue attaching growth units to energetically favorable step and kink sites on an already existing layer than to nucleate new layers.

Kessels et al. (2000) suggested that the stacked layers they observed on synthetic dolomite may form in a manner consistent with the birth and spread model. Birth and spread is somewhat of a hybrid between polynuclear growth and mononuclear growth in that it is characterized by multiple nucleation events, but is ultimately out-paced by the lateral growth component. In this case, attachment of new growth units along the periphery of different surface nuclei creates layers that grow laterally until they intersect and fuse with other layers. Therefore, the birth and spread model could explain some of the geometries observed on synthetic dolomite surfaces, such as stacked layers. In the birth and spread model, individual surface nuclei are responsible for providing attachment sites for new material. Because of this, one would expect to see layers forming at the different nuclei. However, separate, laterally extensive

growth layers within the same plane were not observed. Layers on dolomite are instead stacked on top of one another with steps that are roughly parallel in a manner similar to the periphery of a helical spiral dislocation (Dove and Hochella, 1993; Gratz et al., 1993; De Yoreo et al., 1997; Maiwa et al., 1998; Bosbach et al., 1998; Pina et al., 1998; Jiang et al., 2001). Even more important to the interpretation that layers form by spiral growth is the observation that layers have steps that merge into crystal surfaces and that deep euhedral etch pits develop on etched layer surfaces.

The interpretation that layers are evidence of a spiral growth mechanism is further supported by the fact that growth layers are observed in conjunction with V-shaped euhedral etch pits that form as a result of chemical etching. Euhedral etch pits are hundreds of monolayers deep and are therefore indicative of dissolution at an extended line defect, such as a screw dislocation (see reviews by Heimann, 1982; Brantley et al., 1986; Lasaga and Blum, 1986; Sangwal, 1987). Extended line defects are the site of preferential dissolution because defects have an associated excess free energy (Lasaga, 1990). As a result, dissolution can occur more readily along the defect, which results in a V-shaped etch pit. Point defects, such as precipitates and inclusions may also be sites of etch pits because they too provide an area of elevated reactivity. Point defects, however, only form shallow etch pits because once the pit forms and the point defect is eliminated, there is no drive for further dissolution in a direction normal to the crystal surface. Joshi et al. (1970) and Joshi and Paul (1973) observed the formation of two types of etch pits in synthetic quartz; deep

pyramidal pits and shallow flat-bottomed pits. Upon prolonged etching they noted that the pyramidal pits grew deeper, but that the shallow pits disappeared. They argued that shallow, flat bottom pits corresponded to point defects whereas the deep pointed pits formed at extended line defects. Furthermore, Lin and Shen (1993) showed with TEM that dislocations in willemite corresponded to etch pits that formed on the surface of etched crystals.

Etch pit distributions on synthetic and natural dolomites were observed to be highly variable. Furthermore, most samples had very heterogeneous distributions of etch pits. This is consistent with the findings of Reeder (1982) who reported that dolomite dislocation densities observed with TEM appeared variable and heterogeneous. At this point, it is important to note that deep, V-shaped etch pits may equally form at surface outcrops of edge dislocations as well as a spiral dislocations. Crystal growth naturally introduces any number of lattice defects, but screw dislocations are the only known defect that can facilitate crystal growth. Both edge and screw dislocations may form during growth or deformation, but screw and edge dislocations have very different roles during crystal growth. Spiral (screw) dislocations generally take an active role during growth, whereas edge dislocations, although potentially formed during growth, do not actively participate in the crystal growth process. Etch pits are commonly oriented normal to the growth surface and in many instances, they are slightly tilted and asymmetric. Klapper (1980) showed that spiral dislocations are commonly linear to sublinear and are most often oriented within ~15 degrees of the growth normal in a particular growth sector. As Reeder (1992) points out,

dislocations of this type are common in dolomite. Reeder (1982, 2000) also reported that almost all dislocations are aligned nearly normal to the growth surface in dolomite.

Edge dislocations may also form from processes not associated with growth. In natural crystals, deformation is probably the most frequent cause of this (Reeder, 1982). The synthetic dolomites studied here were never exposed to conditions in which significant deformation would occur. A number of workers using TEM have reported that ideal dolomites have relatively homogeneous microstructures with only dislocations and growth defects (Reeder, 1981; Blake et al., 1982). Reeder (1992) observed that other than in cases where geologic histories preclude high temperatures and stresses, many of the microstructures in sedimentary carbonates have resulted from crystal growth. Barber (1977) noted distinct differences in the dislocation microstructure of dolomite compared to other sedimentary carbonate minerals. Most importantly, dolomite has been observed with TEM to have a significantly lower defect density than limestone or calcite. These differences were attributed to the strong crystallographic control of dislocation orientation (noted above) and to the fact that dolomite has fewer deformation mechanisms than calcite. Rosen et al. (1989) reported a higher density of dislocations in the ideal dolomites compared to the nonideal dolomites with a heterogeneous microstructure that he studied. His results suggest that extended line defects may be more common in ideal dolomites whereas a more heterogeneous microstructure is consistent with a pervasive defect structure.

Radke and Mathis (1980) proposed a model to explain the distinctive macroscopically visible curved faces on saddle dolomite in which Ca substitution for Mg was accompanied by the introduction of edge dislocations. Subsequent TEM work by Reeder (1982) of saddle dolomite showed that many saddle dolomites were characterized by a pervasive array of stacking faults. In addition, parallel growth dislocations were associated with the stacking faults. Reeder (1982) interpreted these to represent active screw dislocations within the different growth sectors.

Although theoretically possible, based on the current observations there is no unequivocal method to distinguish between an etch pit that formed at a screw dislocation, which was utilized during crystal growth and a pit that formed at an edge dislocation. However, the presence of euhedral V-shaped euhedral etch-pits in conjunction with layers that merge into the crystal observed on synthetic dolomite growth surfaces supports the interpretation that ideal dolomites grow primarily by a spiral growth mechanism. In as much as there is no practical way of distinguishing between euhedral etch pits formed by dissolution at screw dislocations that facilitated growth and other types of dislocations, the possibility is very likely that some of the euhedral etch pits are related to edge and perhaps inactive screw dislocations. Based on the above arguments, deformation seems to be an unlikely scenario to explain the introduction of dislocations in dolomite. Furthermore the orientation of most line defects in dolomite, as viewed with TEM, seem to be consistent with that of screw dislocations. These observations in conjunction with the layers observed on synthetic dolomite growth surfaces leads

to the conclusion that a significant proportion of euhedral etch pits on etched dolomite surfaces are related to spiral dislocations that facilitated crystal growth. Otherwise it is extremely difficult to explain how these crystals grew.

4.d. Transition From Polynuclear To Spiral Growth

Crystal growth theory predicts that polynuclear growth and spiral growth dominate under different thermodynamic conditions. Polynuclear growth operates under conditions where the free energy drive is relatively high (Nielsen, 1962; Ohara and Reid, 1973; Sunagawa, 1984). Because polynuclear growth is limited by the formation of surface nuclei, the free energy drive in solution must be great enough to overcome energetic barriers to surface nucleation in order to grow by polynuclear growth. Spiral growth, on the other hand, is predicted for conditions in which the free energy drive is relatively low. Because spiral growth occurs at energetically favorable step and kink sites created on the crystal surface by screw dislocations, the energetically difficult step of surface nucleation is circumvented. In addition to theoretical arguments as a framework for discussing competing growth mechanisms, relative free energies of the crystal surfaces provide a foundation to explain why islands form at relatively high free energy drive and layers form at relatively low free energy drive. Because islands are characterized by a rougher crystal surface compared to layers, islands are indicative of a higher surface free energy (Kessels et al., 2000). Regardless of whether islands nucleate on crystalline defects, like dislocations or defect-free surfaces, surface features with greater surface area require a higher free energy

drive to be stable. Therefore, one might expect the growth mechanism transition during the calcite reactant experiments (from islands to layers at reactant depletion) depicted in figure 61 to correspond to a change from relatively high free energy drive to a relatively low free energy drive in the system.

4.d.1. Energy: According to the experimental design (refer to equation 1), the reactants (calcite and/or aragonite) provided the only source of carbonate for dolomite formation. From pH measurements, Sibley (1990) inferred that calcite dissolution in experimental bombs comes to a steady state within approximately 1 hour at room temperature. At elevated temperatures calcite dissolution is faster, therefore experimental conditions should achieve equilibrium with respect to calcite relatively fast. As a result, hydrothermal bombs are likely to be saturated with respect to calcite (or aragonite) before dolomite begins to form. Because calcite solubility is assumed, the solution $Mg^{2+}:Ca^{2+}$ ratio dictates the free energy drive in the reaction vessels. According to LeChatelier's Principle, a higher solution $Mg^{2+}:Ca^{2+}$ ratio corresponds to a higher degree of free energy drive for the calcite to dolomite replacement reaction (see equation 3) because increasing the reactants should drive the reaction forward, thus producing more product. To this end, higher solution $Mg^{2+}:Ca^{2+}$ ratios have a relatively high free energy drive and lower solution $Mg^{2+}:Ca^{2+}$ ratios result in a relatively low free energy drive for the calcite to dolomite replacement reaction. Based on crystal growth theory, one would predict polynuclear growth to occur at relatively high solution $Mg^{2+}:Ca^{2+}$ ratios and spiral growth at relatively low solution $Mg^{2+}:Ca^{2+}$ ratios. Over the entire range of solution $Mg^{2+}:Ca^{2+}$ conditions studied here,

however, polynuclear growth dominates until reactant depletion when all products are ordered, stoichiometric dolomite. Even the experiment with the lowest initial $\text{Mg}^{2+}:\text{Ca}^{2+}$ ratio (i.e., 0.43) forms dolomite by polynuclear growth prior to reactant depletion. Furthermore, the highest solution $\text{Mg}^{2+}:\text{Ca}^{2+}$ ratio (i.e., 1.5) invariably makes the transition from polynuclear to spiral growth after the calcite is completely consumed. It should be noted at this point that experiments with low solution $\text{Mg}^{2+}:\text{Ca}^{2+}$ ratios (e.g., < 0.66) did not proceed to complete reactant depletion over the duration of the experiment and as a result, never approached the point where the transition from islands to layers is expected. Perhaps one of the most interesting results from these experiments is that in spite of theoretical predictions, crystal growth mechanisms in dolomite are not a function of the $\text{Mg}^{2+}:\text{Ca}^{2+}$ ratio in solution.

A measure of free energy drive for dolomite formation can also be inferred from the reaction rates for the various experiments. Slow reaction rates should indicate conditions nearer to equilibrium, whereas rapid dolomitization should indicate conditions with a relatively high free energy drive. The data show that relatively low solution $\text{Mg}^{2+}:\text{Ca}^{2+}$ ratios corresponded to slow reaction rates and relatively high $\text{Mg}^{2+}:\text{Ca}^{2+}$ ratios correspond to fast reaction rates. Therefore, reaction rates are consistent with the solution $\text{Mg}^{2+}:\text{Ca}^{2+}$ ratios as an indication of the free energy drive in the hydrothermal bombs. In the case of low $\text{Mg}^{2+}:\text{Ca}^{2+}$ ratios, it was difficult to produce dolomite even over very long periods of time. In the experiment with solution $\text{Mg}^{2+}:\text{Ca}^{2+} = 0.43$, for example, one experiment took approximately 1362 hours to form 30% dolomite, compared to only ~28 hours for

the experiment with a solution $\text{Mg}^{2+}:\text{Ca}^{2+}$ ratio = 1.5. Below a solution ratio of $\text{Mg}^{2+}:\text{Ca}^{2+} = 0.66$, the time required to form dolomite increased exponentially with a decreasing solution $\text{Mg}^{2+}:\text{Ca}^{2+}$ ratio (see Figures 12a and 12b). Extrapolating the curve of reaction rate vs. solution $\text{Mg}^{2+}:\text{Ca}^{2+}$ ratio, shows that an initial solution $\text{Mg}^{2+}:\text{Ca}^{2+} = 0.43$ requires a very long time to produce dolomite. Presumably, these long reaction times indicate that an initial $\text{Mg}^{2+}:\text{Ca}^{2+}$ value of 0.43 is seemingly close to the calcite-dolomite equilibrium or at least close enough to it where it is impossible to replace calcite with dolomite on reasonable laboratory time-scales (e.g., months). Furthermore, as the reaction progresses, solution $\text{Mg}^{2+}:\text{Ca}^{2+}$ ratios decrease as dolomite forms at the expense of calcite. Dolomite sequesters Mg^{2+} from solution and liberates Ca^{2+} into solution as the reaction proceeds. Take for example the experiment with an initial solution $\text{Mg}^{2+}:\text{Ca}^{2+}$ of 0.43 (sample 6-17-04-G). At the time of reaction termination (1122 hours), 66% products had formed. As outlined in Table 3, the $\text{Mg}^{2+}:\text{Ca}^{2+}$ ratio in solution would have dropped to below 0.38. The actual calculation yields a solution $\text{Mg}^{2+}:\text{Ca}^{2+}$ ratio of 0.36 when 66% of the calcite is replaced by dolomite with 61 mole% CaCO_3 . Therefore a $\text{Mg}^{2+}:\text{Ca}^{2+}$ ratio of 0.36 is near, but still above the dolomite-calcite stability boundary under the given temperature conditions. Morrow et al. (1994) determined $\log (a_{\text{Ca}^{2+}} / a_{\text{Mg}^{2+}})$ values for the calcite-dolomite stability boundary between 220°C and 240°C for a series of synthetic and natural carbonates to be between 0.4 and 0.9. Converting these values to $\text{Mg}^{2+}:\text{Ca}^{2+}$ ratios yield a calcite-dolomite boundary near 0.4 to 0.125, which is in good agreement with our results. This is also consistent with the

experimental data of Baker and Kastner (1981) and excellent agreement with the results of Rosenberg and Holland (1964). These results suggest that our experiment with final solution $\text{Mg}^{2+}:\text{Ca}^{2+}$ ratios of 0.36 is near the calcite-dolomite stability boundary and therefore solutions are very near equilibrium with respect to dolomite. Therefore, after reactant depletion, when solution $\text{Mg}^{2+}:\text{Ca}^{2+}$ ratios are at their lowest levels (and solid Mg:Ca ratios are at their highest), conditions should be ideal to promote the transition from polynuclear to spiral growth. However, none of the solutions, particularly the experiments with relatively high $\text{Mg}^{2+}:\text{Ca}^{2+}$ ratios, had solution $\text{Mg}^{2+}:\text{Ca}^{2+}$ ratios that approached the lowest starting $\text{Mg}^{2+}:\text{Ca}^{2+}$ ratio of 0.43. This point is important because the experiment with an initial solution $\text{Mg}^{2+}:\text{Ca}^{2+}$ ratio = 0.43 (final $\text{Mg}^{2+}:\text{Ca}^{2+}$ ratio = 0.362) produced islands.

According to the findings presented here, growth mechanisms in dolomite are inconsistent with crystal growth theory in that a low free energy drive with respect to dolomite (i.e. low solution $\text{Mg}^{2+}:\text{Ca}^{2+}$) does not necessarily promote growth by a spiral mechanism before reactant depletion. Likewise, experiments with high free energy drive (i.e. high solution $\text{Mg}^{2+}:\text{Ca}^{2+}$) still proceed to spiral growth after reactant depletion.

Dolomite crystal growth may be analogous to the observations of Dove and Hochella (1993) for calcite nucleation and growth in the presence of growth inhibitors. They showed that at high degrees of supersaturation, surface nucleation continued unimpeded in the presence of phosphate, but that normal growth was obstructed as evidenced by the formation of amorphous nuclei. This

observation was interpreted to reflect surface roughening caused by the sorption of phosphate, which blocks lateral growth sites on calcium carbonate nuclei. If hydrated magnesium acts as a growth inhibitor to dolomite formation, polynuclear growth may dominate over a wide range of conditions because spiral growth is prevented because lateral attachment sites are poisoned.

Although the dolomitization reaction is typically expressed as a replacement reaction in which calcite is replaced by dolomite (refer to equation 1), experimental findings suggest there are, in effect, two reactions that occur in the overall transformation between calcite and ideal dolomite. The first reaction proceeds as calcite is replaced by nonideal dolomite (Equation 4) and the second reaction occurs as nonideal dolomite is replaced by ideal dolomite (Equation 5).



Nonideal dolomite always forms by polynuclear growth and ideal dolomite forms by spiral growth. Therefore, each step in the overall reaction corresponds to a different growth mechanism. The calcite to nonideal dolomite reaction occurs by polynuclear growth, whereas the nonideal dolomite to ideal dolomite reaction proceeds by spiral growth. Because the mechanism transitions from polynuclear to spiral growth after reactant depletion, it might be predicted based on crystal growth theory that the free energy drive is lowered after reactant

depletion. More specifically, that the free energy drive associated with the calcite to nonideal dolomite reaction (and polynuclear growth) is higher than the free energy drive associated with the nonideal dolomite to ideal dolomite reaction (and spiral growth).

The easiest way to examine how the free energy drive for dolomitization changes at reactant depletion is to compare the actual free energies of reaction for the calcite to nonideal dolomite and nonideal dolomite to ideal dolomite reactions. By doing this it may be possible to better understand the factors responsible for changing growth mechanisms after reactant depletion. An important equation to consider when comparing the free energies of reaction is Equation 6:

$$\Delta G_{rxn} = \Delta G_{rxn}^0 + RT \ln Q \quad (\text{Equation 6})$$

In this equation, ΔG_{rxn} is the free energy of reaction, ΔG_{rxn}^0 is the standard free energy of reaction ($\Delta G_{products}^0 - \Delta G_{reactants}^0$), R is the gas constant, T is temperature, and Q is the $\text{Ca}^{2+}:\text{Mg}^{2+}$ activity ratio in solution ($\text{Mg}^{2+}:\text{Ca}^{2+}$) divided by the equilibrium constant (K). In order to solve for the free energy of reaction, one must know the standard free energies for nonideal and ideal dolomite.

Following an approach by Navrotsky and Loucks (1977), Helgeson et al. (1978) used Bragg-William theory (Bragg and Williams, 1934) to determine the thermodynamic consequences of order-disorder in dolomite. According to Helgeson et al. (1978), the standard free energies of formation for a completely

ordered and disordered dolomite are $\Delta G^{\circ}_{\text{formation}} = -517.98\text{kcal/mol}$ and $\Delta G^{\circ}_{\text{formation}} = -515.873\text{kcal/mol}$, respectively. Navrotsky and Capiobanco (1987) determined the enthalpy of formation for an ideal dolomite before and after annealing at 1250°C. Using this value they calculated that the enthalpy of complete cation disorder was approximately 12kJ/mol. Subsequent work by Chai and Navrotsky (1996) and Navrotsky et al. (1999) suggest that this value is even greater at about 20-30kJ/mol. The work of Chai et al. (1995) showed that the enthalpy of formation of natural dolomites with variable Ca content, increased from -10kJ/mol for a nearly stoichiometric sample to +10kJ/mol for the most calcian samples (6 mole% excess calcium). Rock et al. (2001) showed that was shown that standard free energy of formation values for dolomite compiled from various studies ranged from as high as -507.13kcal/mol to as low as -519.25kcal/mol (Wagman et al., 1982; Garrels et al., 1960; Naumov et al., 1974; Robie et al., 1978). Because these values are highly variable, it is still unclear as to what impact Ca-Mg composition and cation order have on the relative energetics of dolomite (Reeder, 2000).

This issue is similar to the problem encountered in assessing magnesium calcite stability because of issues related to whether compositions reflect true thermodynamic equilibrium or kinetically controlled processes (Mackenzie et al., 1983; Arvidson and Mackenzie, 2000). If the free energy drive is responsible for changing growth mechanisms at reactant depletion, it can be reasoned that difference between the standard free energies of formation for nonideal dolomites with islands and ideal dolomites with layers must be considerably

smaller than those contributed by Helgeson et al. (1978). In the same respect, it is important to understand that much of this work indicates that cation order-disorder has significant effects on the thermodynamic properties of dolomite. According to Land (1998), the uncertainties about quantitative effects of stoichiometry and ordering on dolomite solubility remain high. Therefore there is no accurate way of determining the thermodynamic effects on growth mechanism transformation at reactant depletion.

4.d.2. Carbonate: Because the thermodynamic framework for discussing growth mechanisms during the transition between calcite, nonideal dolomite, and ideal dolomite is poorly constrained, we turn to kinetic considerations for an alternative approach. Although dolomitization is written as a replacement reaction, it ultimately proceeds via solution because the reactants must pass through the state of dissolved ionized species (Lippmann, 1973). As a result, the dolomitization reaction can be also written as a dissolution-precipitation reaction:



Although the exact concentrations of calcium, magnesium, and carbonate play no role in determining the free energy drive for dolomitization of $CaCO_3$ (because thermodynamic stability is a function of the $Ca^{2+}:Mg^{2+}$ in solution assuming the solution has equilibrated with calcite), Equation 7 suggests that dolomite kinetics are related to the availability of the reactants, $[Ca^{2+}] [Mg^{2+}] [CO_3^{2-}]$. According to

kinetic growth theory, a larger supply of reactants should help to produce dolomite.

Experimental solutions initially have high concentrations Ca^{2+} and Mg^{2+} , but lack carbonate until calcite begins to dissolve. Although these conditions are not strictly true in nature, they are comparable since seawater's carbonate concentration is lower than the concentrations of Ca^{2+} and Mg^{2+} by approximately two orders of magnitude. Because carbonate concentration in the reaction vessels is dictated by reactant solubility, changes in reactant solubility will affect carbonate activity and, in turn, the ion activity product. At reactant depletion, the solution $a_{\text{Ca}^{2+}}:a_{\text{Mg}^{2+}}$ is effectively constant so the only significant change to occur in solution chemistry is when initial reactants are exhausted and the availability of carbonate is reduced. Therefore, the activity of the carbonate ion in bomb solutions may be the principle variable affecting reaction kinetics and growth mechanisms in the dolomitization reaction.

Although the concentrations of Ca^{2+} , Mg^{2+} , and CO_3^{2-} cannot be directly measured in the reaction vessels during an experiment, the concentration of CO_3^{2-} must have decreased after reaction completion when the calcite was completely consumed and all products were 100% stoichiometric dolomite. At room temperature calcite is more soluble than dolomite and as a result the concentration of carbonate ions will be greater in solutions that are able to equilibrate with calcite. Furthermore, carbonate mineral solubility decreases as temperature increases (exothermic heat of dissolution). This effect is further driven by a decrease in CO_2 solubility with increasing temperature. According to

Langmuir (1997), the relative solubility differences between calcite and dolomite are exacerbated at higher temperatures. Based on thermodynamic data from Nordstrom et al. (1990), Robie et al. (1978), and Tanger and Helgeson (1988), Langmuir (1997) used Equation 8 to calculate the solubility of dolomite as a function of temperature:

$$-\log K_{sp}(\text{dolomite}) = 175.90 + 6835.4/T(K) + 68.727 \log T(K) \quad (\text{Equation 8})$$

According to Langmuir (1997), the solubility of dolomite (based on $K_{sp} = 10^{-17.09}$ at 25°C) decreases nearly 14-fold between 0-90°C, whereas the experimentally determined solubility of calcite reported by Busenberg and Plummer (1982) decreases only six-fold. Assuming this is applicable to the range of conditions studied here, the relative solubility differences between calcite and dolomite are further enhanced by the high temperatures used in the experiments.

Thermodynamic data compiled in Carpenter (1980) also show that for a given solution $\text{Ca}^{2+}/\text{Mg}^{2+}$ ratio, increasing the temperature will shift a solution farther into the dolomite stability field and farther from calcite-dolomite equilibrium. This further confirms that at higher temperatures, dolomite solubility decreases relative to the solubility of calcite. The $K_{sp} = 10^{-17.09}$ at 25°C dolomite used in Langmuir (1997) is very similar to the K_{sp} for the dolomite reported by Robie et al. (1978) that was inferred to be representative of a relatively ideal, but not perfectly ideal dolomite (like the one reported in Helgeson et al., 1978). Because nonideal dolomite acts as the carbonate source (i.e., the reactant) for the formation of

ideal dolomite after reactant depletion, differences in the relative solubilities of calcite and nonideal dolomite at high temperatures may be sufficient to explain the change in growth mechanisms after reactant depletion. Assuming that it approaches equilibrium, carbonate activity must be lowered after calcite is consumed because nonideal dolomite solubility is lower than calcite solubility. As stated previously, the $\text{Mg}^{2+}:\text{Ca}^{2+}$ ratio of the solution is relatively constant because the nonideal dolomite is already stoichiometric. As calcite is consumed and relatively well-ordered stoichiometric dolomite begins to form at the expense of relatively poorly ordered stoichiometric dolomite, carbonate activity $[\text{CO}_3^{2-}]$ in solution decreases because the solubility of the new reactant (nonideal dolomite) is lower than the solubility of the initial reactant (calcite). Therefore, less carbonate is available for dolomite formation once calcite is consumed and the growth mechanism changes. Again, it is important to note that changes in solution chemistry at reaction completion do not affect the thermodynamic stability with respect to dolomite because the energetic drive in the bombs doesn't depend on the carbonate activity. Therefore the changing surface nanotopography from islands to layers at reaction completion may correspond to a kinetic effect related to $[\text{CO}_3^{2-}]$.

The hypothesis that carbonate activity in the hydrothermal bombs is the major factor in determining reaction kinetics and growth mechanisms in dolomite is also consistent with the results from our aragonite experiments. The solubility products of calcite and aragonite at 25°C are $K_{sp} = 10^{-8.52}$ and $K_{sp} = 10^{-8.36}$, respectively (Helgeson et al., 1978). According to the data compiled by

Carpenter (1980) the differences in calcite and aragonite solubility are exaggerated by more than two-fold at 90°C. Because of the high concentration of Ca^{2+} and Mg^{2+} ions in the initial dolomitizing solutions, the compositional effects of aragonite's greater solubility on the initial solution $\text{Mg}^{2+}:\text{Ca}^{2+}$ ratio will be relatively minor (approximately 1.2% at 25°C). Conversely, the solubility of aragonite does lead to a more significant change in the concentration of carbonate in solution. Because there is no initial carbonate, carbonate concentration is more dramatically affected by the solubility of the precursor phase. Based on data reported in Langmuir (1997), the carbonate concentration is approximately 1.9% greater at 25°C, 2.0% greater at 50°C, and 4.4% greater at 90°C in solutions with a mixture of aragonite and calcite, than in experiments with only calcite. The relative differences in solubility of calcite and aragonite are likely to increase with temperature in a manner consistent with the changes between 25°C, 50°C, and 90°C. Assuming a linear relationship between temperature and the relative solubilities of aragonite and calcite (a conservative estimate based on the data above), it is apparent that carbonate concentration in solution is approximately 10% greater at 218°C in aragonite reactant experiments vs. calcite reactant experiments.

Preferential replacement of aragonite when both aragonite and calcite are present can be explained by the fact that the ΔG_{rxn} for the aragonite to dolomite reaction is greater than the ΔG_{rxn} for the calcite to dolomite reaction. Therefore, according to thermodynamic arguments aragonite should dolomitize faster than calcite. However, because thermodynamic factors are unable to fully explain

other aspects of dolomitization kinetics, the role of carbonate availability will be examined. Although the reactant surface area was not determined, the aragonite reactants are finer grained than the calcite reactants. Furthermore, the solubility of aragonite is greater than that of calcite so the dissolution of aragonite must have occurred much more rapidly than the dissolution of calcite and as a result the availability of carbonate for dolomite formation is significantly higher in the aragonite experiments. Selective replacement of aragonite in the aragonite reactant experiments (calcite-aragonite mixture) further stresses the importance of carbonate supply in the dolomitization reaction. It was shown earlier that aragonite's higher solubility would lead to more Ca^{2+} in solution and in turn would slightly reduce the solution $\text{Mg}^{2+}:\text{Ca}^{2+}$. Based on findings from the calcite reactant experiments, a lower solution $\text{Mg}^{2+}:\text{Ca}^{2+}$ ratio should slow the rate of dolomitization. However, the rate of dolomitization was nearly three times faster in the aragonite experiments than any of the calcite experiments. Even the highest solution $\text{Mg}^{2+}:\text{Ca}^{2+}$ ratio in the calcite reactant experiments ($\text{Mg}^{2+}:\text{Ca}^{2+} = 1.5$) took nearly three times longer than the aragonite reactant experiment with a solution $\text{Mg}^{2+}:\text{Ca}^{2+}$ ratio of 1.0. This suggests that the carbonate supply to solution, which is dictated by the solubility of the precursor, has a dramatic effect on dolomite growth.

Dolomite and calcite belong to the same crystal system, whereas aragonite and dolomite are different. Therefore one would expect dolomite to have a better lattice match with calcite and therefore grow easier on calcite, but the dolomite always replaces aragonite before calcite in these experiments. The

concentration of carbonate ions is presumed to be higher near aragonite surfaces during the reaction. This effect is enhanced once calcite solubility is reached in the bombs because further calcite dissolution is prevented and so local zones around aragonite have high carbonate concentrations relative to the calcite surfaces. The aragonite reactants were finer than the calcite reactants and this is likely partly responsible for the increased reaction rate in aragonite reactant experiments. In fact, Sibley and Bartlett (1987) showed that increasing the reactant surface area increased dolomitization rates. They also showed, however, that in experiments comparing the rates of aragonite and calcite reactants of the same size, aragonite was dolomitized significantly faster than calcite. Unfortunately, separating the effects of surface area and mineralogy are difficult given the current data.

In addition to the observation that dolomite selectively replaces aragonite when both aragonite and calcite are present, another observation in support of the carbonate supply argument is that dolomite crystals on aragonite are randomly oriented. This is in contrast to dolomite on calcite, which is always in crystallographic continuity with the calcite substrate. In terms of surface free energy, dolomite nucleation should be much easier on calcite than on aragonite because calcite and dolomite have crystal systems that are much more alike.

The inference that carbonate activity is an important factor in dolomite growth is also consistent with the observation that dolomite forms preferentially on edges and corners of aragonite and calcite in high-temperature synthesis experiments. According to a surface energy standpoint, edges and corners are

poor nucleation sites. However, calcite should dissolve faster in areas, like edges and corners because of the high surface area to volume ratio. Therefore one may expect to find the highest concentration of carbonate near edges and corners during calcite dissolution. Edges and corners may also be the best conversion sites if dolomite nuclei are formed by exchanging Mg^{2+} ions for Ca^{2+} ions in the existing calcite crystal. Although this hypothesis was not tested, it is consistent with the observation that dolomite forms in crystallographic continuity with the calcite substrate.

Lippmann (1967) showed that adding carbonate to $MgCl_2$ solutions allowed norsethite, an ordered, double carbonate mineral $[BaMg(CO_3)_2]$, to replace witherite $[BaCO_3]$ at 20°C and 1 atm. Previously, Chang (1964) showed norsethite could be easily formed by replacing witherite in $MgCl_2$ solutions at 500°C and 15kbar pressure, but witherite could be kept in magnesium chloride solutions with various concentrations for months and years at low-temperature without any evidence of replacement by norsethite (Lippmann, 1973). Forming norsethite by replacement of witherite was argued by Lippmann (1973) to be analogous to dolomitization of calcite. However, even with the addition of carbonate to dolomitization solutions, Lippmann (1973) was unable to form detectable amounts of dolomite in a year. He argued that the problem with dolomitization lies in the similar coordination numbers of Ca and Mg. Because of their larger size, calcium cations are dehydrated easier than magnesium cations and are therefore more readily incorporated into magnesium sites (the enthalpy of hydration for Mg is approximately 20% greater than that of Ca). This argument

exemplifies Graf and Goldsmith's (1956), "simplicity principle", which attempted to explain the occurrence of metastable magnesium-calcites and disordered dolomites in the place of ideal dolomite. Malone et al. (1996) formed Ca-Mg carbonates (41.7 mole% MgCO_3) with no observable ordering reflections at relatively low-temperature (60°C) in $\text{CaCl}_2 - \text{MgSO}_4$ solutions with the addition of carbonate (NaCO_3) on the order of a few days. This suggests that carbonate activity is an important factor in getting magnesium into the carbonate lattice.

A further test of this hypothesis would be to examine dolomites formed on aragonite after aragonite reactant depletion. If the dolomite crystal growth mechanism does not change following aragonite depletion in the aragonite reactant experiments, like it does at reactant depletion in calcite reactant experiments the hypothesis would be further supported. After calcite is completely consumed in the calcite reactant experiments, the solubility of poorly ordered, nonideal dolomite dictates the supply of carbonate to solution because all calcite is depleted. However, calcite remains in the reaction vessels as the principle source of carbonate after reactant depletion in the aragonite reactant experiments. As a result, carbonate concentration should remain relatively high compared to reactant depletion in the calcite reactant experiments. Therefore, complete dolomitization of aragonite in the aragonite reactant experiments may not be followed by a change in growth mechanism.

4.e. Synthetic Dolomite Stoichiometry

The experimental results shown in Figure 13 indicate that the stoichiometry of nonideal dolomite products is highly dependent on the initial $\text{Mg}^{2+}:\text{Ca}^{2+}$ ratio in solution ($R^2=0.97$). Previous high-temperature dolomitization studies are consistent with this in that they have generally shown solutions with lower $\text{Mg}^{2+}:\text{Ca}^{2+}$ produce Ca-rich dolomite and solutions with higher $\text{Mg}^{2+}:\text{Ca}^{2+}$ yield more stoichiometric dolomite (Gaines, 1974; Sibley, 1990; Sibley et al., 1994). Although the relationship between initial solution composition and dolomite stoichiometry is strong ($R^2=0.97$), it is not exactly direct. Despite solutions becoming increasingly Ca-rich as dolomite replaces calcite (see table 3), dolomite composition appears to be independent of percent dolomite by remaining relatively constant until reactant depletion (Figures 14-16). Furthermore, after reactant depletion, $\text{Mg}^{2+}:\text{Ca}^{2+}$ ratios in solution reach their minimum values, yet after reactant depletion synthetic dolomite invariably becomes stoichiometric. Sibley (1990) also noted that in high-temperature dolomitization experiments, the composition of the products remained relatively constant, while the solution $\text{Mg}^{2+}:\text{Ca}^{2+}$ decreased from 0.66 to 0.53 after half of the calcite was replaced by a 65 mole% CaCO_3 product. Moreover, he noted that the observed transition to stoichiometric dolomite at reactant depletion occurred when the solution chemistry was at its lowest value and nearly constant. These observations suggest that the stoichiometry of nonideal dolomite only reflects the solution $\text{Mg}^{2+}:\text{Ca}^{2+}$ ratio at the beginning of growth and not the solution chemistry as it changes.

Aragonite reactant experiments with initial solution $\text{Mg}^{2+}:\text{Ca}^{2+} = 1.0$ yield more Ca-rich dolomite than dolomite formed from calcite reactant experiments with the same initial solution $\text{Mg}^{2+}:\text{Ca}^{2+}$. Aragonite is more soluble than calcite and as a result, the concentration of Ca^{2+} will be higher in solutions that equilibrate with aragonite than those that equilibrate with calcite. However, because of the high initial concentrations of Ca^{2+} and Mg^{2+} in experimental solutions, the effects of aragonite's greater solubility have only a relatively minor effect on the solution $\text{Mg}^{2+}:\text{Ca}^{2+}$ ratio (approximately 1.2% at 25°C). Because the effects of aragonite and calcite solubility on solution $\text{Mg}^{2+}:\text{Ca}^{2+}$ are difficult to determine at 218°C, they may account for the observed stoichiometric differences between dolomite formed in the calcite reactant experiment and those formed in the aragonite reactant experiment.

Although dolomite bulk composition remains relatively constant with reaction progress, the composition of individual islands is likely to be variable. If the composition and degree of cation order of individual islands were identical, one might expect islands to coalesce into layers upon continued growth. According to our observations, islands do not coalesce into layers, but instead remain distinct surface features as polynuclear growth proceeds. Furthermore, our chemical etching experiments suggest that island interfaces remain distinct components of the crystalline microstructure even long after formation. TEM observations also indicate that the microstructure of natural nonideal Ca-rich dolomites is heterogeneous due to distinct compositional and structural domains

(Reeder and Wenk, 1979; Reeder, 1981, 1992, 2000; Schubel et al., 2000; Frisia, 1994). This will be discussed in more depth in subsequent sections.

4.f. Synthetic Dolomite Cation Order

In the calcite reactant experiments, the degree of cation order (ordering ratios) in synthetic dolomites formed prior to reactant depletion with islands have values between 0.0 and 0.45, whereas synthetic dolomites formed after reactant depletion with layers have ordering ratios of 0.5 to 0.88. This suggests that a higher degree of cation order is achieved after the reactant is consumed during spiral growth. However it could be argued that cation order is related to dolomite stoichiometry because all well ordered dolomites are stoichiometric. Figure 22 indicates that prior to reactant depletion, the degree of cation order is seemingly independent of dolomite stoichiometry ($R^2 = 0.034$). Cation order generally increases with reaction progress, but dolomite stoichiometry remains relatively constant. Although a certain abundance of magnesium is necessary for cation order to occur, the results here indicate that cation order is independent of dolomite stoichiometry. This is further supported by the observation that many of the stoichiometric dolomites produced in high $Mg^{2+}:Ca^{2+}$ solutions have ordering ratios that are lower than Ca-rich dolomites from lower $Mg^{2+}:Ca^{2+}$ solutions.

Changes in the degree of cation order with time (Figures 19 and 20) also indicate changing growth mechanisms after reactant depletion. The results show that degree of cation order increases relatively rapidly during the growth of nonideal dolomite before all calcite is consumed. The rate at which cation order

increases slows considerably after the calcite is consumed and products are 100% stoichiometric dolomite (indicated by a shallower slope). This is precisely the time when the change from island to layer nanotopography on dolomite surfaces occurs. According to crystal growth theory, spiral growth is a slower growth mechanism than polynuclear growth (Sunagawa, 1984; refer to Figure 3). Therefore after reactant depletion, a slowing rate of increase for cation order with time is consistent with dolomite changing from polynuclear growth to spiral growth. Note that the experiment with solution $Mg^{2+}:Ca^{2+} = 0.66$ does not follow the trend of decreasing slope ($R^2 = 0.93$; Figure 21). Because the growth rate is already relatively slow compared to experiments with higher solution $Mg^{2+}:Ca^{2+}$ ratios, the change in rate of ordering after reactant depletion in the $Mg^{2+}:Ca^{2+} = 0.66$ experiment may not be as dramatic.

Because ideal dolomite is thermodynamically stable relative to nonideal dolomite, some factor must cause slow nucleation or crystal growth of ideal dolomite in order for nonideal dolomite to form first. Because it is possible to produce stoichiometric, but poorly ordered dolomite in our high $Mg^{2+}:Ca^{2+}$ experiments, it seems reasonable that cation ordering may be a factor to consider in explaining why nonideal dolomite forms before ideal dolomite. Although Ca-enrichment has been shown to destabilize dolomite (Navrotsky and Capobianco, 1987; Chai et al., 1995), calcium is incorporated more easily into the lattice than magnesium. In the laboratory, Glover and Sippel (in Bathurst, 1975, page 542) were able to produce magnesium calcites at room temperature and atmospheric pressure. Although compositions had cation proportions equal

to that of some dolomites, the magnesium calcites were completely disordered. Morrow et al. (1994) argued that the precipitation of partially ordered, metastable dolomite of stoichiometric composition is favored over that of ideal dolomite because of nonspecified kinetic inhibitions. This is in contrast to other studies that invoke thermodynamic arguments.

Kazmierczak et al. (1982) reported the activation energy for precipitating calcite to be $9.4 \pm 0.9 \text{ kcal mol}^{-1}$. Assuming that calcite and magnesite grow by identical mechanisms, Arvidson and Mackenzie (2000) reported the activation energy of magnesite to be $22.2 \text{ kcal mol}^{-1}$ based on data from Lippmann (1973). Arvidson and Mackenzie (2000) plotted activation energy as a function of carbonate composition by drawing a line between the calcite and magnesite values. Arvidson and Mackenzie (1999) calculated the activation energy for Ca-rich protodolomite (poorly ordered) to be $31.9 \text{ kcal mol}^{-1}$. This value agreed relatively well with the predicted value for a carbonate of the same composition. Gaines (1980) synthesized relatively well-ordered dolomites and calculated the enthalpy of formation to be $\sim 5.5 \text{ kcal mol}^{-1}$ above the value predicted by the extrapolation by Arvidson and Mackenzie (2000). Because the composition was stoichiometric, the additional energy is assumed to represent the effect of cation ordering in the dolomite structure. The additional activation energy calculated by Gaines (1980) is also in good agreement with the value of $5.5 \text{ kcal mol}^{-1}$ that Arvidson and Mackenzie (2000) calculated from the data of Malone et al. (1996) for the rate of recrystallization of disordered Ca-Mg carbonate to ordered-phases between 149°C and 197°C .

For comparable reaction progress, the degree of cation order in dolomite produced during aragonite reactant experiments is considerably lower than in dolomite produced during calcite reactant experiments. This is likely related to the fact that the rate of dolomitization was significantly higher in the aragonite reactant experiments. Ordering reflects how crystalline material (e.g., ions or molecules) is deposited into energetically favorable attachment sites. The processes of nucleation and crystal growth typically occur when material attaches to a surface followed by surface diffusion to energetically favorable (ideal) attachment sites (Gratz et al., 1991). When nucleation and growth rates are extremely high, attachment of new material may out compete surface diffusion and poor ordering may result. Aragonite reactant experiments demonstrate a linear relationship between cation order and time ($R^2 = 0.83$). More specifically, no change in the rate of increasing cation order with reaction progress is observed after the aragonite is completely consumed. However, if dolomite formed in the aragonite experiments never transitions from polynuclear to spiral growth after aragonite is consumed, a change in the rate of increasing order would not be expected at reactant depletion.

4.g. Synthetic Dolomite Recrystallization

The only source of carbonate for ideal dolomite after reactant depletion is poorly ordered stoichiometric (nonideal) dolomite. Immediately after reactant depletion dolomite still has a relatively low degree of order, and is therefore metastable and an energetic drive towards equilibrium still exists. Because

layers appear only after calcite reactant depletion when dolomite products are already stoichiometric, they indicate a transition between poorly ordered (nonideal) dolomite and well-ordered (ideal) dolomite (refer to Figure 61). According to Bathurst (1975), recrystallization can be defined in terms of a diagenetic fabric change without accompanying change in carbonate mineralogy. Growth layers on synthetic dolomite are interpreted, in this context, to be indicative of recrystallization. After reactant depletion, cation order and surface nanotopography change without a concomitant change in dolomite composition. Therefore recrystallization is understood to include changes in ordering and surface nanotopography.

Machel (1997) suggested the use of the term “significant recrystallization” to describe a modification in the original texture, ordering, chemical composition, or magnetic properties that is larger than the original range during dolomitization. The use of this term is warranted because all synthetic dolomites displaying evidence of recrystallization (i.e., layers) have higher degree of cation order than any synthetic dolomites with islands. As the degree of cation order increases in dolomite, excess strain energy in the crystal must decrease as the internal microstructure approaches an ideal form. As layers become more pervasive with increasing reaction times after 100% replacement, the degree of cation order continues to increase as well. Therefore significant recrystallization has occurred after the appearance of layers on dolomite surfaces.

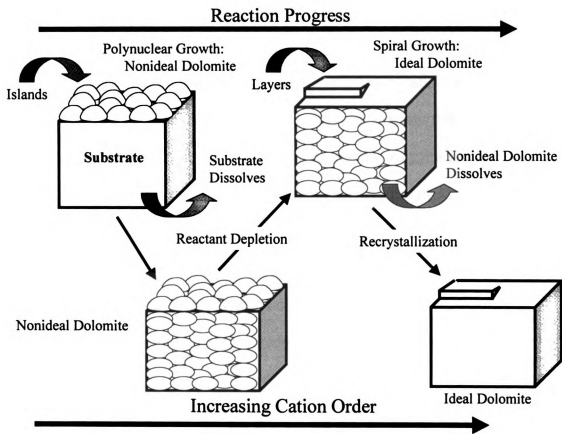


Figure 61. Growth mechanism summary diagram for dolomitization.

The observations that synthetic dolomite nanotopography does not change as a function of reaction progress, except after reactant depletion and that nanotopography does not change with solution $Mg^{2+}:Ca^{2+}$ ratio are also consistent with recrystallization. These observations indicate that polynuclear growth dominates over a wide range of solution conditions prior to reactant depletion. Furthermore, despite highly variable starting solutions and nonideal dolomite stoichiometries, all dolomite surfaces are covered with layers after reactant depletion. In as much as layers occur over a wide range of conditions, they provide a measure of recrystallization that is independent of solution chemistry and stoichiometry of the nonideal precursor dolomite.

4h. Natural Dolomite Growth Mechanisms

Most natural stoichiometric dolomites included in this study are relatively well-ordered (0.96-1.33), whereas most nonstoichiometric dolomites are relatively poorly ordered (0.458-0.824). In most cases, surface nanotopography can generally be differentiated according to stoichiometry alone. For instance, all nonstoichiometric dolomites have islands, but so do a few stoichiometric dolomites. These include the dolomites from Spain (samples 8-9-84-3 and 8-9-84-5) and Abu Dhabi (GWP287 120-130), which are stoichiometric and have island-covered surfaces. The above dolomites have relatively low ordering ratios (0.44-0.67), however, and are therefore considered nonideal. Furthermore, a nonstoichiometric Mississippian dolomite from Kentucky has an ordering ratio of 1.167, which is higher than some of the stoichiometric samples.

This sample has islands. However, the nonstoichiometric composition (i.e., excess calcium) indicates that the sample is nonideal. According to the results presented here, dolomite surface nanotopography is related to ideality, a combination of stoichiometry and cation order.

4.h.1. Nonideal Dolomite and Polynuclear Growth: Observations of dissolution islands are relatively rare in comparison to those of etch pits. There is, however, another dissolution feature that is somewhat analogous to the dissolution islands reported here. During dissolution experiments, Lin and Shen (1995) observed the formation of etch hillocks (smooth, topographically high surface features) prior to the development of etch pits on willemite crystal surfaces. They reasoned that the hillocks resulted from dissolution-resistant impurities contained within the willemite lattice. Other etch hillocks have been interpreted to form due to local surface contaminations (Batterman, 1957), etch resistant impurities (Stadler, 1963; Lin and Shen, 1995), reaction products, precipitates (Tuck, 1975; Rozgonyi et al., 1976), and gas bubbles attached to the surface (Weyher and Van Enckevort, 1983). Regardless of the exact mechanism involved with their occurrence, etch hillocks are generally understood to form on the crystal surface where dissolution is suppressed (Tuck, 1975). Therefore relative dissolution rates at various surface locations dictate the development of hillocks (Tuck and Baker, 1973). Islands have also formed on calcite as a result of dissolution in the laboratory (Kirkland et al., 1999) and islands on natural kaolinites have been interpreted to form by dissolution (Zbik and Smart, 1998). Dove and Hochella (1993) reported that calcite surfaces were characterized by

the presence of flat, rounded islands with flat tops in some of their experiments. They interpreted these features as being remnant growth islands that were exhumed during undersaturated conditions.

The formation of dislocations at the interface between nanoparticles as shown by Penn and Banfield (1998), suggests that it is not unreasonable to expect a defect-laden boundary between adjacent growth islands. Preferential dissolution at the interface between islands indicates that there is some driving force such as chemical or structural discontinuity at the interface between adjacent islands. The relatively high-energy interface between individual growth islands can therefore be utilized during etching to uncover an island nanotopography in ancient dolomites.

Using FESEM, Jones (2004) observed that chemically etched Ca-rich, Miocene-age dolomite cements exhibited “blocky topography”. Individual “blocks” were described as square or elongate topographic highs with rounded edges and corners. Blocks generally measure between 250 and 500 nanometers wide and less than 1 micron long. The edges between individual blocks were relatively straight, but curved edges were not uncommon. The features were observed to occur pervasively across the surfaces of Ca-rich dolomite cements. Jones (2004) also noted that the blocks were oriented perpendicular to the dominant dolomite growth face. Furthermore, the corners of dolomite crystals that represented multiple growth faces were characterized by multiple block orientations. The size, shape, and orientation of blocks on Ca-rich

dolomite observed by Jones (2004) are consistent with the islands observed with AFM. No euhedral etch pits were reported.

In addition to looking at hillocks as areas of suppressed dissolution, as Tuck (1975) suggested, it is helpful to consider the interface between hillocks (islands) as areas of enhanced dissolution. The presence of distinct growth islands on synthetic dolomite surfaces in and of itself suggests a physical mismatch between adjacent islands that serves as the site of elevated free energy. The ability to etch and uncover these growth features is further evidence of lattice mismatch between adjacent growth islands. The finding that islands are easily exposed on natural nonideal dolomite with chemical etching, even after hundreds of millions of years, suggests that islands maintain a pervasive defect network that was formed during polynuclear growth. According to Reeder (1992), solid-state diffusion is recognized as a relatively slow process; therefore defect microstructures formed during growth are likely to remain unmodified long after growth. If two adjacent islands have even slightly different orientation, structure, stoichiometry, or cation order, and come into contact with one another during crystal growth, their crystal lattices will be different, thus producing surface tension at the island-island interface. Surface tension between islands would result in elevated reactivity at the interface and would therefore serve as the site of preferential dissolution during chemical etching. Because the interface between islands follows the shape of an island, dissolution is able to uncover the polynuclear growth microstructure.

According to models of dissolution, the reactivity of island interfaces must be higher than the reactivity of the islands themselves, otherwise islands would dissolve and the interfaces would be resistant. However, it is possible to argue that euhedral etch pits are not observed because the reactivity of the island interfaces is higher than the reactivity of other naturally occurring defects. Although this may represent a limitation to uncovering other defects, the argument is not important to the interpretation that islands form by a polynuclear growth mechanism. The presence of dislocations in dolomites with island-covered surfaces does not preclude the interpretation that growth occurred by polynuclear growth. Because growth islands occur pervasively on dolomite surfaces, the free energy drive must have been high enough to support nucleation dominated growth.

Because empirical observations of islands as dissolution features are limited compared to etch pits, observations from growth and dissolution experiments for synthetic dolomites become an extremely useful analog for interpreting natural etching features. Dissolution islands on natural nonideal dolomites (Figures 50-52) are very similar to synthetic dolomite growth (Figures 32-34) and dissolution (Figure 46) islands. As a result, etch features on natural dolomites are interpreted in a manner consistent with the AFM observations of synthetic dolomite crystal surfaces. Because islands appear to be ubiquitous in nonideal dolomites they are not interpreted as post reaction surface precipitates, reaction products formed during dissolution, or etch resistant impurities. Islands

on natural and synthetic nonideal dolomites are interpreted as growth features that have been exposed during chemical etching.

4.h.2. Ideal Dolomite and Spiral Growth: The euhedral etch pits on natural dolomite (Figures 53-56) have similar size, shape, and orientation as the euhedral etch pits on synthetic dolomites (Figures 47-49). Because of this, natural dolomites are interpreted according to the observations from high-temperature synthetic dolomites as well as theoretical predictions for interface-controlled dissolution. Spiral growth in synthetic dolomite is inferred from the presence of steps and layers on ideal dolomite surfaces as well as the occurrence of euhedral etch pits following dissolution. Therefore the presence of euhedral etch pits on natural ideal dolomites are interpreted as evidence for spiral growth.

Deep euhedral etch pits form equally at spiral and edge dislocations because both promote preferential dissolution and it is not possible to distinguish the two by means of chemical etching. Although significant deformation of synthetic dolomites in the bombs likely did not occur, some of the natural dolomites studied here may have been subjected to conditions favorable for deformation. Consider, however, that euhedral etch pits are observed only in ideal dolomites and were never observed in nonideal dolomite. Deformation probably did occur in some of the natural dolomites studied here, but it is rather unlikely that deformation preferentially affects ideal dolomites.

Herman and White (1985) analyzed surface topography on polished natural dolomite crystals after dissolution in distilled water. After 200 hours of

dissolution, the etched single crystal had ledges and steps with consistently oriented pits that ranged from microns to tens of microns in diameter. In the rock specimen, dissolution occurred preferentially along grain boundaries after 200 hours, but Herman and White (1985) also observed that surfaces were covered by etch pits with steps that descended into the crystal. Luttge et al. (2003) used vertical scanning interferometry to analyze natural dolomite surfaces following experimental dissolution runs. After 8 hours of dissolution in mild hydrochloric acid (0.001mol/L; pH = 3), dolomite surfaces exhibited variously-shaped etch pits that measured up to 20 μ m in width and ~1.7 μ m in depth. Groups of pits have consistent orientation. Luttge et al. (2003) argued that dissolution occurred at inter-pit areas on dolomite surfaces. According to Luttge et al. (2003) vertical scanning interferometry has a vertical resolution of 2nm and a lateral resolution of 0.5 to 1.2 μ m (depending on the objective). The etch features on natural and synthetic dolomite observed with AFM (both etch pits and islands) are typically tens to hundreds of nanometers in diameter and would therefore not be resolvable using this instrument (VSI). As a result, the inter-pit dissolution observed by Luttge et al. (2003) may actually have occurred at pits or islands that were not resolvable.

4.i. Surface Topography And Internal Microstructure

TEM observations of ancient dolomite microstructures indicate that ideal dolomites are characterized by a homogeneous microstructure whereas nonideal (Ca-rich) dolomites exhibit heterogeneous and modulated microstructure (Barber,

1977; Reeder and Wenk, 1979; Reeder, 1981, 1983, 1992, 2000; Wenk et al., 1983; Van Tendello et al., 1985; Rosen et al., 1989; Frisia, 1994; Schubel et al., 2000). A number of these TEM studies (e.g., Reeder, 1981, 1992, 2000) have discovered that nonideal dolomites are composed of chemical and/or structural domains, which cause the appearance of modulations. The modulations have wavelengths that measure nanometers to tens of nanometers (up to 400 Angstroms). Modulations have been attributed to local compositional heterogeneities and/or fluctuations in cation ordering (Reeder and Wenk, 1979; Reeder, 1981, 1992, 2000; Reeder and Prosky, 1986; Miser et al., 1987; Fouke and Reeder, 1992). High-resolution TEM (HRTEM) images have confirmed the presence of individual domains in nonstoichiometric dolomite (Schubel et al., 2000). Furthermore, that these domains have cation distributions different from ideal dolomite and from one another. This suggests that domains are compositionally distinct and are characterized by different degrees of cation order (Reeder, 2000). Reeder (2000) argued that modulations found in nonideal dolomites were largely a result of strain associated with the structure of individual domains. He suggested that variations in the size, shape and, perhaps local distortions of adjacent zones could explain the occurrence of distinct domains in Ca-rich, nonideal dolomite.

Schubel et al. (2000) reported the occurrence of a heterogeneous, modulated microstructure in ancient Ca-rich dolomites despite a wide range of inferred dolomitizing conditions and reaction mechanisms. Dolomitizing environments reportedly ranged from low-temperature (<50°C) vadose

conditions to relatively high-temperature (<177°C) hydrothermal conditions. These observations suggest that similar dolomite microstructures occur over a wide range of temperature and formation conditions. Fouke and Reeder (1992) interpreted such differences in microstructures to indicate that ideal and nonideal dolomites formed by different growth processes. The ability to detect growth islands in ancient nonideal dolomites with the use of chemical etching suggests that islands remain as separate entities, which is consistent with the idea that dolomite has a pervasive crystalline defect microstructure. If two growth islands with different composition, ordering, or orientation (as suggested by the TEM results) intersect one another, lattice mismatch is likely to occur and therefore should result in a defective interface. In order for individual growth islands to remain distinct, there must be a surface tension associated with the interface between growth islands. Without an interfacial free energy growth islands would just grow together and form a continuous growth layer.

Although the size of islands and modulations are not identical, there is reason to believe that surface nanotopography and crystalline microstructure are directly related. First, the range of island sizes overlaps the range of modulation wavelengths. Secondly, modulations have been interpreted as growth features because they occur in an orientation that is sub-parallel to the growth direction. Even in areas with multiple growth sectors, modulations are observed to be consistent with the growth direction (Reeder, 2000). This is consistent with the AFM observations because regardless of what cleavage face is analyzed, islands are always observed in nonideal samples.

Ideal dolomite microstructures are homogeneous when viewed with TEM (Barber, 1977; Reeder and Wenk, 1979; Reeder, 1981, 1983, 1992, 2000; Wenk et al., 1983; Van Tendello et al., 1985; Rosen et al., 1989; Frisia, 1994; Schubel et al., 2000). This suggests that growth occurred in a way that promotes a homogeneous microstructure. Rosen et al. (1989) reported a higher density of dislocations in the ideal dolomites with homogeneous microstructure compared to the nonideal dolomites with a heterogeneous microstructure that he studied. His results suggest that extended line defects may be more common in ideal dolomites whereas a more heterogeneous microstructure is consistent with a pervasive defect structure.

4.j. Similarities Between Synthetic and Natural Dolomites

Because discrepancies exist between the conditions in which dolomite is synthesized in the laboratory and those generally recognized as being associated with natural dolomitization, one might scrutinize comparisons between them. Despite the lack of direct evidence indicating high-temperature experimental results are applicable to low-temperature natural dolomites, a number of observations, in addition to the similarities between surface nanotopography observed here, imply that empirical findings from high-temperature experiments are consistent with natural, low-temperature dolomites.

4.j.1. Induction Period: Although there is no theoretical basis for predicting an induction period, high-temperature synthetic dolomitization experiments are characterized by a long induction period and relatively short

growth period. The data presented here show that the length of the induction period is highly dependent on the solution chemistry and mineralogy of the reactant. Other studies have shown that temperature, the reactant surface area, and the amount of sulfate in solution can also have dramatic effects on the length of the induction period (Land, 1967; Gaines, 1974; Baker and Kastner, 1981; Sibley and Bartlett, 1987). In nature, seawater is supersaturated with respect to dolomite, yet many sediments consisting of aragonite and calcite exist in marine waters for millions of years without being dolomitized. This demonstrates that natural environments can have a long induction period for dolomitization. Furthermore, the observation that many ancient marine limestone deposits contain no dolomite despite evidence suggesting these rocks were submerged in seawater for extensive periods of time is also consistent with the idea of an induction period for natural dolomite. On the other hand, the existence of Holocene dolomite deposits suggests that dolomite can and does form relatively rapidly ($\sim 10^3$ years) in natural environments (Baltzer et al., 1994; Purser et al., 1994; Warthman et al., 2000). Therefore the existence of modern dolomites suggests an induction period for natural dolomitization that is on the order of ~ 1000 years or longer. Arvidson and Mackenzie (1997) argued against an induction period in natural dolomites, suggesting that the induction period itself is an artifact of high-temperature synthesis experiments. Because the majority of carbonate minerals that reside in marine waters (which are supersaturated with respect to dolomite) have no detectable amounts of dolomite, we interpret this to be consistent with the experimental results that indicate an induction period for

dolomitization. Moreover, many natural carbonate rocks show evidence of finer grained components being preferentially dolomitized. This will be discussed further in a subsequent section, but suffice it to say at this point that this is consistent with experimental findings, which show reactant surface area plays a major role in the induction period for dolomitization.

4.j.2. Reaction Rate: The observation that dolomitization in high-temperature synthesis experiments proceeds relatively rapidly once the induction period is over is consistent with the findings of Lumsden and Chimahusky (1980) and Sperber et al. (1984). These studies reported that most dolomitized-limestones in the rock record have dolomite/limestone ratios that are between 90% and 100% dolomite, which indicates that once dolomitization begins, most limestone are completely replaced. Given and Wilkenson (1987) plotted the distribution of dolomite content in Phanerozoic carbonates based on data from Baum et al. (1985), Chilingir (1956), Langbein et al. (1984), Lumsden and Chimahusky (1980), Marschner (1968), and Sperber et al., (1984) to show that a majority of carbonate samples have either a very low percentage of dolomite (~20%) or a very high percentage of dolomite (~97%). This is consistent with the observation that most synthetic dolomitization experiments start out relatively slowly compared to the rapid replacement phase.

The contacts between limestone and dolomite are generally abrupt (Sibley et al., 1994). Furthermore, Choquette and Steinen (1980) reported that these transitions are characterized by a decrease in the number of dolomite rhombohedra, but no change in crystal size across the contact. These

observations are consistent with an induction period as well as a rapid replacement period observed in high-temperature synthetic experiments. Sibley et al. (1994) argued that if limestone-dolomite contacts correspond to transition zones where limestone resides in potentially dolomitizing solutions of different duration, then completely dolomitized rock may indicate only a slightly longer duration in the fluid than the undolomitized limestone. Based on these observations, it seems evident that the same process, or processes inherent to the dolomitization reaction result in either minor or complete dolomitization of carbonate sediments in both high-temperature and low-temperature reactions.

4.j.3. Selective Replacement: Sibley and Bartlett (1987) reported that the reactant surface area greatly influenced the length of the induction period in hydrothermal bomb experiments. They showed that the rate of dolomitization decreased for finely ground calcite, medium calcite, and coarse calcite, respectively. They also showed that the induction period was longer for finely ground aragonite, medium aragonite, and coarse aragonite, respectively. These observations are consistent with nucleation theory, which predicts that finer reactants have more active nucleation sites per unit mass and should therefore have a higher nucleation rate. Sibley and Bartlett (1987) and this study show that high-temperature synthetic dolomites selectively replace aragonite when the solid reactant is a mixture of calcite and aragonite. Sibley and Gregg (1986) also reported that in high-temperature synthesis experiments with mixtures of low magnesium calcite and aragonite, the aragonite was completely dolomitized before any calcite showed signs of replacement. Katz and Matthews (1977) and

Gaines (1980) showed that aragonite is dolomitized faster than LMC in high-temperature synthesis experiments. The data presented here also show that the induction period of aragonite is nearly four times shorter than calcite experiments with the same solution $Mg^{2+}:Ca^{2+}$ ratio. This rapid rate of dolomitization is attributed to both the greater surface area and the mineralogy of the aragonite reactant. Although each individually could possibly account for the increased dolomitization rate, both have been experimentally shown to influence reaction rates. The observations from Sibley and Bartlett (1987) are interpreted to be analogous to selective dolomitization of fine-grained components in natural limestone reported by Murray and Lucia (1967). Furthermore, McKenzie (1981) and Patterson and Kinsman (1982) reported that dolomite selectively replaces aragonite in modern sabkhas.

4.j.4. Crystal Size Distributions: Crystal size distributions (CSD) contain information about nucleation and crystal growth (Marsh, 1988). Therefore it is reasonable to use CSD for comparisons between synthetic and natural dolomites. Although the inability to unambiguously interpret the separate effects of nucleation and growth presents a major limitation in interpreting CSD, certain constraints can be established, thus making CSD more useful in understanding similarities between natural and synthetic dolomites. Sibley et al. (1993) determined CSD for natural dolomites Recent to Cambrian in age by counting crystals in thin-section and scanning electron photomicrographs. They analyzed dolomites from Belize (Recent), the Saluda Formation (Ordovician), the Trenton Limestone (Ordovician), and the Bonneterre Dolomite (Cambrian) and reported

that many of the natural dolomite samples were unimodally distributed and characterized by a coarse-skewed lognormal distribution. Gregg et al. (1992) looked at Holocene dolomites from Belize and reported that the CSD were nearly lognormal. Kessels (2001) showed zone widths for 1400 dolomite crystals from the Saluda Formation were coarse-skewed.

The synthetic dolomites studied here display coarse-skewed CSD. Furthermore, Malone et al. (1996) experimentally investigated recrystallization of Ca-rich dolomite at 50°C to 200°C for up to one year in solutions with ionic strength near that of seawater. CSD frequency plots produced from their cumulative percent crystal size data reveal coarse-skewed CSD for the synthetic dolomite products. Therefore the CSD for synthetic dolomites representing a wide range of formation conditions are consistent with those reported for a number of naturally occurring sedimentary dolomites.

4.j.5. Mimetic Replacement: When dolomite replaces the precursor carbonate in a way that preserves the shape and texture of cements or allochems, replacement is reported as mimetic. Nonmimetic replacement destroys the original fabric of the precursor phase. Mimetic replacement occurs when the abundance of dolomite nuclei is sufficient and nuclei have the proper orientation with respect to the precursor phase (Bullen and Sibley, 1984). Because mimetic/nonmimetic replacement fabrics reflect information about crystal growth and nucleation, it is relevant to compare natural and synthetic dolomite in this context. Bullen and Sibley (1984) dolomitized a variety of fossils in hydrothermal bombs (at 250°C). They observed that the fossils that displayed

mimetic replacement in the experiments commonly exhibit mimetic replacement in nature (e.g., Cullis, 1904; Murray, 1964; Sibley, 1982). Furthermore, the fossils that showed nonmimetic replacement in the high-temperature experiments were consistent with the types of fossils that do not undergo mimetic replacement in nature. Bullen and Sibley (1984) also pointed out that coralline algae underwent rapid dolomitization in the experiments and are commonly selectively dolomitized in nature, whereas microcrystalline, LMC fossils preferentially resist dolomitization in high-temperature experiments and in nature. Sibley et al. (1993) reported that dolomite commonly nucleates epitaxially on calcite, thus preserving the crystallographic orientation of cements and allochems. Aragonite, on the other hand, is replaced by dolomite in a way that preserves structures, but not crystallographic orientation in cements and allochems. Bullen and Sibley (1984) also reported that LMC and HMC fossils were more apt to be mimetically replaced than aragonite fossils. This is interpreted to be consistent with the observation that dolomite rhombohedra are randomly oriented on aragonite, but invariably oriented in crystallographic continuity with the calcite substrate.

4.j.6. Stoichiometry: Compositional zoning in dolomites is often used as evidence for establishing a relationship between dolomite composition and the chemistry of the dolomitizing fluids (Katz, 1971; Richter, 1974; Cander et al., 1988). Thermodynamic considerations suggest that the Mg:Ca ratio in dolomite should be positively and proportionally related to the activity ratio in the liquid (Sass and Katz, 1982). Sass and Katz (1982) argued that the two activity ratios cannot be proportionally related based on the observation that $Mg^{2+}:Ca^{2+}$ ratios

vary widely in natural solutions, but dolomite compositions are relatively well constrained (0.74 to 1.0). The high-temperature synthetic experiments presented here indicate a strong correlation between the solution $Mg^{2+}:Ca^{2+}$ ratio and the stoichiometry of nonideal dolomite products formed prior to reactant depletion ($R^2 = 0.97$). At relatively low $Mg^{2+}:Ca^{2+}$ ratios, the rate of dolomite formation is relatively slow, and the first dolomite products are initially Ca-rich. At relatively high solution $Mg^{2+}:Ca^{2+}$ ratios, the rate of dolomitization is relatively rapid and initial dolomite products are more stoichiometric. These observations are consistent with the findings from a number of studies that have examined natural dolomites (Schmidt, 1965; Katz, 1971; Richter, 1974; Patterson and Kinsman, 1974; Sass and Katz, 1982; Sass and Bein, 1988). Patterson and Kinsman (1974) observed increasing Ca-enrichment with increasing depth that followed a decrease in the $Mg^{2+}:Ca^{2+}$ ratio of local pore waters of a sabkha environment. They interpreted this to represent a geologic situation where increasing isolation resulted in lowering $Mg^{2+}:Ca^{2+}$ ratios in solution. Sass and Katz (1982) suggested that dolomite stoichiometry and solution $Mg^{2+}:Ca^{2+}$ ratios were related based on observations from a Cretaceous carbonate sequence in the Judean Mountains in Israel. Their data show greater compositional variations and more Ca-enrichment in dolomites found lower in the section. Based on dolomite Na/Ca ratios and isotope data, they interpreted the compositional changes with depth to reflect the degree of isolation from overlying seawater. The shallower, more stoichiometric dolomites were interpreted to represent earlier, less isolated crystallization, whereas deeper, Ca-rich dolomites crystallized from older, more

modified solutions. Rosen et al. (1989) proposed that the Mg:Ca in dolomites of the Coorong region reflect the solution $Mg^{2+}:Ca^{2+}$ ratio of the parent fluids. TEM observations of growth microstructures and geochemical (isotopic) analyses implied that Mg-rich dolomites underwent rapid precipitation from brines with highly elevated $Mg^{2+}:Ca^{2+}$ ratios, whereas the Ca-rich dolomites precipitated more slowly from solutions that were less evaporative. Mg-rich dolomites exhibited extremely defect-rich microstructures and heavy $\delta^{18}O$ values.

Despite a decreasing $Mg^{2+}:Ca^{2+}$ ratio in solution as the dolomite replaces calcite, synthetic dolomite composition is invariably stoichiometric after reactant depletion. This is consistent with the findings of Schmidt (1965), Langbein et al. (1984), Lumsden and Chimahusky (1980), and Sperber et al. (1984), who showed that dolomite in partially dolomitized limestone is generally more calcium-rich whereas completely dolomitized rocks are found to be more stoichiometric. This is also consistent with the observation from our experiments that over most solution $Mg^{2+}:Ca^{2+}$ ratios studied here, initial products are generally Ca-rich, but become stoichiometric after reactant depletion regardless of the solution $Mg^{2+}:Ca^{2+}$ ratio or the stoichiometry of initial products. It is noteworthy to mention at this point that although no relationship was observed between the percent product and dolomite stoichiometry in the calcite reactant experiments, other high-temperature dolomitization studies have reported increasing dolomite stoichiometry with reaction progress (e.g., Nordeng and Sibley, 1994). However, the results presented here and those of Sibley (1990) suggest that there is no simple relationship between the solution composition and

that of the solid product. The stoichiometry of dolomites formed prior to reactant depletion is clearly a function of the initial solution chemistry, but all experiments proceeding to reactant depletion were stoichiometric. Therefore, without knowledge of the solution chemistry, stoichiometric dolomites must be interpreted with caution.

4.j.7. Cation Order: The experimental results suggest that although dolomite stoichiometry is related to the initial $\text{Mg}^{2+}:\text{Ca}^{2+}$ chemistry of the parent fluids, the degree of cation order is a function of reaction progress and is independent of solution chemistry. Although it was possible to form compositionally stoichiometric dolomite directly from calcite, the dolomite was nonetheless characterized by a low degree of cation order and therefore interpreted as nonideal. Ordering increased throughout the reaction, both before and after reactant depletion, albeit at a much slower rate after the calcite reactant was consumed. Synthetic dolomites formed prior to reactant depletion are always less ordered than dolomites formed after reactant depletion. Ordering ratios achieved by synthetic nonideal dolomites with growth islands ranged from 0.0 to 0.45, whereas synthetic ideal dolomites with layers had ordering ratios that ranged from 0.5 to 0.88. This indicates that dolomites formed earlier in the reaction are generally poorly ordered compared to those formed later. Gregg et al. (1992) showed that the degree of cation order in natural dolomites from Belize increased with depth without a concomitant increase in stoichiometry. These observations are consistent with the experimental data presented here, which show cation ordering and dolomite stoichiometry are independent. Furthermore,

better cation order is achieved with a spiral growth mechanism than during polynuclear growth. This observation is consistent with the observations of natural dolomite samples reported here, which suggest ideal dolomites correspond to a spiral growth mechanism whereas nonideality corresponds to dolomites that grew by a polynuclear growth mechanism.

Many recent sedimentary dolomites have a low degree of cation order and are Ca-rich. Garcia et al. (2001) reported on the occurrence of primary dolomite lake deposits. Dolomites were calcium-rich (51-54 mol% CaCO₃) with ordering ratios that ranged from 0.27 to 0.48 ($\bar{X} = 0.36$). In a DSDP report, Bottcher et al. (1998) noted relatively low cation ordering for Pliocene and Miocene dolomites. The degree of ordering ranged between 0.39 and 0.56 ($\bar{X} = 0.45$). Other modern dolomite from the Coorong area, Australia (Von der Borch and Jones, 1976; Rosen et al., 1988), Sugarloaf Key, Florida (Carballo et al., 1987), Ojo de Liebre, Mexico (Pierre et al., 1984), West Caicos, British West Indies (Perkins et al., 1994) and Western Australia (DeDekker and Last, 1988) have been reported to be Ca-rich and poorly-ordered.

Based on laboratory work and observations from modern and relatively recent environments, Bathurst (1975) proposed that a high Mg²⁺:Ca²⁺ ratio was required for dolomite ordering. He argued that a high Mg activity relative to Ca in the solution is required to give the chemical potential necessary to achieve the high degree of order in the dolomite lattice. According to our experimental results, ordering is neither a function of dolomite stoichiometry nor a function of the Mg²⁺:Ca²⁺ ratio in solution. More specifically, low Mg²⁺:Ca²⁺ ratios were

observed to be equally as efficient in producing ordered dolomites than higher solution $Mg^{2+}:Ca^{2+}$ ratios. Some solutions with lower $Mg^{2+}:Ca^{2+}$ ratios (e.g., 0.66) produced dolomites with a higher degree of cation order in less time than it took some experiments with higher solution $Mg^{2+}:Ca^{2+}$ (e.g., 1.5). This is interesting because lower solution $Mg^{2+}:Ca^{2+}$ ratios have slower dolomitization rates and ordering increases with reaction progress, therefore we would predict ordering to increase at a slower rate in low $Mg^{2+}:Ca^{2+}$ solutions.

4.k. Implications for Natural Dolomite

The similarities between natural and synthetic dolomites discussed in the previous section permit observations from synthetic dolomite experiments to be used to infer factors that affect the kinetics of dolomitization in natural settings with a reasonable level of confidence. One of the geologically significant inferences based on the empirical findings is that solution $Mg^{2+}:Ca^{2+}$ ratios do not dictate crystal growth mechanisms in natural dolomite. This is striking because according to crystal growth theory, one would predict spiral growth to occur under relatively low solution $Mg^{2+}:Ca^{2+}$ ratios and polynuclear growth during relatively high solution $Mg^{2+}:Ca^{2+}$ ratios. As demonstrated by the experimental results, however, crystal growth mechanisms are independent of solution $Mg^{2+}:Ca^{2+}$ ratios over the entire range included in this study. According to seawater curves for Mg^{2+} and Ca^{2+} from Lowenstein et al. (2001) and Horita et al. (2002), $Mg^{2+}:Ca^{2+}$ ratios have changed considerably throughout the Phanerozoic. Though there is no way of knowing the exact compositions of dolomitizing fluids,

one can assume that most natural dolomite deposits formed from relatively normal seawater or seawater derivatives. If this is correct, it is reasonable to infer that a wide range of solution $\text{Mg}^{2+}:\text{Ca}^{2+}$ ratios is represented by the natural samples studied here. To this end, nonideal dolomites formed by polynuclear growth occur over a wide range of geologic time periods and formation conditions. For example, based on the seawater chemistry curves of Lowenstein et al. (2001) and Horita et al. (2002), nonideal dolomites from the Ordovician, a period of relatively low $\text{Mg}^{2+}:\text{Ca}^{2+}$ ratios, have the same island nanotopography as recent dolomites that formed during geologic time periods with relatively high $\text{Mg}^{2+}:\text{Ca}^{2+}$ ratios. Furthermore, the natural nonideal dolomites studied here, which formed by polynuclear growth, range from 54 mol% CaCO_3 to stoichiometric. This further suggests that natural nonideal dolomites form by a polynuclear mechanism independently of dolomite stoichiometry, an inference consistent with the empirical observations.

Earlier discussions emphasized the idea that the transition from polynuclear growth to spiral growth is indicative of recrystallization in synthetic dolomite. Because the surface features observed on natural ideal and nonideal dolomites are consistent with observations of synthetic surface nanotopography, it may be possible to interpret natural dolomite in the same context. For example, if two natural stoichiometric dolomites were both determined to have ordering ratios of 0.8, and the first was observed to have an etched surface covered with islands and the second with layers and euhedral etch pits, the latter would be interpreted as a recrystallized dolomite. This is not to say that the

dolomite with islands is not recrystallized, only that layers with pits would be clear evidence of recrystallization according to the experimental observations.

However, because the transition from polynuclear to spiral growth in the high-temperature synthesis experiments occurs only after calcite reactant depletion, it is not easy to distinguish between the effects of recrystallization and inferred changes in carbonate ion concentration. Because the relationship between Ca^{2+} , Mg^{2+} , and CO_3^{2-} in nature is often unknown, one cannot determine whether spiral growth indicates the process of recrystallization, or dolomite formation under conditions where the carbonate ion concentration at the growth interface is low. According to the carbonate concentration argument, it may be possible to directly form a dolomite with layers, without the presence of a nonideal dolomite precursor, if the carbonate concentration is low enough.

Mimetic replacement of CaCO_3 by dolomite indicates that dolomitization may proceed by micrometer or smaller scale dissolution-precipitation. As a result, carbonate concentration in the bulk solution should be much less important than the carbonate concentration at the interface between growing a dolomite crystal and the dissolving carbonate substrate. Following this argument, the growth mechanism may be more indicative of the carbonate ion concentration at the surface of the precursor phase (e.g., calcite or nonideal dolomite) than the carbonate concentration in solution. Two observations from this study support the importance of carbonate ion concentration at the growth interface. First, dolomite nucleation occurs preferentially on the edges and corners of calcite. One presumes nucleation would not readily occur at corners

and edges because a nucleus on a corner or edge would have a relatively small contact area with the substrate. This small contact area would cause the nucleus to have a relatively high surface free energy. The same size nucleus in a kink site would have a much larger contact area with the substrate and, therefore, a lower surface free energy. As a result, the nucleus in the kink site would be more stable than the nucleus on an edge or corner. In order for the nucleus on the edge to become more stable than a nucleus in a kink site, it would have to be considerably larger. To this end, nuclei on edges and corners may be much larger than those in surface kinks because edges and corners (of CaCO_3) are likely to dissolve faster and dissolution of the substrate is the source of carbonate ions for the growing dolomite. Second, selective dolomitization of aragonite occurs when both calcite and aragonite are present. A bomb solution that equilibrates with respect to aragonite should allow dolomite to form readily on calcite. In fact, based on surface energy considerations, it is more favorable for dolomite to grow on calcite instead of aragonite because calcite and dolomite have the same crystal system. Furthermore, dolomite should form on calcite in bombs with mixed calcite-aragonite faster than it forms in bombs with just calcite because the carbonate ion concentration in the bombs with calcite and aragonite must be higher than in the bombs with just calcite. However, in bombs with mixed aragonite and calcite reactant, dolomite does not form on the calcite. These observations are consistent with the model that surface concentration of carbonate ions has a greater effect on the kinetics of dolomitization than surface

free energy of equivalent size nuclei or bulk solution carbonate ion concentration arguments.

There is no mechanistic basis in crystal growth theory that explains why dolomite growth mechanisms change when reactants are depleted in the synthesis experiments. The free energy drive (based on the $Mg^{2+}:Ca^{2+}$ in solution) is relatively constant at reactant completion and so is the composition of the dolomite phase. However, after reactant calcite depletion, ideal dolomite utilizes carbonate from the dissolving nonideal dolomite, whereas prior to reactant depletion nonideal dolomite uses the dissolving calcite substrate as its carbonate source. The substrates, calcite and nonideal dolomite, have different solubility products. Following this idea, it may be possible that differences in solubility are able to explain the change in growth mechanisms at reactant depletion. Given the K_{sp} values for nonideal dolomite and calcite from Helgeson et al. (1978), one can calculate the carbonate concentration in solution for each of the substrates. If the concentration of Ca^{2+} is fixed, for example at 10^{-3} , then for dolomite dissolution, the concentration of Mg^{2+} must be the same as Ca^{2+} because for every mole of Ca^{2+} that dissolves a mole of magnesium is also dissolved. This means that the concentration of Mg^{2+} is also 10^{-3} . For a nonideal dolomite with $K_{sp} = 10^{-16.52}$, the concentration of Ca^{2+} times concentration of Mg^{2+} is 10^{-6} , and the concentration of CO_3^{2-} squared must be $10^{-10.52}$. That means the concentration of CO_3^{2-} in solution would be $10^{-5.26}$ when nonideal dolomite is dissolved. Now for calcite, if $K_{sp} = 10^{-8.52}$ and given that Ca^{2+} is 10^{-3} , the concentration of CO_3^{2-} must be $10^{-5.52}$. This simple calculation demonstrates that

the carbonate concentration differences for calcite and nonideal dolomite are relatively minor. Therefore, the solubility products of calcite and nonideal dolomite provide very little insight into the observed growth mechanism change between nonideal dolomite formed on calcite and ideal dolomite formed on nonideal dolomite substrates.

From field data, it is well known that dolomite weathers more slowly than calcite (Cowell and Ford, 1980; Atkinson 1983). This has also been confirmed by experiment when Chou et al. (1989) showed that calcite dissolved eight to nine times faster than dolomite. In contrast, Busenberg and Plummer (1982) showed that it took different dolomite specimens 25-250 times longer than calcite to dissolve. The kinetic details of calcite dissolution seem to be well understood (Plummer et al., 1979), but dolomite dissolution is not (Busenberg and Plummer, 1982; Chou et al., 1989), except far from equilibrium. Under a range of PCO_2 values, Busenberg and Plummer (1982) measured dissolution rates for a variety of natural dolomite samples. From this data, a rate expression in terms of three forward and one backward reaction was derived. Busenberg and Plummer (1982, 1989) proposed that the $CaCO_3$ part of dolomite dissolves more readily than the $MgCO_3$ component. Consequently, the rate of dolomite dissolution is dependent on the rate of the $MgCO_3$ dissolution. Chou et al. (1989) later demonstrated a difference of four orders of magnitude in the rate constants between magnesite and calcite.

The rate of dissolution for dolomite and calcite are significantly different. This indicates that the carbonate flux to the growth surface must be highly

dependent on the nature of the substrate. Because the rate of dissolution of nonideal dolomite is significantly lower than the rate of dissolution of calcite (Busenberg and Plummer, 1982; Chou et al., 1989), the carbonate ion flux to the surface of a dissolving nonideal dolomite grain must be lower than at the surface of a dissolving calcite grain. Therefore, a nonideal dolomite substrate will have a lower carbonate ion concentration at a dolomite growth/substrate dissolution interface than a calcite substrate. Without the presence of a nonideal dolomite precursor for ideal dolomite to grow on, the carbonate flux to the dolomite growth interface would be dictated by more soluble substrates, such as calcite and aragonite. It has been shown experimentally that calcite and aragonite reactants support polynuclear growth of nonideal dolomite under a wide range of conditions. Only when the substrate and the carbonate source changes to nonideal dolomite, does the growth mechanism change from polynuclear to spiral. Therefore, the observation of layers only on ideal dolomite is consistent with the carbonate flux argument in that a nonideal dolomite precursor is necessary for spiral growth. Therefore, it is reasonable to suggest that layers are only associated with ideal dolomite because it is only with a nonideal dolomite precursor that the carbonate flux to the interface between the dissolving substrate and growing dolomite is low enough to allow spiral growth to outcompete polynuclear growth.

If a nonideal dolomite must exist in order to provide a substrate for spiral growth, then the ideal dolomite with evidence of spiral growth inevitably replaced an older dolomite substrate. In the experiments, the formation of ideal dolomite

took place after the nonideal dolomite was already stoichiometric. Therefore, the only changes to occur between the nonideal and ideal phases were in the degree of cation order and the surface nanotopography. Mineral replacement of this sort is consistent with what is generally accepted as recrystallization. Therefore, an ideal dolomite that grew by spiral growth should be interpreted as a recrystallized dolomite.

Dolomite solubility increases with excess calcium content and with decreasing cation order (Carpenter, 1980). It is, therefore, reasonable to suggest, at least on thermodynamic grounds, that nonideal dolomite (either poorly ordered and/or Ca-rich) is susceptible to recrystallization. Although the persistence of nonstoichiometric, nonideal dolomite in seawater over millions of years is a common phenomena (e.g., Lumsden, 1988), some studies show that recrystallization occurs in relatively recent dolomitic sediments (e.g., Gregg et al., 1992). Land (1992) proposed that most ancient dolomites have been recrystallized; furthermore that it is only through multiple recrystallization events that the formation of ideal dolomite is possible. Progressive recrystallization is consistent with the experimental observation, which show that the degree of cation order continues to increase throughout dolomitization. Furthermore, the experimental observations presented here indicate that ideal dolomite only forms by replacing a metastable, nonideal dolomite precursor. In addition, modern dolomites are characteristically nonideal (typically Ca-rich and poorly ordered), whereas ancient dolomites are generally more ideal.

Providing that conditions are constant, systems tend toward equilibrium with the passage of time. This suggests that older nonideal dolomites have a greater potential for recrystallization because older rocks are increasingly exposed to conditions that may favor dolomitization, such as influx of pore fluids, as well as elevated temperatures and pressures (Lumsden and Chimahusky, 1980). Fuchtbauer (1972) noted the calcium content of natural dolomites decreased in response to increasing diagenetic change. Sperber et al. (1984) observed a paucity of Ca-rich dolomites in samples Jurassic in age and older (2 of 55 samples), whereas Lumsden and Chimahusky (1980) observed that 43 of 290 pre-Cenozoic dolomites were Ca-rich. Therefore, it is not clear whether there is a relationship between dolomite stoichiometry and age. However, given enough time, solutions supersaturated with respect to dolomite should yield dolomite with compositions and cation order that tend toward ideality. This hypothesis is consistent with our experimental results, which show that dolomite always achieves a stoichiometric composition and relatively high degree of order given long enough.

Because there is currently no independent test of recrystallization for dolomite, previous studies have relied on geochemical tests, a somewhat tenuous approach, as our experiments have shown, when trying to identify recrystallization in dolomite. As the synthesis experiments have shown, examining geochemistry alone is not sufficient in attempting to identify recrystallization. First, there is no change in nonideal dolomite stoichiometry until the point of reactant depletion, despite a continually increasing degree of cation

order. Secondly, nonideal dolomite stoichiometry only reflects the composition of the solution during the start of dolomitization, but following reactant depletion all dolomite is stoichiometric.

Recrystallization has important implications for using dolomite geochemistry to infer conditions about the environment of formation. In particular, if a dolomite is recrystallized, its stoichiometry may no longer reflect the chemistry of the solution from which it initially formed, but instead reflect conditions during the latest recrystallization event. As the experiments here have shown, dolomite stoichiometry may also not reflect the solution from which it formed if it has recrystallized. All synthetic dolomites, regardless of the solutions from which they formed, were stoichiometric after reactant depletion. As Land (1980) reported, most ancient dolomite is trace-element depleted relative to Holocene dolomites. This suggests that either Holocene dolomite is formed under significantly different formation conditions than ancient dolomite, or that most ancient dolomites have been recrystallized. If the latter is true, valuable geochemical information about the original formation conditions has been lost.

According to the seawater curves of Lowenstein et al. (2001) and Horita et al. (2002) the Ordovician corresponds to low seawater $Mg^{2+}:Ca^{2+}$ ratios. This is interesting because some Ordovician dolomites included in this study are Ca-rich with surfaces covered with islands, whereas others are ideal and are characterized by layers with etch pits. According to the arguments described above, nonideal Ordovician dolomites presumably represent rocks that have not

been fully recrystallized and may even contain information about the original dolomitizing conditions, whereas ideal Ordovician dolomites with layers likely represent rocks that have been recrystallized. As the synthesis experiments have shown, examining geochemistry alone is not sufficient in attempting to identify recrystallization. First of all, there is no change in nonideal dolomite stoichiometry until the point of reactant depletion, despite a continually increasing degree of cation order. Furthermore, nonideal dolomite stoichiometry seems only to reflect the composition of the initial solution. Following reactant depletion, however, all dolomite is stoichiometric. As the earlier discussions alluded to, the surface nanotopography approach may be a powerful tool that offers an independent assessment of recrystallization for ancient dolomites.

Based on the premise that relatively high solution $Mg^{2+}:Ca^{2+}$ concentrations should promote dolomite-dominated carbonate rocks as well as more stoichiometric dolomite, Lumsden and Chimahusky (1980) initially postulated that the percent dolomite in a carbonate rock should be directly related to its stoichiometry. This is consistent with the data of Schmidt (1965) and Langbein et al. (1984), who showed a relationship between percent dolomite and dolomite stoichiometry in some ancient dolomitic carbonate rocks. Swart and Melim (2000) reported an R^2 of 0.13 between the percent dolomite and stoichiometry in Tertiary sediments of the Great Bahama Bank. Gregg et al. (2001) reported an R^2 of 0.115 between the percent dolomite and stoichiometry in sediments from Belize. The relatively low correlation coefficients make it difficult to accurately discern if, in fact, there is a physical relationship. The data

presented in this study from a suite of stratigraphically related samples from Abu Dhabi (GWP samples) also demonstrate a possible relationship between percent dolomite and dolomite stoichiometry. The results plotted in Figure 62 show a correlation between dolomite composition (reported as degrees 2-theta) and the

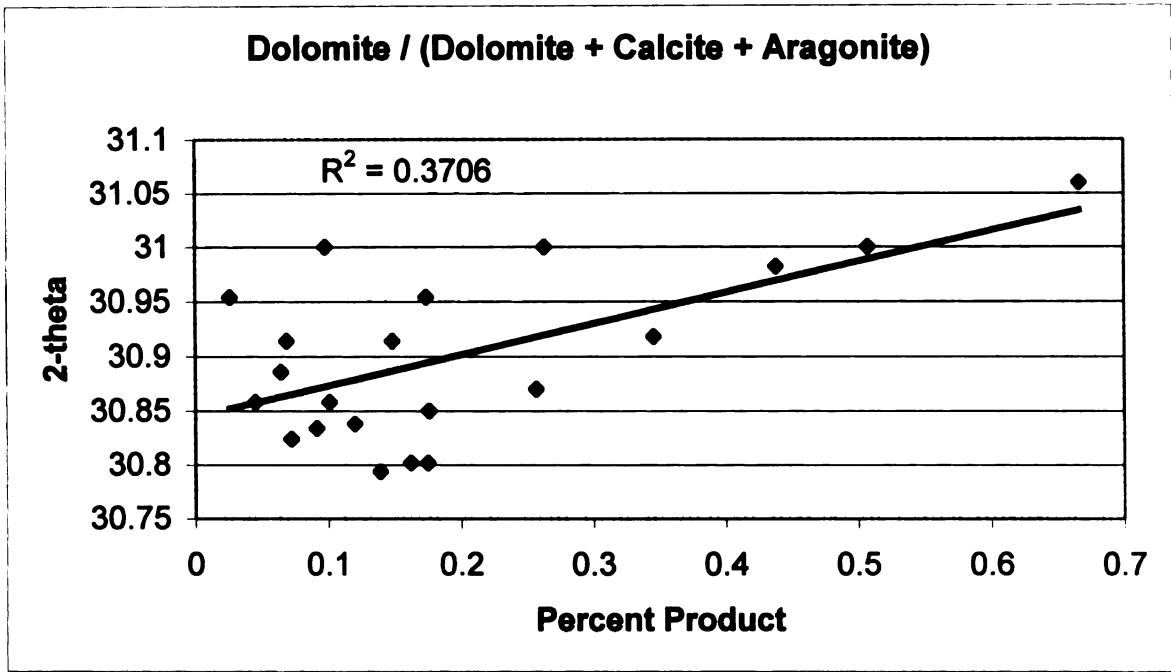


Figure 62. 2-theta (i.e. dolomite stoichiometry) vs. percent dolomite for GWP data from Abu Dhabi, $R^2=0.3706$. Note: 2-theta values are proportional to dolomite stoichiometry.

percent products [dolomite: (dolomite + calcite + aragonite) ratio] in the rock ($R^2=0.37$).

A correlation between percent dolomite in a carbonate rock and dolomite stoichiometry can be interpreted in two different ways. First, it may be interpreted to indicate that dolomite stoichiometry is dependent on reaction progress. In other words, the dolomite becomes increasingly stoichiometric as more dolomite replaces the precursor carbonate. However, a second interpretation, one more consistent with the experimental observations, is more appropriate. It postulates that variations in percent dolomite and dolomite stoichiometry are the result of different solution chemistry. Our high-temperature experiments clearly demonstrate that dolomite stoichiometry is highly dependent on the initial solution $Mg^{2+}:Ca^{2+}$ ratio and that stoichiometry remains remarkably steady throughout the reaction prior to reactant depletion. These findings indicate that no correlation exists between reaction progress (i.e., the percent dolomite in the carbonate fraction) and dolomite stoichiometry (in contrast to the findings of Malone et al., 1996). Based on the low correlation coefficients discussed earlier for percent dolomite and dolomite stoichiometry in natural rocks, it appears that the experimental results and natural observations coincide relatively well. Recall that the experiments show that the rate of dolomitization was also heavily dependant on solution $Mg^{2+}:Ca^{2+}$ ratios. In conjunction with the observed correlation between solution $Mg^{2+}:Ca^{2+}$ and nonideal dolomite stoichiometry, higher initial solution $Mg^{2+}:Ca^{2+}$ and hence faster growth rates produce greater abundances of more stoichiometric dolomite. Therefore,

correlations between percent products and dolomite stoichiometry, such as the ones observed by Schmidt (1965) and Langbein et al. (1984) for geologically related rocks, are interpreted to indicate that dolomitization occurred in a geological environment with variable solution $Mg^{2+}:Ca^{2+}$ ratios at the time of dolomite initiation. The argument here rests on the idea that dolomite does not become more stoichiometric simply because the percent dolomite in the rock increases, but that more dolomite (i.e., higher percent product) and more stoichiometric dolomite form because a higher solution $Mg^{2+}:Ca^{2+}$ ratios lead to faster rates of dolomitization. In ancient carbonate rocks where the percent dolomite does correlate with dolomite stoichiometry (e.g., Schmidt, 1965 and Langbein et al., 1984), areas with higher percentage of dolomite and lower Ca-enrichment would be interpreted to indicate initial solutions with higher $Mg^{2+}:Ca^{2+}$ and faster growth rates, not just to represent an area in which dolomitization has progressed further with time. Conversely, areas with a lower percentage of dolomite in the carbonate rock and more Ca-enrichment suggest lower $Mg^{2+}:Ca^{2+}$ in solution and in turn slower growth rates. Therefore the driving force behind correlations between stoichiometry and percent dolomite are likely due to differences in the $Mg^{2+}:Ca^{2+}$ ratio in solution at the onset of dolomitization. Furthermore, this may indicate an environment in which the solution chemistry is geologically controlled. One geologically reasonable, and potentially common situation is envisioned where Mg-rich fluids migrate downward and dolomitize carbonate sediments. During the migration the $Mg^{2+}:Ca^{2+}$ ratio of these solutions is reduced as Mg^{2+} is consumed and Ca^{2+} is liberated during the replacement

reaction. Therefore, sediments nearer to the Mg-rich fluids are dolomitized faster and have more stoichiometric compositions, whereas sediments lower in the section and farther away from the source of Mg-rich fluids are dolomitized more slowly and end up being more Ca-rich.

Lumsden and Chimahusky (1980) noted that dolomites became increasingly Ca-rich with increasing distance from overlying evaporite beds in the Salina-Niagaran Suite (Sanders and Horicon wells). Zenger (1996) observed a similar pattern in the dolomites of the Red River Formation in eastern Montana. Both studies interpreted this correlation to indicate a change in solution $Mg^{2+}:Ca^{2+}$ ratio with distance from the overlying dolomitizing solutions. In particular, they suggested that dolomite formed by downward seeping fluids that become increasingly depleted in Mg^{2+} as dolomite precipitates. This suggests that geologic controls on $Mg^{2+}:Ca^{2+}$ ratios in nature may also explain the correlation between percent dolomite and dolomite stoichiometry observed by Schmidt (1965) and Langbein et al. (1984). If the $Mg^{2+}:Ca^{2+}$ in dolomitizing solutions is geologically controlled, we might predict a correlation between dolomite stoichiometry and percent dolomite in the rock. Once again, according to our experiments, carbonate sediments closer to the source of magnesium will dolomitize faster and have a more stoichiometric composition, whereas deposits down section will be exposed to solutions with lower $Mg^{2+}:Ca^{2+}$ ratios and therefore have slower rates dolomitization and more Ca-rich compositions.

Graf and Goldsmith (1958) first documented a covariance between evaporite conditions and near-stoichiometric dolomite. Fuchtbauer and

Goldsmith (1965) found dolomites in evaporite-related deposits have more stoichiometric compositions than normal marine deposits. Fuchtbauer (1972) also noted the stoichiometric dolomite is associated with evaporite basin conditions as well as the presence of anhydrite. Fuchtbauer (1974) related calcium content in dolomite to the salinity of dolomitizing fluids. He documented a change from Ca-rich to nearly stoichiometric dolomite in going from humid to arid modern environments. Lumsden and Chimahusky (1980) observed that dolomicrites have a bimodal distribution in which near stoichiometric samples (50-52% CaCO₃) consist of mainly evaporitic rocks, whereas Ca-rich samples (53-55% CaCO₃) were mostly from non-evaporitic setting. These observations are important because evaporitic settings promote higher Mg²⁺:Ca²⁺ ratios in dolomitizing solutions due to precipitation of gypsum and calcite (Alderman, 1965; Land, 1967). The occurrence of accessory anhydrite in dolomites and limestones with near-stoichiometric dolomite supports the interpretation that high Mg²⁺:Ca²⁺ ratios in solution result in near-stoichiometric dolomite (Fuchtbauer, 1974). Higher Mg²⁺:Ca²⁺ also correspond to higher dolomitization rates, which is consistent with the occurrence of dolomite in modern environments with high evaporation rates (Illing et al., 1965; Deffeyes et al, 1965; Shinn et al., 1965).

Although percent dolomite and dolomite stoichiometry seem to covary in some cases where carbonate rocks are stratigraphically related (e.g., Schmidt, 1965; Langbein et al., 1984; Figure 62-GWP), the correlation is lacking when unrelated rocks are examined. Lumsden and Chimahusky (1980) observed no correlation between percent dolomite in carbonate rocks and dolomite

stoichiometry ($R^2 = 0.037$) for 290 Phanerozoic shelf carbonates from the U.S. Sperber et al. (1984) examined an additional 54 carbonate samples and also observed no correlation, suggesting that dolomite stoichiometry is independent of reaction progress for geologically unrelated samples. These findings are consistent with the experimental results (Figure 14), which indicate that the dolomite stoichiometry is independent of percent dolomite when data from all the experiments are compared. Because the data presented in Lumsden and Chimahusky (1980) and Sperber et al. (1984) include carbonate rocks from many different and unrelated depositional environments, a relationship between stoichiometry and percent dolomite is not expected, nor is it observed.

Based on the empirical findings, one would predict that times of higher $Mg^{2+}:Ca^{2+}$ in seawater would correspond to times of greater dolomite abundance because it would form faster. However, the Early Paleozoic is a period of high dolomite/limestone ratio (Given and Wilkenson, 1987 and references therein; Sun, 1994 and references therein), but low inferred seawater $Mg^{2+}:Ca^{2+}$ ratios (Lowenstein et al, 2001). No correlation between these secular variations of the dolomite/limestone ratio and seawater $Mg^{2+}:Ca^{2+}$ chemistry throughout the Phanerozoic implies that either (1) $Mg^{2+}:Ca^{2+}$ ratio of seawater was not a major factor determining the amount of dolomite in ancient rocks, (2) extensive dolomitization in the early Paleozoic may have actually lowered seawater $Mg^{2+}:Ca^{2+}$ ratios, as proposed by Wilkenson and Algeo (1989), or (3) dolomitization of most carbonate rocks occurs in fluids that are significantly different from seawater. The second hypothesis does not preclude the

importance of $Mg^{2+}:Ca^{2+}$ ratios in natural dolomitization. However, it does imply that other factors may have been more important. The third hypothesis is consistent with the idea that dolomitizing fluids are generally seawater derivatives (Given and Wilkenson, 1987), but not necessarily normal seawater. As it stands, unmodified seawater appears to be relatively inefficient at dolomitizing sediments as modern and many ancient marine carbonates have not been dolomitized.

The experimental results presented here are consistent with the argument of Clayton et al. (1968), Lippmann (1973), and Hardie (1987), that carbonate may be a major factor in affecting dolomitization kinetics. As Hardie (1987) notes, high $Mg^{2+}:Ca^{2+}$ ratios are not necessary to increase the solubility product of dolomite, particularly when carbonate is readily available. But as Burns et al. (2000) outlined, secular variations in seawater alkalinity are also unable to explain dolomite abundance through the Phanerozoic. As discussed in Lippmann (1973), however, a more local source of carbonate in marine environments may be supplied by anaerobic bacterial sulfate reduction. Vasconcelos and McKenzie (1997) proposed the microbial dolomite model as a means to explain dolomitization of recent sediments in the lagoonal waters of Lagoa Vermelha, Rio De Janeiro, Brazil. The model is appealing in two respects: as a part of their normal metabolic processes, sulfate reducing bacteria 1) release carbonate into solution (in the form of CO_3^{2-} or HCO_3^-), and 2) remove sulfate, a proposed kinetic inhibitor to dolomitization (see Baker and Kastner, 1981). Therefore microbial sulfate reduction would in effect, create an

environment on the submicrometer-scale that is more favorable for dolomite formation. The model is supported by the findings of Warthmann et al. (2000), who produced dolomite at low temperatures (30°C) using sulfate-reducing bacteria. Furthermore, Burns et al. (2000) showed a correlation between periods of extensive dolomitization and times during the Phanerozoic when redox conditions were favorable for anaerobic bacteria. The similarities between the high-temperature inorganic dolomites and ancient, low-temperature dolomites presented here are remarkable. Although available data for organogenic dolomites is extremely limited, they do indicate spherulitic growth and not growth islands. At this point, it is still difficult to evaluate whether organogenic dolomites are capable of explaining observations of natural dolomites in the same way that the high-temperature experiments can.

5. CONCLUSIONS

High-temperature dolomitization of calcite or aragonite reactants is characterized by the formation of an initial poorly ordered, nonideal synthetic dolomite. Following reactant depletion, initial nonideal dolomite products are later replaced by relatively well-ordered, ideal dolomite. Dolomitization rates are highly dependent on the initial solution $\text{Mg}^{2+}:\text{Ca}^{2+}$ ratio. High solution $\text{Mg}^{2+}:\text{Ca}^{2+}$ ratios dolomitized reactants relatively rapidly (e.g., 30 hours), whereas low solution $\text{Mg}^{2+}:\text{Ca}^{2+}$ ratios require very long reaction times (e.g., >1000 hours). The stoichiometry of the initial nonideal dolomite is also highly dependent on the starting $\text{Mg}^{2+}:\text{Ca}^{2+}$ ratio in solution ($R^2 = 0.97$). Relatively high solution $\text{Mg}^{2+}:\text{Ca}^{2+}$ ratios yield initial products that are stoichiometric, whereas lower solution $\text{Mg}^{2+}:\text{Ca}^{2+}$ ratios yield initial products that are calcium-rich. The stoichiometry of the nonideal dolomite remains relatively steady prior to reactant depletion despite a solution chemistry that continually evolves with reaction progress. After reactant depletion, dolomite is stoichiometric regardless of the initial or final solution $\text{Mg}^{2+}:\text{Ca}^{2+}$ ratio, suggesting that the relationship between solution $\text{Mg}^{2+}:\text{Ca}^{2+}$ and dolomite stoichiometry is not direct. Cation order increases with reaction progress as reactants are dolomitized. After calcite reactant depletion, ordering continues to increase as ideal dolomite forms at the expense of nonideal dolomite. In some experiments, ordering increases more slowly after reactant depletion.

Two distinct nanometer-scale growth features, described here as islands and layers, characterize synthetic dolomite growth surfaces. Prior to calcite reactant depletion, growth islands are observed on the surfaces of nonideal dolomite. Islands are analogous to surface nuclei observed on other minerals and are consistent with a model of polynuclear growth. After calcite reactant depletion, ideal dolomite nanotopography is characterized by layers with steps that emerge from the crystal. Layer geometry is consistent with a theoretical model of spiral growth. According to crystal growth theory, polynuclear growth is indicative of conditions where the free energy drive is relatively high, whereas spiral growth is indicative of conditions where the free energy drive is relatively low. Calcite reactant experiments demonstrate, however, that despite highly variable solution $Mg^{2+}:Ca^{2+}$ ratios, nonideal synthetic dolomites always grow by a polynuclear mechanism prior to calcite reactant depletion and ideal dolomites by a spiral mechanism after calcite reactant depletion. These findings contradict the hypothesis proposed by Sibley et al. (1987) that induction period of dolomitization marks a change in growth mechanisms from polynuclear to spiral growth.

A number of observations presented here indicate that dolomitization may proceed by micrometer or smaller scale dissolution-reprecipitation. After calcite reactant depletion, the flux of carbonate to the dolomite growth interface must be lowered because $[CO_3^{2-}]$ is dictated by slower dissolving nonideal dolomite. This suggests that rate of dissolution of the reactant and thus the flux of carbonate to dolomite growth surfaces dictate dolomitization kinetics in high-temperature synthesis experiments. The importance of carbonate flux to the growth interface

is further supported by the observations that dolomite preferentially replaces aragonite when both calcite and aragonite are present, and that dolomite nuclei form preferentially on the edges and corners of calcite. The present observations contradict predictions based on crystal growth theory. However, although growth mechanisms are processes that must obey thermodynamics, they are ultimately dictated by geochemical kinetics. Therefore, theoretical growth models may not be able to fully explain complex geochemical phenomenon for complex minerals like dolomite. Furthermore, because growth layers are only observed after all initial calcite reactants are consumed, they are indicative of recrystallization in high-temperature synthetic dolomite.

Chemically etched synthetic dolomites that grew by polynuclear and spiral growth yield islands and euhedral etch pits, respectively. Dissolution islands are indistinguishable from the growth islands observed on synthetic dolomite growth surfaces. Euhedral etch pits occur on relatively flat surfaces and are interpreted to form by preferential dissolution along linear defects, such as spiral dislocations. Chemically etched natural dolomites exhibit dissolution islands and deep euhedral etch pits on flat layers. Despite a large range of ages and stoichiometries, Ca-rich and relatively poorly ordered stoichiometric (nonideal) dolomites are invariably characterized by dissolution islands. Relatively well-ordered and stoichiometric (ideal) dolomites are characterized by deep euhedral etch pits on broad flat layers. Islands and etch pits observed on natural dolomites are nearly identical to islands and etch pits found on etched synthetic dolomite crystal surfaces. This suggests that by using chemical etching, it is

possible to uncover ancient nanometer-scale growth features on the surfaces of natural dolomite crystals.

The findings presented here also demonstrate the importance of examining mineral textures when attempting to understand the evolution of ancient carbonate rocks. Growth layers on ideal dolomite appear to be indicative of a growth mechanism that only occurs during the replacement of a nonideal dolomite precursor. It is only with slow dissolving nonideal dolomite substrate that carbonate flux to the ideal dolomite growth interface is low enough for spiral growth to out compete polynuclear growth. Without the presence of a nonideal dolomite precursor for ideal dolomite to grow on, the carbonate flux to the dolomite growth interface would be dictated by more soluble substrates, such as calcite and aragonite. Therefore the presence of layers appears indicative of recrystallization in ideal dolomite.

The dolomite problem is rooted in the kinetics of nucleation and growth. Because of sluggish kinetics at low temperatures, high-temperature synthetic dolomites are often used to better understand dolomitization in natural settings. To this end, similarities between natural and synthetic dolomite nanotopography suggests that synthetic and natural dolomites form by the same crystal growth mechanisms despite large discrepancies in formation conditions. Therefore, synthetic dolomite should be used as a proxy for natural low temperature dolomite with a higher level of confidence than previously acknowledged. Therefore, a long induction period followed by rapid dolomitization is the best model to explain the absence of dolomite in modern environments.

REFERENCES CITED

- Alderman, A.R., 1965, Dolomitic sediments and their environment in the South-East Australia, *Geochimica et Cosmochimica Acta*, Vol. 29, pp. 1355-1365.
- Avidson, R.S. and Mackenzie, F.T., 1997, Tentative kinetic model for dolomite precipitation rate and application to dolomite distribution, *Aquatic Geochemistry*, Vol. 2, pp. 273-298.
- Avidson, R.S. and Mackenzie, F.T., 1999, The dolomite problem: control of precipitation kinetics by temperature and saturation state *American Journal of Science*, Vol. 299, pp. 257-288.
- Avidson, R.S. and Mackenzie, F.T., 2000, Temperature dependence of mineral precipitation rates along the CaCO₃-MgCO₃ join, *Aquatic Geochemistry*, Vol. 6, pp. 249-256.
- Astilleros, J.M., Pina, C.M., Fernandez-Diaz, L., and Putnis, A., 2002, Molecular-scale surface processes during the growth of calcite in the presence of manganese, *Geochimica et Cosmochimica Acta*, Vol. 66, No. 18, pp. 3177-3189.
- Atkinson, T.C., 1983, Growth mechanisms of speleothems in Castleguard Cave, Columbian Icefields, Alberta, Canada, *Arctic Alpine Research*, Vol. 15, pp. 523–536.
- Avrami, M., 1939, Kinetics of phase change, I. General theory, *Journal of Chemical Physics*, Vol. 7, pp 1103-1112.
- Baker, P.A. and Kastner, M., 1981, Constraints on the formation of sedimentary dolomite, *Science*, Vol. 213, No. 4504, pp. 214-216.
- Baltzer, F., Kenig, F., Boichard, R., Plaziat, J.C., and Burser, B.H., 1994, Organic matter distribution, water circulation and dolomitization beneath the Abu Dhabi Sabkha (UAB), in *Dolomites: A Volume in Honor of Dolomieu*, Purser, B.H., Tucker, M.E., and Zenger, D.H., eds., Special Publication, International Association of Sedimentologists, Vol. 21, pp. 409-427.
- Banfield, J.F., Welch, S.A., Zhang, H., Ebert, T.T., and Penn, R.L., 2000, Aggregation-based crystal growth and microstructure development in natural iron oxyhydroxide biomineralization products, *Science*, Vol. 289, pp. 751-754.
- Barber, D.J., 1977, Defect microstructures in deformed and recovered dolomites, *Tectonophysics*, Vol. 39, pp. 193-213.

- Bathurst, R.G.C., 1975, Carbonate Sediments and Their Diagenesis, Developments in Sedimentology, Vol. 12, Elsevier Scientific, New York.**
- Battermann, B.W., 1957, Hillocks, pits, and etch rate in germanium crystals, Journal of Applied Physics, Vol. 28, pp. 1236-1241.**
- Baum, G.R., Harris, W.B., Drez, P.E., 1985, Origin of dolomite in the Eocene Castle Hayne Limestone, North Carolina, Journal of Sedimentary Research, Vol. 55, No. 4, pp. 506-517.**
- Becke, F., 1890, Tschernarks Min. Petr. Mitteil, Vol. 11, p. 349.**
- Berner, R.A., 1978, Rate control on mineral dissolution under earth surface conditions, American Journal of Science, Vol. 278, pp. 1235-1252.**
- Berner, R.A., 1981, Kinetics of weathering and diagenesis, In, Lasaga, A.C. and Kirkpatrick, R.J., eds., Kinetics of Geochemical Processes: MSA, Reviews in Mineralogy, Vol. 8, pp. 111-134.**
- Berner, R.A., and Morse, J.W., 1974, Dissolution kinetics of calcium carbonate in sea water, IV. Theory of calcite dissolution, American Journal of Science, Vol. 274, pp. 108-134.**
- Berner, R.A., and Holdren, G.R., 1977, Mechanism of feldspar weathering: Some observational evidence, Geology, Vol. 5, No. 6, pp. 369-372.**
- Blake, D.F., Peacor, D.R., and Wilkenson, B.H., 1982, The sequence and mechanism of low-temperature dolomite formation: Calcian dolomite in a Pennsylvanian echinoderm, Journal of Sedimentary Petrology, Vol. 52, pp. 59-70.**
- Blum, A.E., Yund, R.A., and Lasaga, A.C., 1990, The effect of dislocation density on the dissolution rate of quartz, Geochimica et Cosmochimica Acta, Vol. 54, pp.283-297.**
- Bosbach, D. and Rammensee, W., 1994, In situ investigation of growth and dissolution on the (010) surface of gypsum by Scanning Force Microscopy, Geochimica et Cosmochimica Acta, Vol. 58, No. 2, pp. 843-849.**
- Bosbach, D., Hall, C, and Putnis, A., 1998, Mineral precipitation and dissolution in aqueous solution: in-situ microscopic observations on barite with atomic force microscopy, Chemical Geology, Vol. 151, pp. 143-160.**
- Bottcher, M.E., Mart, Y, and B, H.J., 1998, Data Report: Geochemistry of Pliocene and Miocene carbonates from the Eratosthenes Seamount (Site 965), Proceedings of the Ocean Drilling Program, Scientific Results, Vol. 160, pp. 447-451.**

- Bragg, W.L. and Williams, E.J., 1934, The effect of thermal agitation on atomic arrangements in alloys, Royal Society of London Proceedings, Vol. 145A, pp. 699-730.
- Brantley, S.L., Crane, S.R., Crerar, D.A., Hellmann, R., and Stallard, R., 1986, Dissolution at etch pits in quartz, *Geochimica et Cosmochimica Acta*, Vol. 50, pp. 2349-2361.
- Budd, D.A., 1997, Cenozoic dolomites of carbonate islands: their attributes and origin, *Earth Science Reviews*, Vol. 42, pp. 1-47.
- Bullen, S.B. and Sibley, D.F., 1984, Dolomite selectivity and mimic replacement, *Geology*, Vol. 12, pp. 655-658.
- Burns, S.J., McKenzie, J.A., and Vasconcelos, C., 2000, Dolomite formation and biogeochemical cycles in the Phanerozoic, *Sedimentology*, Vol. 47, pp. 49-61.
- Burton, W.K., Cabrera, N., and Frank, 1951, *Philosophical Transaction Royal Society of London A*, Vol. 243, pp. 299.
- Busenberg, E. and Plummer, L.N., 1982, The kinetics of dissolution of dolomite in CO₂H₂O systems at 1.5 to 65°C and 0 to 1 ATM PCO₂, *American Journal of Science*, Vol. 282, pp. 45-78.
- Busenberg, E. and Plummer, N.L., 1989, Thermodynamics of magnesian calcite solid-solutions at 25° C and 1 atm total pressure, *Geochimica et Cosmochimica Acta*, Vol. 53, Issue 6, pp.1189-1208.
- Cabrera, N. and Levine, M.M., 1956, *Philosophy Magazine*, Vol. 1, pp. 450.
- Cander, H.S., Kaufman, J., Daniels, L.D., and Meyers, W.J., 1988, Regional dolomitization of shelf carbonates in the Burlington-Keokuk Formation (Mississippian), Illinois and Missouri: Constraints from cathodoluminescent zonal stratigraphy, In *Sedimentology and Geochemistry of Dolostones*, SEPM Special Publication, No. 43, pp. 129-144.
- Carballo, J.D., Land, L.S., and Miser, D.E., 1987, Holocene dolomitization of supratidal sediments by active tidal pumping, Sugarloaf Key, Florida, *Journal of Sedimentary Petrology*, Vol. 57, pp. 153-165.
- Carpenter, A.B., 1980, The Chemistry of dolomite formation I: The stability of dolomite, in Zenger, D.H., Dunham, J.B., and Ethington, R.L., eds. *Concepts and Models of Dolomitization*: SEPM Special Publication, Vol. 28, pp. 111-121.
- Chai, L., and Navrotsky, A, 1996, Thermochemistry of carbonate-pyroxene equilibria, *Contributions to Mineralogy and Petrology*, Vol. 114, pp. 139-147.

- Chai, L., Navrotsky, A., and Reeder, R.J., 1995, Energetics of calcium-rich dolomite, *Geochimica et Cosmochimica Acta*, Vol. 59, pp. 939-944.
- Chang, L.L.Y., 1964, Synthesis of $\text{MBa}(\text{CO}_3)_2$ compounds. *American Mineralogist*, Vol. 49, pp. 1142-1143.
- Chilingar, G.V., 1956, Relationship between Ca/Mg ratio and geological age, *American Association of Petroleum Geologists Bulletin*, Vol. 40, pp. 2256-2266.
- Choquette, P.W. and Steinen, R.P., 1980, Mississippian non-supratidal dolomite, Ste. Genevieve Limestone, Illinois Basin: Evidence for mixed-water dolomitization, in Zenger, D.H., Dunham, J.B., and Ethington, R.L., eds. *Concepts and Models of Dolomitization: SEPM Special Publication*, Vol. 28, pp. 163-196.
- Chou, K., Garrels, R.M. and Wollast, R., 1989, Comparative study of the kinetics and mechanisms of dissolution of carbonate minerals, *Chemical Geology*, Vol. 78, pp. 269–282.
- Clayton, R.N., Jones, R.F. and Berner, R.A., 1968, Isotope studies of dolomite formation under sedimentary conditions, *Geochimica et Cosmochimica Acta*, Vol. 43, pp. 415-432.
- Cowell, D.W. and Ford, D.C., 1980, Hydrochemistry of a dolomite karst: the Bruce Peninsula of Ontario, Canada. *Journal of Earth Science*, Vol. 17, pp. 520–526.
- Cullis, C.G., 1904, Then mineralogical changes observed in the ocores of the Funafuti boring, in Bonney, T.G., ed., *The atoll of Funafuti*, Royal Society of London, pp. 392-420.
- DeDekker, P. and Last, W.M., 1988, Modern dolomite deposition in continental, saline lakes, western Victoria, Australia, *Geology*, Vol. 16, pp. 29-32.
- Deelman, J.C., 1981, Dolomite formation: Why thermodynamics failed, *N. Jb. Miner. Abh.*, Vol. 141, pp. 30-58.
- Deer, W.A., Howie, R.A., and Zussman, J., 1992, *An Introduction to the Rock-Forming Minerals*, Longman.
- Deffeyes, K.S., Lucia, F.J., and Weyl, P.K., 1965, Dolomitization of Recent and Plio-Pleistocene sediments by marine evaporite waters on Bonaire, Netherlands Antilles, In L.C. Pray and R.C. Murray, eds., *Dolomitization and limestone diagenesis*, SEPM special publication, Vol. 13., pp. 71-88.

- De Yoreo, J.J., Land, T.A., Rashkovich, L.N., Onischenko, T.A., Lee, J.D., Monovskii, O.V., and Zaitseva, N.P., 1997, The effect of dislocation cores on growth hillock vicinity and normal growth rates of KDP {101} surfaces, Journal of Crystal Growth, Vol. 182, pp. 442-460.**
- Dove, P.M. and Hochella Jr, M.F., 1993, Calcite precipitation mechanisms and inhibition by orthophosphate: In situ observations by Scanning Force Microscopy, Geochimica et Cosmochimica Acta, Vol. 57, pp. 705-714.**
- Eggleston, C.M., 1994, High-resolution scanning probe microscopy: tip-surface interaction, artifacts and applications in mineralogy and geochemistry, In Scanning Probe Microscopy of Clay Minerals, Eds. Nagy, K.L. and Blum, A.E., Clay Minerals Society, Boulder, CO, pp. 3-90.**
- Folk, R.L., Chafetz, H.S., and Tiezzi, P.A., 1985, Bizarre forms of depositional and diagenetic calcite in hot-springs travertines, central Italy, in Schneidermann, N., and Harris, P.M., eds., Carbonate Cements, SEPM Special Publication Vol. 36, pp. 349-369.**
- Folk, R.L., 1993, SEM imaging of bacteria and nanobacteria in carbonate sediments and rocks, Journal of Sedimentary Petrology, Vol. 25 no. 6, pp. 990-999.**
- Folk, R.L. and Land, L.S., 1975, Mg/Ca ratio and salinity: Two controls over crystallization of dolomite, American Association of Petroleum Geologists Bulletin, Vol. 59, pp. 60-68.**
- Fouke, B.W. and Reeder, R.J., 1992, Surface structural controls on dolomite composition: Evidence from sectoral zoning, Geochimica et Cosmochimica Acta, Vol. 56, pp. 4015-4024.**
- Frank, F.C., 1951, Capillary equilibria of dislocated crystals, Acta Crystallographica, Vol. 4, pp. 497-501.**
- Friedman, G.M. and Sanders, J.E., 1967, Origin and occurrence of dolostones: In G.V. Chilingar, H.J. Bissell, and R.W. Fairbridge, Eds., Carbonate Rocks, Part A, Elsevier, New York, pp. 267-348.**
- Frisia, S., 1994, Mechanisms of complete dolomitization in a carbonate shelf: comparison between the Norian Dolomia Principale (Italy) and the Holocene of Abu Dhabi Sabkha, Special Publication, Int. Ass. Sediment, Vol. 21, pp. 55-74.**
- Fuchtbauer, H., 1972, Influence of salinity on carbonate rocks of the Zechstein formation, northwest Germany, In: Geology of saline deposits, ed. G. Richter-Bernburg, Unesco, Paris, pp. 23-31.**

- Fuchtbauer, H., 1974, Sediments and Sedimentary Rocks, Halsted Press, New York.**
- Fuchtbauer, H. and Goldschmidt., H., 1965, Beziehungen zwischen calciumgehalt und bildungs-bedingungen der dolomite, Geologische Rundschau, Vol. 55., pp. 29-40.**
- Gaines, A.M., 1968, An experimental investigation of the kinetics and mechanism of the formation of dolomite, PhD Dissertation, The University of Chicago.**
- Gaines, A.M., 1974, Protodolomite synthesis at 100°C and atmospheric pressure, Science, Vol. 55, pp. 84-101,**
- Gaines, A.M., 1980, Dolomitization kinetics: recent experimental studies, SEPM Special Publication No. 28, pp. 81-86.**
- Garcia Del Cura, M.A., Calvo, J.P., Ordonez, S., Jones, B.F., and Canaveras, J.C., 2001, Petrographic and geochemical evidence for the formation of primary, bacterially induced lacustrine dolomite: La Roda "white earth" (Pliocene, central Spain), Sedimentology, Vol. 48, pp. 897-915.**
- Garrels, R.M. and Thompson, M.E., 1962, A chemical model for sea water at 25°C and one atmosphere total pressure, American Journal of Science, Vol. 260, pp. 57-66.**
- Garrels, R.M., Thompson, M.E., and Siever, R., 1960, Stability of some carbonates at 25°C and 1 atmosphere total pressure, American Journal of Science, Vol. 258, pp. 402-418.**
- Gilman, J.J., Knudson, C., and Walsh, W.P., 1958, Journal of Applied Physics, Vol. 29, pp. 601.**
- Given, R.K. and Wilkenson, B.H., 1987, Dolomite abundance and stratigraphic age: Constraints on rates and mechanisms of Phanerozoic dolostone formation, Journal of Sedimentary Petrology, Vol. 57, No. 6, pp. 1068-1078.**
- Goldsmith, J.R. and Graf, D.L., 1958, Structural and compositional variations in some natural dolomites, Journal of Geology, Vol. 66, pp. 678-693.**
- Graf, D.L. and Goldsmith, J.R., 1956, Some hydrothermal synthesis of dolomite and protodolomite, Journal of Geology, Vol. 64, pp. 173-187.**
- Graf, D.L., Blyth, C.R., and Stemmler, R.S., 1967, One dimensional disorder in carbonates. Illinois State Geological Survey Circular, Vol. 408.**

- Grandstaff, D.E., 1978, Changes in surface area and morphology and the mechanism of forsterite dissolution, *Geochimica et Cosmochimica Acta*, Vol. 42, pp. 1899-1901.
- Gratz, A., Manne, S., and Hansma, P.K., 1991, Atomic force microscopy of atomic-scale ledges and etch pits formed during dissolution of quartz, *Science*, Vol. 251, Issue 4999, pp. 1343-1346.
- Gratz, A.J., Hillner, P.E., and Hansma, P.K., 1993, Step dynamics and spiral growth on calcite, *Geochimica et Cosmochimica Acta*, Vol. 57, pp. 491-495.
- Gregg, J.M., Howard, S.A, and Mazzullo, S.J., 1992, Early diagenetic recrystallization of Holocene (<3000 years old) peritidal dolomites, Ambergris Cay, Belize, *Sedimentology*, Vol. 39, pp. 143-160.
- Gregg, J. M., Shelton, K. L., Johnson, A. W., Somerville, I. D., and Wright, W. R., 2001, Dolomitization of the Waulsortian Limestone (Lower Carboniferous) Irish Midlands: *Sedimentology*, Vol. 48, pp. 745-766.
- Hardie, L.A., 1987, Dolomitization: a critical view of some current views, *Journal of Sedimentary Petrology*, Vol. 57, pp. 166-183.
- Hartman, P., 1982, On the growth of dolomite and kaolinite crystals, *N. Jb. Miner. Mh.*, pp. 84-92.
- Heimann, R.B., 1975, *Auflosung von Kristallen – Theorie und Technische Anwendung*, Springer, New York, Russ. Translation, 1979, *Rastvorenije Kristallov (Nedra, Leningrad)*.
- Heimann, R.B., 1982, Principles of chemical etching, in: *Crystals – Growth, Properties and Applications*, ed. J. Grabmaier, Springer, Berlin, Vol. 8.
- Helgeson, H.C., Delany, J.M., Nesbitt, H.W., and Bird, D.K., 1978 Summary and critique of the thermodynamic properties of rock-forming minerals, *American Journal of Science*, Vol. 278-A, pp. 229.
- Heraty, L.J., 1988, In-situ AFM examination of calcite nanomorphology in the presence of know anionic growth inhibitors SO_4^{2-} and PO_4^{3-} , Masters Thesis, Michigan State University.
- Herman, J.S. and White, W.B., 1985, Dissolution kinetics of dolomite: Effects of lithology and fluid flow velocity, *Geochimica et Cosmochimica Acta*, Vol. 49, pp. 2017-2026.
- Hillner, P.E., Gratz, A.J., Manne, S., and Hansma, P.K., 1992, Atomic-scale imaging of calcite growth and dissolution in real time, *Geology*, Vol. 20, pp. 359-362.

-Hochella, M.F., 1990, Atomic structure, microtopography, composition, and reactivity of mineral surfaces, In. M.F. Hochella and A.F. White eds., Mineral – Water interface geochemistry, Reviews in Mineralogy, Vol. 23, pp. 87-128.

-Hochella, M.F. Jr., Eggleston, C.M., Elins, V.B., and Thompson, M.S., 1990, Atomic structure and morphology of the albite {101} surface: An atomic-force microscope and electron diffraction study, American Mineralogist, Vol. 75, pp. 723-730.

-Horita, J, Zimmermann, H, and Holland, H., 2002, Chemical evolution of seawater during the Phanerozoic: Implications from the record of marine evaporites, Geochimica et Cosmochimica Acta, Vol. 66, No. 21, pp. 3733-3756.

-Horn, F.H., 1952, Screw dislocations, etch figures, and holes, Philosophical Magazine, Vol. 43, pp. 1210-1213.

-Hsu, K., 1963, Solubility of dolomite and composition of Florida ground waters, Journal of Hydrology, Vol. 1, pp. 288-310.

-Hull, D. and Bacon, D.J., 1984, Introduction to Dislocations, Pergamon Press, Oxford, UK.

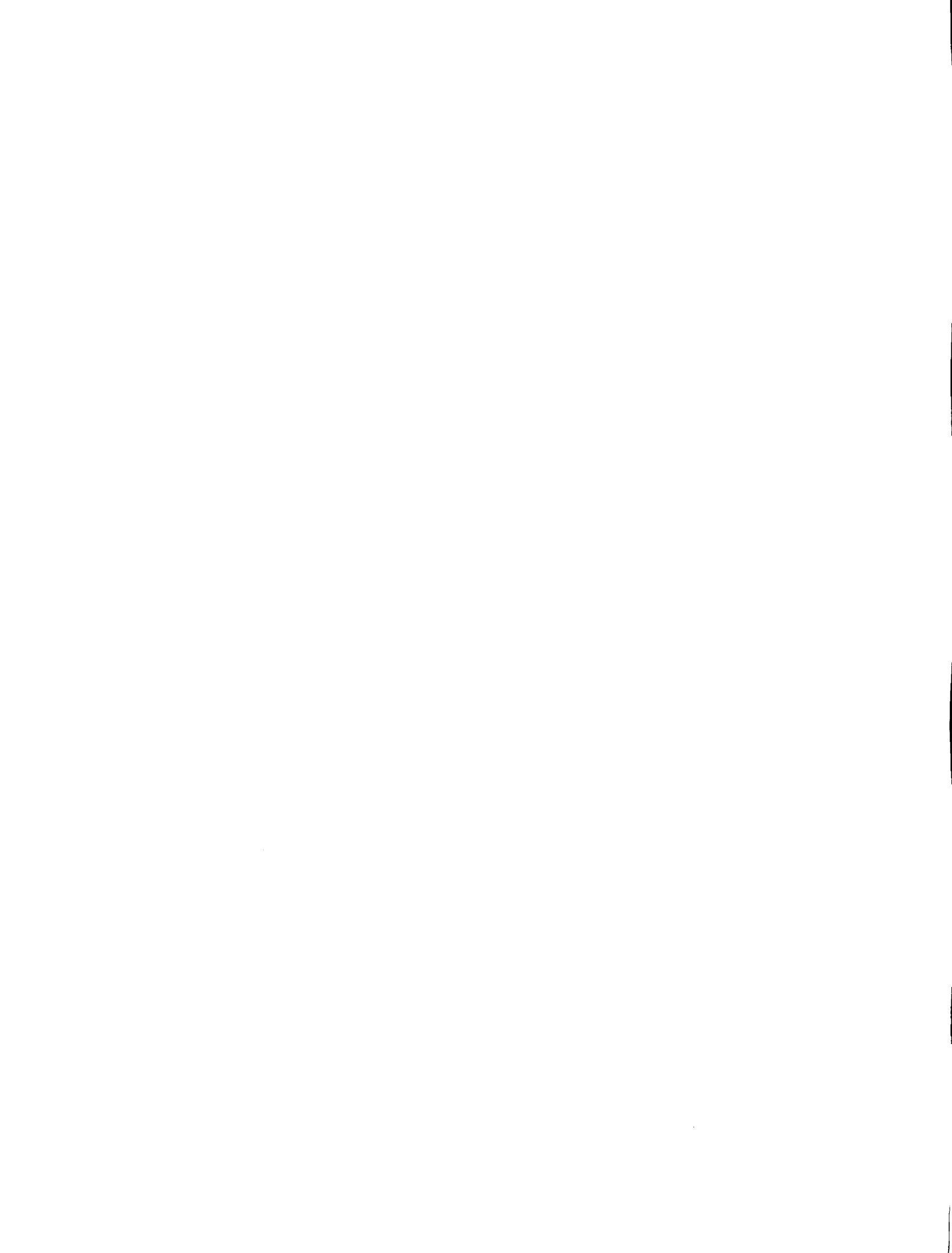
-Illing, L.V., Wells, A.J., and Taylor, J.C.M., 1965, Penecontemporary dolomite in the Persian Gulf, In L.C. Pray and R.C. Murray, eds., Dolomitization and limestone diagenesis, SEPM special publication, Vol. 13., pp. 89-111.

-Jiang, X.N., Yuan, D.R., Sun, D.L., Lu, M.K., Zhang, G.H., and Guo, S.Y., 2001a, Atomic Force Microscopy studies on growth mechanisms and defect formations on (110) faces of Cadmium Mercury Thiocyanate crystals, Crystal Research Technology, Vol. 36, No. 6, pp. 601-608.

-Jiang X.N., Xu D., Sun D.L., Yuan D.R., Lu M.K., Zhang G.H., and Fang Q, 2001b, Formation of small straight steps among large rough steps on the {110} face of cadmium mercury thiocyanate crystal, Journal of Crystal Growth, November 2001, Vol. 233, No. 1, pp. 318-325(8).

-Johnston, W.G., 1962, Dislocation etch pits in non-metallic crystals, In: Progress In Ceramic Science Vol. 2, (Ed. J.E Burke).

-Jones, B., Luth, R.W., and MacNeil, A.J., 2001, Powder X-ray diffraction analysis of homogeneous and heterogeneous sedimentary dolostones, Journal of Sedimentary Research, Vol. 71, No. 5, pp. 790-799.



- Jones, B., 2004, Petrography and significance of zoned dolomite cements from the Cayman Formation (Miocene) of Cayman Brac, British West Indies, Journal of Sedimentary Research, Vol. 74, pp. 95-109.**
- Joshi, M.S., Kotru, P.N., and Ittyachen, M.A., 1970, Kristallografiya, Vol. 15, pp. 103.**
- Joshi, M.S. and Paul, B.K., 1973, Mineralogical Magazine, Vol. 39, pp. 482.**
- Katz, A., 1971, Zoned dolomite crystals, Journal of Geology, Vol. 79, pp. 38-51.**
- Katz, A. and Matthews, A., 1977, The dolomitization of CaCO₃: an experimental study at 252-295°C, Geochimica Cosmochimica Acta, Vol. 41, 297-308.**
- Kazmierczak, T.F., Tomson, M.B., and Nancollas, G.H., 1982, Crystal growth of calcium carbonate. A controlled composition kinetic study, Journal of Physical Chemistry, Vol. 86, pp. 103-107.**
- Keith, R.E., and Gilman, J.J., 1960, Dislocation etch pits and plastic deformation in calcite, Acta Metallurgica, Vol. 8, pp. 1-10.**
- Kessels, L.A., Sibley, D.F., and Nordeng, S.H., 2000, Nanotopography of synthetic and natural dolomite crystals, Sedimentology, Vol.47, pp.173-186.**
- Kessels, L.A., 2001, Interpreting crystal growth kinetics of ancient dolomites, PhD Dissertation, Michigan State University.**
- Kirkland, B.L., Lynch, F.L., Rahnis, M.A., Folk, R.L., Molineux, I.J., and McLean, R.J.C., 1999, Alternative origins for nanobacteria-like objects in calcite, Geology, Vol. 27, No. 4, pp. 347-350.**
- Kirkpatrick, R.J., 1981, Kinetics of crystallization of igneous rocks, in Eds. A.C. Lasaga and R.J. Kirkpatrick, Kinetics of Geochemical Processes, Reviews in Mineralogy, Vol. 8, Chapter 8, pp. 321-398**
- Klapper, H., 1980, Defects in non-metal crystals. In: Characterization of Crystal Growth Defects by X-Ray Methods, eds., B.K. Tanner, D.K. Bowen, Plenum Press, new York, pp. 133-160.**
- Krauskopf, K.B. and Bird, D.K., 1995, Introduction to Geochemistry, McGraw-Hill, New York.**
- Land, L.S., 1967, Diagenesis of skeletal carbonates, Journal of Sedimentary Petrology, Vol. 37, pp. 914-930.**

- Land, L.S., 1980, The isotopic and trace element geochemistry of dolomite: the state of the art, SEPM Special Publication No. 28, Eds., D.L. Zenger, J.B. Dunham, and R.L. Ethington, pp. 87-110.
- Land, L.S., 1985, The origin of massive dolomite, *Journal of Geological Education*, Vol. 33, 112-125.
- Land, L. S. and Macpherson, G. L., 1992, Origin of Saline Formation Waters, Cenozoic Section, Gulf of Mexico Sedimentary Basin: AAPG Bulletin, Vol. 76, pp. 1344–1362.
- Land, L.S., 1998, Failure to precipitate dolomite at 25°C from dilute solution despite 1000-fold oversaturation after 32 years, *Aquatic Geochemistry*, Vol. 4, pp. 361-368.
- Langbein, R. von, Landgraf, K.F., and Milbrodt, E., 1984, Calciumüberschüsse im Dolomit als Indikator des Sedimentationsmilieus in deonischen Karbonatgesteinen: *Chemie der Erde*, Vol. 43, pp. 217-227.
- Langmuir, D., 1997, *Aqueous Environmental Geochemistry*, Prentice Hall, New Jersey, pp. 193-230.
- Lasaga, A.C., and Blum, A.E., 1986, Surface chemistry, etch pits and mineral-water reactions, *Geochimica et Cosmochimica Acta*, Vol. 50, pp. 2363-2379.
- Lasaga, A.C., 1990, Atomic treatment of mineral –water surface reactions, In: Hochella Jr, M.F. and White, A.F., eds. *Mineral-Water Interface Geochemistry*, *Reviews in Mineralogy*, Vol. 23, pp. 17-85.
- Liang, Y., Baer, D.R., McCoy, J.M., Amonette, J.E., and LaFemina, J.P., 1996, Dissolution kinetics at the calcite-water interface, *Geochimica et Cosmochimica Acta*, Vol. 60, pp. 4883-4887.
- Lin, C.C. and Shen, P., 1993, Role of screw axis in dissolution of willemite, *Geochimica et Cosmochimica Acta*, Vol. 57, pp. 1649-1655.
- Lin, C.C. and Shen, P., 1995, Incubation time of etch pits at dislocation outcrops, *Geochimica et Cosmochimica Acta*, Vol. 59, No. 14, pp. 2955-2963.
- Lippmann, F., 1967, Die syntheses des norsethite bei 20°C und 1 at. Ein Modell zur Dolmitisierung, *Neues Jahrb. Mineral. Monatsh.*, pp. 23-29
- Lippmann, F., 1973, *Sedimentary Carbonate Minerals*, Springer-Verlag, Berlin.

- Lorens, R.B., 1981, Sr, Cd, Mn, and Co distribution coefficients in calcite as a function of calcite precipitation rate, *Geochimica et Cosmochimica Acta*, Vol. 45, pp. 553-561.**
- Lowenstein, T.K., Timofeeff, M.N., Brennan, S.T., Hardie, L.A., and Demicco, R.V., 2001, Oscillations in Phanerozoic seawater chemistry: evidence from fluid inclusions. *Science*, Vol. 294, pp. 1086-1088.**
- Lumsden, D.N., 1979, Discrepancy between thin sections and X-ray estimates of dolomite in limestone, *Journal of Sedimentary Petrology*, Vol. 49, pp. 429-436.**
- Lumsden, D.N., 1988, Characteristics of deep marine dolomite, *Journal of Sedimentary Petrology*, Vol. 58, pp. 1023-1031.**
- Lumsden, D.N. and Chimahusky, J.S., 1980, Relationship between dolomite nonstoichiometry and carbonate facies parameters, In: *Concepts and Models of Dolomitization* (Eds. D.H Zenger, J.B. Dunham and R.L. Ethington), Special Publication Society of Economic Paleontologists and Mineralogists, Vol. 28, pp. 111-121.**
- Luttge, A., Winkler, U., and Lasaga, A.C., 2003, Interferometric study of the dolomite dissolution: A new conceptual model for mineral dissolution, *Geochimica et Cosmochimica Acta*, Vol. 67, pp. 1099-1116.**
- Machel, H. , 1997, Recrystallization versus neomorphism, and the concept of 'significant recrystallization' in dolomite research, *Sedimentary Geology*, Vol. 113, pp. 161-168.**
- MacInnes, I.N. and Brantley, S.L., 1992, The role of dislocations and surface morphology in calcite dissolution, *Geochimica et Cosmochimica Acta*, Vol. 56, pp. 1113-1126.**
- MacInnes, I.N. and Brantley, S.L., 1993, Development of etch pit size distributions on dissolving minerals, *Chemical Geology*, Vol. 105, pp. 31-49.**
- Mackenzie, F.T., Bischoff, W.D., Bishop, F.C., Loijens, M., Schoonmaker, J. and Wollast, R., 1983, Magnesian calcites: low temperature occurrence, solubility and solid-solution behavior, in *Carbonate: Mineralogy and Chemistry, Reviews in Mineralogy*, ed. Reeder, R.J., Minerals Society of America, Vol. 11, Chapter 4, pp. 97-144.**
- Maiwa, K., Plomp, M., van Enckevort, W.J.P., and Bennema, P., 1998, AFM observation of barium nitrate (111) and (100) faces: spiral growth and two dimensional nucleation growth, *Journal of Crystal Growth*, Vol. 186, pp. 214-223.**

- Malone, M.J., Baker, P.A., and Burns, S.J., 1994, Recrystallization of dolomite: evidence from the Monterey Formation (Miocene), California, *Sedimentology*, Vol. 41, pp. 1223-1239.**
- Malone, M.J., Baker, P.A., and Burns, S.J., 1996, Recrystallization of dolomite: An experimental study from 50-200°C, *Geochimica et Cosmochimica Acta*, Vol. 60, No. 12, pp. 2189-2207.**
- Marschner, H., 1968, Ca-Mg distribution in carbonates from the Lower Keuper in NW Germany, in Muller, G and Friedman, G.M., eds., *Recent Developments in Carbonate Sedimentology in Central Europe*, Springer-Verlag, New York, pp. 128-135.**
- Marsh, B.D., 1988, Crystal size distribution (CSD) in rocks and the kinetics and dynamics of crystallization: I. Theory, *Contributions to Mineralogy and Petrology*, Vol. 99, pp. 277-291.**
- Mazzullo, S.J., 1992, Geochemical and neomorphic alteration of dolomite: A review, *Carbonates and Evaporites*, Vol. 7, pp. 21-37.**
- McClay, K.R., 1977, Pressure solution and cobble creep in rocks and minerals: a review, *Journal of the Geological Society of London*, Vol. 134, pp. 57-70.**
- McKenzie, J.A. 1981, Holocene dolomitization of calcium carbonate sediments from the coastal sabkhas of Abu Dhabi, U.A.E.: A stable isotope study: *Journal of Geology*. Vol. 89, pp. 185–198.**
- Meike, A., 1990a, A micromechanical perspective on the role of dislocations in selective dissolution, *Geochimica et Cosmochimica Acta*, Vol. 54, pp. 3347-3352.**
- Meike, A, 1990b, Considerations for quantitative determination of the role of dislocations in selective dissolution, *Earth-Science Reviews*, Vol. 29, pp. 309-320.**
- Miser, D.E., Swinnea, J.S., and Steinfink, H., 1987, TEM observations and X-ray crystal structure refinement of a twinned dolomite with a modulated microstructure, *American Mineralogist*, Vol. 72, pp. 188-193.**
- Morrow, D.W. and Ricketts, B.D., 1988, Experimental investigation of sulfate inhibition of dolomite and its mineral analogues, In: Shukla, V., and Baker, P.A., eds., *Sedimentology and Geochemistry of Dolostones: SEPM Special Publication*, Vol. 43, pp. 25-38.**
- Morrow, D.W., Gorham, B.L., and Wong, J.N.Y., 1994, Dolomite-calcite equilibrium at 220 to 240°C at saturation vapour pressure: Experimental data, *Geochimica et Cosmochimica Acta*, Vol. 58, pp. 169-177.**

- Morse, J.W., and Arvidson, R.S., 2002, The dissolution kinetics of major sedimentary carbonate minerals, *Earth Science Reviews*, Vol. 58, No. 1-2, pp. 51-84.
- Murphy, W.M., 1989, Dislocation and feldspar dissolution, *European Journal of Mineralogy*, Vol. 1, pp. 315-326.
- Murray, R.C., 1964, Preservation of primary structures and fabrics in dolomite, in Imbrie, J. and Newell, N., eds., *Approaches to paleoecology*: New York, John Wiley, pp. 388-403.
- Murray, R.C. and Lucia, F.J., 1967, Cause and control of dolomite distribution by rock selectivity, *Geological Society of America Bulletin*, Vol. 78, pp. 21-35.
- Murray, R.C. and Pray, L.C., 1965, Dolomitization and limestone diagenesis-An introduction: In L.C. Pray and R.C. Murray, Eds., *SEPM Special Publication*, Vol. 13, pp. 1-2.
- Naumov, G.B., Ryzhenko, B.N., and Khodakovsky, I.L., 1974, in Barnes, I. and Speltz, V., eds., *Handbook of thermodynamic data*, USGS Water Research Reports 74-001, pp. 239.
- Navrotsky, A. and Capobianco, C., 1987, Enthalpies of formation of dolomite and magnesian calcite, *American Mineralogist*, Vol. 79, pp. 782-787.
- Navrotsky, A., Dooley, D., Reeder, R., and Brady, P., 1999, Calorimetric studies on the energetics of order-disorder in the system $Mg_{1-x}Fe_xCa(CO_3)_2$, *American Mineralogist*, Vol. 84, pp. 1622-1626.
- Navrotsky, A. and Loucks, D., 1977, Calculation of subsolidus phase relations in carbonates and pyroxenes, *Physics and Chemistry of Minerals*, Vol. 1, pp. 109-127.
- Nielsen, A.E., 1964, *Kinetics of Precipitation*, Macmillan, New York.
- Nordeng, S.H. and Sibley, D.F., 1994, Dolomite stoichiometry and Ostwald's Step Rule, *Geochimica et Cosmochimica Acta*, Vol. 58, pp. 191-196.
- Nordstrom, D.K., Plummer, L.N., Langmuir, D., Busenberg, E., May, H.M., Jones, B.F., and Parkhurst, D.L., 1990, Revised chemical equilibrium data for major water-mineral reactions and their limitations, In eds. Melchior, D.C., and Bassett, R.L., *Chemical modeling of aqueous systems II*, American Chemical Society, pp. 398-413.
- Ohara, M. and Reid, R.C., 1973, *Modeling Crystal Growth Rates From Solution*. Prentice Hall, Engelwood Cliffs, NJ, New York.

- Ohnesorge, F. and Binnig, G., 1993, True atomic resolution by atomic force microscopy through repulsive and attractive forces, *Science*, Vol. 260, pp. 1451-1456.
- Paquette, J., Hojatollah, V., and Mountjoy, E., 1999, Novel TEM approaches to imaging of microstructures in carbonates: Clues to growth mechanisms in calcite and dolomite, *American Mineralogist*, Vol. 84, pp. 1939-1949.
- Paquette, J. and Reeder, R.J., 1990, New type of compositional zoning in calcite: Insight into crystal-growth mechanisms, *Geology*, Vol. 18, pp. 1244-1247.
- Paquette, J. and Reeder, R.J., 1995, Relationship between surface structure, growth mechanism, and trace element incorporation in calcite, *Geochimica et Cosmochimica Acta*, Vol. 59, No. 4, pp. 735-749.
- Pande, D.R. and Vadrabade, S.R., 1990, Etch pits on basal cleavage faces of apophyllite crystals, *Mineralogical Magazine*, Vol. 54, pp. 559-565.
- Patel, A.R., Bahl, O.P, and Vagh, A.S., 1965, *Acta Crystallographica*, Vol. 19, pp. 757 and 1025.
- Patterson, R.J. and Kinsman, D.J.J., 1982, Formation of diagenetic dolomite in coastal sabkha along the Arabian (Persian) Gulf, *AAPG Bulletin*, Vol. 66, No. 1, pp. 28-43.
- Penn, R.L. and Banfield, J.F., 1998, Imperfect oriented attachment: dislocation generate in defect-free nanocrystals, *Science*, Vol. 281, pp. 969-971.
- Perkins, R.D., Dwyer, G.S., Rosoff, D.B., Fuller, J., Baker, P.A., and Lloyd, R.M., 1994, Salina sedimentation and diagenesis: West Caicos, British West Indies, *International Association of Sedimentologists, Special Publication*, Vol. 21, pp. 37-54.
- Pierre, C., Ortlieb, L., and Person, A., 1984, Supratidal evaporitic dolomite at Ojo de Liebre lagoon: mineralogical and isotope arguments for primary crystallization, *Journal of Sedimentary Petrology*, Vol. 54, pp. 1049-1061.
- Pina, C.M., Becker, U., Risthaus, P., Bosbach, D., and Putnis, A., 1998, Molecular-scale mechanisms of crystal growth in barite, *Nature*, Vol. 395, pp. 483-486.
- Pina C.M., Enders M., and Putnis A., 2000, The composition of solid solutions crystallizing from aqueous solutions: the influence of supersaturation and growth mechanisms, *Chem. Geol.*, Vol. 168, pp. 195-210.

-Pina, C.M., Putnis, A., and Astilleros, J.M., 2004, The growth mechanisms of solid solutions crystallizing from aqueous solutions, *Chemical Geology*, Vol. 204, pp. 145-161.

Plummer, L.N., Parkhurst, D.L. and Wigley, T.M.L., 1979, Critical review of the kinetics of calcite dissolution and precipitation. In: Jenne, E. Editor, 1979. *Chemical Modelling — Speciation, Sorption and Kinetics in Aqueous Systems* American Chemical Society, Washington, D.C., pp. 537–573.

-Porsche, J., Ruf, A, Geiger, M., and Scholz, F., Size control of self-assembled InP/GaP quantum islands, *Journal of Crystal Growth*, Vol. 195, pp. 591-595.

-Purser, B., Tucker, M., and Zenger, D, 1994, Problems, progress and future research concerning dolomites and dolomitization, in *Dolomites: A Volume in Honor of Dolomieu*, Special Publication of the International Association of Sedimentologists, No. 21., pp. 3-20.

-Radke, B.M. and Mathis, R.L., 1980, On the formation and occurrence of saddle dolomite, *Journal of Sedimentary Petrology*, Vol. 50, pp. 1149-1168.

-Randazzo, A.F. and Cook, D.J., 1987, Characterization of dolomite rocks from coastal mixing zone of the floridian aquifer, USA, *Sedimentary Geology*, Vol.

-Reeder, R.J., 1981, Electron optical investigation of sedimentary dolomites, *Contributions to Mineralogy and Petrology*, Vol. 76, pp. 148-157.

-Reeder, R.J., 1982, Crystal growth defects in sedimentary carbonate minerals, *Estudios Geologica*, Vol. 38, pp. 179-183.

-Reeder, R.J., 1983, Crystal chemistry of the rhombohedral carbonates. In Reeder, R.J. Ed., *Carbonates: Mineralogy and Chemistry*, *Reviews in Mineralogy*, Vol. 11, pp. 1-47.

-Reeder, R.J., 1992, Carbonates: Growth and alteration microstructures. In. *Minerals and reactions at the atomic scale; transmission electron microscopy*, *Reviews in Mineralogy*, Vol. 27, pp. 380-424.

-Reeder, R.J., 2000, Constraints on cation order in calcium-rich sedimentary dolomites, *Aquatic Geochemistry*, Vol. 6, pp. 213-226.

-Reeder, R.J. and Prosky J.L., 1986, Compositional sector zoning in dolomite, *Journal of Sedimentary Petrology*, Vol. 56, pp. 237-247.

-Reeder, R.J. and Sheppard, C.E., 1984, Variation of lattice parameters in some sedimentary dolomites, *American Mineralogist*, Vol. 69, pp. 520-527.

- Reeder, R.J. and Wenk, H.R., 1979, Microstructures in low temperature dolomites. *Geophysical Review Letter*, Vol. 6, pp. 77-80.
- Richter, D.K., 1974, Entstehung und diagenese der Devonischen und Permotriassischen Dolomite in der Eifel: In *Contributions to Sedimentology*, Vol. 2, Schweizerbartsche Verlagsbuchhandlung, Stuttgart, pp. 101.
- Robie, R.A., Hemingway, B.S., and Fisher, J.R., 1978, Thermodynamic properties of minerals and related substances at 298.15K and 1 bar pressure and at higher temperatures, *U.S. Geological Survey Bulletin*, Vol. 1452, pp. 456.
- Rock, P.A., Manell, G.K., Casey, W.A., and Walling, E.M., 2001, Gibbs energy of formation of dolomite from electrochemical cell measurements and theoretical calculations, *American Journal of Science*, Vol. 301, pp. 103-111.
- Rosen, M.R., Miser, D.E., and Warren, J.K., 1988, Sedimentology, mineralogy, and isotopic analysis of Pellet Lake, Coorong region, South Australia, *Sedimentology*, Vol. 35, pp. 105-122.
- Rosen, M.R., Miser, D.E., Starcher, M.A., and Warren, J.K., 1989, Formation of dolomite in the Coorong region, South Australia, *Geochimica et Cosmochimica Acta*, Vol. 53, pp. 661-669.
- Rosenberg, P.E. and Holland, H.D., 1964, Calcite-dolomite-magnesite stability relations in solutions at elevated temperatures, *Science*, Vol. 145, pp. 700-701.
- Royce, C.R., Wadell Jr., J.S., and Petersen, L.E., 1971, X-ray determination of calcite-dolomite: an evaluation, *Journal of Sedimentary Petrology*, Vol. 41, pp. 483-488.
- Rozgonyi, G.A., Mahajan, S., Read, M.H., and Brasen, D., 1976, Sources of oxidation-induced stacking faults in Czochralski silicon wafers, *Applied Physics Letters*, Vol. 29, pp. 531-533.
- Sangwal, K., 1987a, *Etching of Crystals: Theory, Experiment, and Application*, North-Holland, Oxford.
- Sangwal, K., 1987b, Etching processes and the investigation of minerals, In: *Geochemistry and Mineral Formation in the Earth Surface*, eds. R. Rodriguez-Clemente and Y. Tardy, *Proceedings of the international meeting, Geochemistry of the earth surface and processes of mineral formation*.
- Sass, E. and Bein, A., 1988, Dolomites and salinity: a comparative geochemical study, in Shukla, V. and Baker, P.A., eds., *Sedimentology and Geochemistry of Dolostones: SEPM Special Publication*, Vol. 43, pp. 223-233.

- Sass, E. and Katz, A., 1982, The origin of platform dolomites: new evidence, American Journal of Science, Vol. 282, pp. 1184-1213.**
- Sayles, F.L. and Fyfe, W.S., 1973, The crystallization of magnesite from aqueous solution, Geochimica et Cosmochimica Acta, Vol. 37, pp. 87-99**
- Schmidt, V., 1965, Facies, diagenesis, and related reservoir properties in the Gigas Beds (Upper Jurassic), northwestern Germany: In, Prey, L.C. and Murray, R.C., eds., Dolomitization and Limestone Diagenesis: SEPM, Special Publication, Vol. 13, pp. 124-169.**
- Schubel, K.A., Elbert, D.C., and Veblen, D.R., 2000, Incommensurate c-domain superstructure in calcian dolomite from the Latemar buildup, Dolomites, Northern Italy, American Mineralogist, Vol. 85, pp 858-862.**
- Shinn, E., Ginsburg, R.N., and Lloyd, R.M., 1965, Recent supratidal dolomite from Andros Island, In L.C. Pray and R.C. Murray, eds., Dolomitization and limestone diagenesis, SEPM special publication, Vol. 13., pp. 112-123.**
- Sibley, D.F., 1982, The origin of common dolomite fabrics, Journal of Sedimentary Petrology, Vol. 50, pp. 1149-1168.**
- Sibley, D.F. and Bartlett, T.R., 1987, Nucleation as a rate limiting step in dolomitization, International Symposium on Crystal growth Processes in the Sedimentary Environment, 2nd, Granada, 1986, Madrid, Institute de Geologica, C.S.I.C, pp. 733-741.**
- Sibley, D.F., Dedoes, R.E., and Bartlett, T.R., 1987, Kinetics of dolomitization, Geology, Vol. 15, 1112-1114.**
- Sibley, D.F. and Gregg, J.M., 1987, Classification of dolomite rock texture, Journal of Sedimentary Petrology, Vol. 57, pp. 967-975.**
- Sibley, D.F., Gregg, J.M., Brown, R.G., and Laudon, P.R., 1993, Dolomite crystal size distribution, in Rezak, R., and Lavoie, D., eds., Carbonate Microfabrics: New York, Springer-Verlag, pp. 195-208.**
- Sibley, D.F., Nordeng, S.H., and Borkowski, M.L., 1994, Dolomitization kinetics in hydrothermal bombs and natural settings, Journal of Sedimentary Research, Vol. A64, No. 3, pp. 630-637.**
- Sibley, D.F., 1990, Unstable to stable transformations during dolomitization, Journal of Geology, Vol. 98, 739-748.**

- Sperber, C.M., Wilkinson, B.H., and Peacor, D.R., 1984, Rock composition, dolomite stoichiometry, and rock/water reactions in dolomitic carbonate rocks, *The Journal of Geology*, Vol. 92, No. 6, pp. 609-622.
- Stadler, H.L., 1963, Etched hillocks in BaTiO₃, *Journal of Applied Physics*, Vol. 34, pp. 570-573.
- Stipp, S.L.S., Eggleston, C.M., and Nielsen, B.S., 1994, Calcite surface structure observed at microtopographic and molecular scales with atomic force microscopy (AFM), *Geochimica et Cosmochimica Acta*, Vol. 58, No. 14, pp. 3023-3033.
- Sun, S.Q., 1994, A reappraisal of dolomite abundances and occurrence in the Phanerozoic, *Journal of Sedimentary Research, Section A* 64, No. 2, pp. 396-404.
- Sunagawa, I., 1977, Natural crystallization, *Journal of Crystal Growth*, Vol. 42, pp. 214-223.
- Sunagawa, I., 1981, Characteristics of crystal growth in nature as seen from the morphology of mineral crystals, *Bulletin Mineralogie*, Vol. 104, pp. 81-87.
- Sunagawa, I., 1984, Growth of crystals in nature. In: *Materials Science of the Earth's Interior*, Ed. I. Sunagawa, Terra Scientific Publishing, Tokyo, pp. 63-105.
- Swart, P.K. and Melim, L.A., 2000, The origin of dolomite in Tertiary sediments from the Great Bahama Bank, *Journal of Sedimentary Research*, Vol. 70, pp. 738-748.
- Tanger, J.C. IV, and Helgeson, H.C., 1988, Calculation of the thermodynamic and transport properties of aqueous species at high pressures and temperatures, Revised equations of state for the standard partial molal properties of ions and electrolytes, *American Journal of Science*, Vol. 288, pp. 19-98.
- Tuck, B. and Baker, A.J., 1973, Chemical etching of {111} and {100} surfaces of InP, *Journal of Materials Science*, Vol. 8, pp. 1559-1566.
- Tuck, B., 1975, The chemical polishing of semiconductors, *Journal of Materials Science*, Vol. 10, pp. 321-339.
- Usdowski, E., 1994, Synthesis of dolomite and geochemical implications, In *Dolomites: A Volume in Honor of Dolomieu*, Eds. B.H. Purser, M.E. Tucker, and D.L. Zenger, International Association of Sedimentology, Special Publication, Vol. 21, pp. 345-360.

- Van Tendello, G., Wenk, H.R., and Gronsky, R., 1985, Modulated structures in calcian dolomite: A study by electron microscopy, Physics and Chemistry of Minerals, Vol. 12, pp. 333-341.**
- Vasconcelos, C, McKenzie, J.A., Bernasconi, S., Grujic, D, and Tien, A., 1995, Microbial mediation as a possible mechanism for dolomite formation at low temperature, Nature, Vol. 377, pp. 220-222.**
- Vasconcelos, C. and McKenzie, J.A., 1997, Microbial mediation of modern dolomite precipitation and diagenesis under anoxic conditions (Lagoa Vermelha, Rio De Janeiro, Brazil), Journal of Sedimentary Research, Vol. 67, No. 3, pp. 378-390.**
- Vennegues, P., Beaumont, B., Haffouz, S., Vaille, M., and Gibart, P., 1998, Influence of in situ sapphire surface preparation and carrier gas on the growth mode of GaN in MOVPE, Journal of Crystal Growth, Vol. 187, pp. 167-177.**
- Vogel, F.L., Pfann, W.G., Corey, H.E., Thomas, E.E., 1953, Physics Review, Vol. 90, pp. 489.**
- Von Der Borch, C.C. and Jones, J.B., 1976, Spherular modern dolomite from the Coorong area, South Australia, Sedimentology, Vol. 23, pp. 587-591.**
- Wagman, D.D., Evans, W.H., Parker, V.B., Schumm, R.H., Halow, I., Bailey, S.M., Churney, K.L., and Nuttall, R.L., 1982, The NBS tables of chemical thermodynamic properties: selected values for inorganic and C₁ and C₂ organic substances in SI units, Journal of Physical and Chemical Reference Data, Vol. 11 (Supplement No. 2), pp. 392.**
- Walton, A.G., 1969, Nucleation in Liquids and Solutions, Zettlemoyer, AC Nucleation, New York.**
- Warthman, R., van Lith, Y, Vasconcelos, C., McKenzie, J.A., and Karpoff, A.M., 2000, Bacterially induced dolomite precipitation in anoxic culture experiments, Geology, Vol. 28, No. 12, pp. 1091-1094.**
- Wenk, H.R., Barber, D.J., Reeder, R.J., 1983, Microstructures in carbonates. In Carbonates: Mineralogy and Chemistry (ed. R.J. Reeder); Reviews in Mineralogy Vol. 11, pp. 301-367.**
- Wenk, H.R., Hu, M.S., and Frisia, S., 1993, Partially ordered dolomite-Microstructural characterization of Abu-Dhabi sabkha carbonates, American Mineralogist, Vol. 78, pp. 769-774**

-Weyher, J. and Van Enkevort, W.J.P., 1983, Selective etching and photoetching of {100} in gallium arsenide CrO_3 -HF aqueous solutions. II., The Nature of etch hillocks, *Journal of Crystal Growth*, Vol. 63, pp. 292-298.

-Wilkenson, B.H. and Algeo, T.J., 1989, Sedimentary carbonate record of calcium magnesium cycling, *American Journal of Science*, Vol. 289, pp. 1158-1194.

-Zbik, M. and Smart, R. St C., 1998, Nanomorphology of kaolinities: comparative SEM and AFM studies. *Clays and Clay Minerals*, Vol. 46, pp. 153-160.

-Zenger, D.H., 1996, Dolomitization of the "C" zone, Red River Formation (Upper Ordovician) in a deep core, Williston basin, Richland County, eastern Montana, *Contributions to Geology, University of Wyoming*, Vol. 31, No. 1, pp. 57-75.

MICHIGAN STATE UNIVERSITY LIBRARIES



3 1293 02736 7857